

MATRIX FRACTURE INTERACTION IN SANDSTONE ROCKS
DURING CARBON DIOXIDE, METHANE AND NITROGEN INJECTION

A THESIS SUBMITTED TO
THE GRADUATE SCHOOL OF NATURAL AND APPLIED SCIENCES
OF
MIDDLE EAST TECHNICAL UNIVERSITY

BY

SEVTAÇ BÜLBÜL

IN PARTIAL FULFILLMENT OF THE REQUIREMENTS
FOR
THE DEGREE OF DOCTOR OF PHILOSOPHY
IN
PETROLEUM AND NATURAL GAS ENGINEERING

JUNE 2012

Approval of the thesis:

**MATRIX FRACTURE INTERACTION IN SANDSTONE ROCKS
DURING CARBON DIOXIDE, METHANE AND NITROGEN INJECTION**

submitted by **SEVTAÇ BÜLBÜL** in partial fulfillment of the requirements for the degree of **Doctor of Philosophy in Petroleum and Natural Gas Engineering Department, Middle East Technical University** by,

Prof. Dr. Canan Özgen
Dean, Graduate School of **Natural and Applied Sciences** _____

Prof. Dr. Mahmut Parlaktuna
Head of Department, **Petroleum and Natural Gas Engineering** _____

Prof. Dr. Mahmut Parlaktuna
Supervisor, **Petroleum and Natural Gas Eng. Dept., METU** _____

Examining Committee Members

Prof. Dr. Ender Okandan
Petroleum and Natural Gas Engineering Dept.,METU _____

Prof. Dr. Mahmut Parlaktuna
Petroleum and Natural Gas Engineering Dept.,METU _____

Prof. Dr. Salih Saner
Petroleum and Natural Gas Engineering Dept.,METU- NCC _____

Assoc. Prof. Dr. Yusuf Uludağ
Chemical Engineering Dept., METU _____

Asst. Prof. Dr. Çağlar Sınayuç
Petroleum and Natural Gas Engineering Dept.,METU _____

Date:

18.06.2012

I hereby declare that all information in this document has been obtained and presented in accordance with academic rules and ethical conduct. I also declare that, as required by these rules and conduct, I have fully cited and referenced all material and results that are not original to this work.

Name, Last name: Sevtaç BÜLBÜL

Signature:

ABSTRACT

MATRIX FRACTURE INTERACTION IN SANDSTONE ROCKS DURING CARBON DIOXIDE, METHANE AND NITROGEN INJECTION

Bülbül, Sevtaç

Ph.D., Department of Petroleum and Natural Gas Engineering

Supervisor: Prof. Dr. Mahmut Parlaktuna

June 2012, 167 pages

The aim of the study is to investigate matrix-fracture interaction, gas oil gravity drainage (GOGD) and diffusion mechanisms with CO₂, N₂ and CH₄ gas injection in a fractured system. Effects of injected gas type, initial gas saturation and diffusion coefficient on oil recovery are studied by an experimental and simulation work.

In the experimental study, Berea sandstone cores are placed in a core holder and the space created around the core is considered as a surrounding fracture. System is kept at a pressure of 250 psi by CO₂, N₂ and CH₄ gases and at a reservoir temperature of 70 °C.

Experiments with cores having similar initial saturations resulted in the highest n-decane recovery in CO₂ experiment followed by CH₄ and N₂. The highest

solubility of CO₂ in n-decane and density difference between CO₂ and CO₂-n-decane mixture are considered as the reason of results.

CO₂ injection tests with n-decane and brine saturated core with and without initial gas saturation indicate that availability of initial gas saturation in matrix increased recovery.

A simulation study is continued using CMG (Computer Modeling Group Ltd.) WinProp (Microsoft Windows™ based Phase-Behavior and Fluid Property Program) and GEM (Generalized Equation-of-State Model Compositional Reservoir Simulator). Simulation results of CO₂ experiment with initial gas show that dominant effect of GOGD decreases and diffusion becomes more effective at final production stages. Simulation study indicates an immediate, sharp decrease in oil saturation in matrix. Oil in matrix migrates into fractures and moves downward as a result of GOGD with gas injection.

Keyword: Matrix-Fracture Interaction, Gas-Oil Gravity Drainage, Diffusion, CO₂, N₂ and Methane Injection, Oil Recovery

ÖZ

KUMTAŞI KAYAÇLARDA KARBONDİOKSİT, METAN VE NİTROJEN ENJEKSİYONU SIRASINDAKİ MATRİKS ÇATLAK ETKİLEŞİMİ

Bülbül, Sevtaç

Doktora, Petrol ve Doğal Gaz Mühendisliği Bölümü

Tez Yöneticisi: Prof. Dr. Mahmut Parlaktuna

Haziran 2012, 167 sayfa

Çalışmanın amacı, çatlaklı bir sistemde CO₂, CH₄ ve N₂ enjeksiyonu sırasında meydana gelen matriks-çatlak etkileşimi, gaz-petrol gravite drenajı ve difüzyon mekanizmalarını incelemektir. Enjekte edilen gaz türünün, başlangıç gaz doymuşluğunun ve difüzyon katsayısının petrol kazanımı üzerindeki etkileri deney ve simülasyon çalışması ile incelenmiştir.

Deneysel çalışma sırasında, Berea kumtaşı karotlar karot tutucuya yerleştirilmiş ve karotun etrafında kalan boşluk karotu çevreleyen bir çatlak olarak değerlendirilmiştir. Sistem CO₂, N₂ ve CH₄ gazları ile 250 psi basınç değerinde tutulmuştur. Sistem sıcaklığı, rezervuar sıcaklığı değeri olarak alınan 70 °C'dir.

Benzer başlangıç doymuşluklarına sahip karot örnekleri ile yürütülmüş deneyler sonucunda en yüksek kazanım değeri CO₂ ile yürütülmüş deneyde elde edilmiştir. Kazanım sıralamasında CO₂ deneyinden sonra sırasıyla CH₄ ve N₂ deneyleri

gelmektedir. n-dekandaki en yüksek çözünürlük değerinin CO₂'ye ait olması ve CO₂ ile CO₂-n-dekan karışımı arasındaki yoğunluk farkı, bu sonuçların nedeni olarak değerlendirilmiştir.

n-dekan ve tuzlu su ile doyurulmuş karot ile yapılan başlangıç gaz doymuşluğu bulunan ve bulunmayan CO₂ enjeksiyonu testleri, matrikste başlangıç gaz doymuşluğu bulunmasının kazanımı arttırdığını göstermektedir.

CMG (Computer Modeling Group Ltd.) WinProp (Microsoft Windows™ based Phase-Behavior and Fluid Property Program) ve GEM (Generalized Equation-of-State Model Compositional Reservoir Simulator) kullanılarak bir simülasyon çalışması yapılmıştır. Başlangıç gaz doymuşluğu ile yürütülen CO₂ deneyinin simülasyon sonuçları, üretimin son aşamalarında gaz petrol gravite drenajının baskın etkisinin azaldığını ve difüzyonun daha etkin bir hal aldığını göstermektedir. Simülasyon çalışması, petrolün matrikste ani ve keskin azalmasını göstermektedir, Matriksteki petrol çatlaklara göç etmekte ve gaz enjeksiyonu ile gaz petrol gravite drenajının sonucu olarak aşağı doğru hareket etmektedir.

Anahtar Kelimeler: Matriks-Çatlak Etkileşimi, Gaz-Petrol Gravite Drenajı, Difüzyon, CO₂, N₂ ve Metan Enjeksiyonu, Petrol Kazanımı

To My Family

ACKNOWLEDGEMENTS

I would like to express my sincere thanks to my thesis advisor Prof. Dr. Mahmut PARLAKTUNA for his support, encouragement, advice and guidance throughout the study. Without his invaluable insights, this study would not have been accomplished.

I would like to thank Thesis Supervising Committee Members, Prof. Dr. Ender OKANDAN, Prof. Dr. Mahmut PARLAKTUNA and Assoc. Prof. Dr. Yusuf ULUDAĞ for their guidance and insights throughout the study. I would like to express my gratitude to all the Thesis Examining Committee Members, Prof. Dr. Salih SANER and Asst. Prof. Dr. Çağlar SINAYUÇ.

I would like to acknowledge Shell Global Solutions International for funding the research presented in this thesis (Contract No. 4600004372). I also would like to thank Marco WELLING and Suzanne HANGX from Shell for their valuable contribution to the study.

I would like to thank Naci DOĞRU for his help and contribution during the experiments and in the construction of the experimental set-up. I also want to thank Murat ÇALIŞKAN and Nazım ERGÜN for their help during experiments.

I would also like to thank Can ERCAN from the Turkish Petroleum Corporation (TPAO) Research Center for his contribution to the study.

I also wish to thank my dear friends; Chansthalmaa DALKHAA, who I have shared not only simply the same laboratory but also friendship and encouragement during this study. Emre ÖZGÜR, Mehmet SORGUN, Aslı GÜNDOĞAR and

Oytun ÖRS, my officemates and dear friends who were always standing beside me throughout the study. Reza Ettehadı OSGOUEI, Tuğçe BAYRAM, Gizem GÜL and Göker ERTUNÇ, who I appreciate invaluable friendship and contribution of them.

Finally, I would like to express my deepest gratitude to my family for their endless love, support and encouragement throughout my life. Without their presence and support, it would not be possible for me to complete this study and surely, I would not be the person that I am today. My final thanks go to my little nephew Tuna, who suggested helping me in the preparation of my thesis several times, although he is only 6 years old and has recently learnt how to read and write.

TABLE OF CONTENTS

ABSTRACT	iv
ÖZ.....	vi
ACKNOWLEDGEMENTS.....	ix
TABLE OF CONTENTS.....	xi
LIST OF TABLES.....	xiv
LIST OF FIGURES.....	xv
CHAPTERS	
1. INTRODUCTION	1
2. THEORY.....	3
2.1. Gas Oil Gravity Drainage (GOGD) in Fractured Reservoirs.....	3
2.1.1. Governing Equations of Gas-Oil Gravity Drainage Mechanism.....	9
2.2. Diffusion in Naturally Fractured Reservoirs.....	16
2.3. Miscibility Considerations	19
3. PREVIOUS EXPERIMENTAL AND SIMULATION WORK.....	24
3.1. Experimental Studies Carried Out On Matrix-Fracture Interaction, Gas-Oil Gravity Drainage and Gas Injection Processes.....	24
3.2. Simulation Studies Carried Out On Matrix-Fracture Interaction, Gas-Oil Gravity Drainage and Gas Injection Processes.....	35
4. STATEMENT OF PROBLEM.....	40
5. EXPERIMENTAL STUDY.....	41
5.1. Experimental Setup	41
5.2. Experimental Procedure.....	49

6. EXPERIMENTAL RESULTS AND DISCUSSION.....	51
6.1. Core Sample Characterization.....	51
6.2. Experiments carried out with CO ₂ , CH ₄ and N ₂ Injection.....	53
6.3. Comparison of Experiments carried out with CO ₂ Injection.....	62
6.4. Comparison of Recovery Factors Obtained in Tests with CO ₂ , CH ₄ and N ₂	63
7. SIMULATION RESULTS AND DISCUSSION.....	70
7.1. CMG (Computer Modeling Group Ltd.) WinProp (Microsoft Windows™ based Phase-Behavior and Fluid Property Program).....	71
7.2. Data Preparation by using CMG Builder for CMG GEM (Generalized Equation-of-State Model Compositional Reservoir Simulator).....	79
7.3. Results of Simulation Study carried out with CO ₂ , CH ₄ and N ₂ Injection Experiments.....	86
8. CONCLUSION.....	108
9. RECOMMENDATIONS.....	112
REFERENCES.....	113
APPENDICES	
A. SPECIFICATIONS OF N-DECANE.....	122
B. SPECIFICATIONS OF THE EQUIPMENT USED IN THE EXPERIMENTAL SETUP.....	125
C. RESULTS OF XRD ANALYSIS.....	129
D. RESULTS OF CORE ANALYSIS CARRIED OUT AT TPAO.....	132

E. SOLUBILITY OF CO ₂ , CH ₄ AND N ₂ IN N-DECANE AT 70 °C AND 250 PSI.....	138
F. MIXTURE DENSITY AND VISCOSITY OF N-DECANE-CO ₂ , CH ₄ & N ₂	141
G. PENG ROBINSON EQUATION OF STATE.....	145
H. INPUT FILE PREPARED FOR MODELING CO ₂ EXPERIMENT.....	149
VITA.....	161

LIST OF TABLES

TABLES

Table 6. 1. KCl Aqueous Solution Saturated and Dry Weights of Core Samples.	52
Table 6.2. List of Experiments	54
Table 6. 3. Weight of Core samples after Brine, n-decane Saturation.....	55
Table 6. 4. Initial Saturations.....	55
Table 6. 5. Original Oil in Place for each Experiment.....	56
Table 6. 6. Properties of n-decane, CO ₂ , CH ₄ and N ₂ at 250 psi and 70 °C (NIST Chemistry WebBook, 2011).	65
Table 6. 7. Mixture and Component Densities Calculated with Peng-Robinson Equation of State (Peng and Robinson, 1976).....	68
Table 6.8. Diffusion coefficients for CO ₂ and CH ₄ in n-decane at 250 psia, 70 °C	69

LIST OF FIGURES

FIGURES

Figure 2. 1. Matrix and Fracture Network System with Open Flow Channels (Reiss, 1980)	2
Figure 2. 2. Process of Oil Production under Gravity Drainage Drive in a Conventional Reservoir (Cole, 1969; Ahmed and McKinney, 2005).....	4
Figure 2. 3. Cross Section of a Conventional Gravity Drainage Reservoir and its Oil Saturation Profile (Hall, 1961).....	5
Figure 2. 4. A Conventional Reservoir with (a) Constant Pressure Maintenance ...	6
Figure 2. 5. Processes and Zones during Gas Oil Gravity Drainage in Fractured Reservoirs (Clemens and Wit, 2001).	8
Figure 5.1. Schematic of the System Used For Saturating the Core with Brine ...	42
Figure 5.2. Core Holder with its Pressure Gauge Used for Saturating the Core with Brine	42
Figure 5. 3. Schematic of the System Used For Saturating the Core with.....	43
Figure 5. 4. Core Holder with its Pressure Transducers Used for Saturating the Core with n-decane.....	44
Figure 5. 5. Schematic of the System Used For the Experiments	45
Figure 5. 6. Core Holders Used for the Experiments.....	45
Figure 5. 7. Core Cleaning Apparatus.....	46
Figure 5. 8. Data Logging System with Different Modules of Temperature and Pressure Measurements	47
Figure 5. 9. Flowchart Developed By LabVIEW Software for Data Logging, Recording and Visualization.....	48
Figure 5. 10. Experimental Set-up with Its Components	49

Figure 6.1. Cumulative n-decane production with CO ₂ injection- Test-1, Core E1	57
Figure 6. 2. Cumulative n-decane production with CO ₂ injection- Test-2, Core E2	57
Figure 6. 3. Cumulative n-decane production with CH ₄ injection- Test-3, Core E1	58
Figure 6. 4. Cumulative n-decane production with N ₂ injection- Test-4, Core E2	58
Figure 6. 5. Recovery Factors with CO ₂ injection, Test -1, Core E1	60
Figure 6. 6. Recovery Factors with CO ₂ injection, Test – 2, Core E2	61
Figure 6. 7. Recovery Factors with CH ₄ injection, Test – 3, Core E1	61
Figure 6. 8. Recovery Factors with N ₂ injection, Test – 4, Core E2	62
Figure 6. 9. Comparison of Experiments carried out with CO ₂ Injection	63
Figure 6. 10. Recovery Factors with CO ₂ , CH ₄ and N ₂ injection	64
Figure 7. 1. CMG WinProp Steps for Modelling Phase Behavior of Reservoir Fluids	71
Figure 7. 2. CMG WinProp Component Selection	73
Figure 7. 3. CMG WinProp- Composition	73
Figure 7. 4. CMG WinProp Two-Phase Envelope Construction	74
Figure 7. 5. P-T Phase Boundaries for n-decane- CO ₂ System for Different Primary CO ₂ compositions (0.01-0.9)	74
Figure 7. 6. P-T Diagram with primarily 0.001 mole fraction of CO ₂ (Exp-1)	75
Figure 7. 7. P-T Diagram with primarily 0.055 mole fraction of CO ₂ (Exp-2)	75
Figure 7. 8. P-T Diagrams with primarily 0.067 mole fraction of CH ₄ (Exp-3)	76
Figure 7. 9. P-T Diagrams with primarily 0.083 mole fraction of N ₂ (Exp-4)	76
Figure 7. 10. P-X diagram for n-decane and CO ₂ system with primarily 0.001 mole fraction of CO ₂ (Exp-1)	77
Figure 7. 11. P-X diagram for n-decane and CO ₂ system with primarily 0.055 mole fraction of CO ₂ (Exp-2)	78

Figure 7. 12. P-X diagram for n-decane and CH ₄ system with primarily 0.067 mole fraction of CH ₄ (Exp-3)	78
Figure 7. 13. P-X diagram for n-decane and N ₂ system with primarily 0.083 mole fraction of N ₂ (Exp-4).....	79
Figure 7. 14. Reservoir Simulation Settings for CMG GEM.....	80
Figure 7. 15. Radial Grid System Created with 20 Divisions in the r Direction...	80
Figure 7. 16. 3 D View of the Radial Grid System with 20 layers along the k-direction	81
Figure 7. 17. Layers along the k Direction in the Grid System.....	81
Figure 7. 18. Property Specification	83
Figure 7. 19. Permeability in i Direction for Matrix and Fracture Blocks.....	83
Figure 7. 20. Changes in Permeability Values in Different Layers in the Areal View	84
Figure 7. 21. Relative Permeability Curve constructed by the CMG Builder.....	84
Figure 7. 22. User specified Initial Conditions.....	85
Figure 7. 23. Well Constraints and Well Events Specified.....	86
Figure 7. 24. Radial Grid System with 3 Divisions along the r Direction and 3 Layers along the K- Direction (Down) for Experiment-1	87
Figure 7. 25. Simulation Results without Diffusion for CO ₂ Experiment-1	88
Figure 7. 26. Defining Gas Phase Matrix- Fracture Diffusion Coefficient in CMG Builder	89
Figure 7. 27. Simulation Results with Diffusion for CO ₂ Experiment-1	90
Figure 7. 28. Radial Grid System with 3 Divisions along the r Direction and 3 Layers along the K- Direction (Down) for Experiment-2	91
Figure 7. 29. Simulation Results with Diffusion for CO ₂ Experiment-2.....	93
Figure 7. 30. Oil and Gas Saturation in Fractures with a Spacing of 1×10 ⁻⁵ m in Matrix at 884, 908 and 932 hours	93
Figure 7. 31. Block 1,1,2; Block 1,1,20 and Block 1,1,39.....	94
Figure 7. 32. Oil Saturation Values in Matrix for Block 1,1, 2; Block 1,1,20 and Block 1,1,39	95

Figure 7. 33. Oil Saturation Values in Fracture for Block 1,1,2; Block 1,1,20 and Block 1,1,39	96
Figure 7. 34. Gas Saturation Values in Matrix for Block 1,1,2; Block 1,1,20 and Block 1,1,39	97
Figure 7. 35. Gas Saturation Values in Fracture for Block 1,1,2; Block 1,1,20 and Block 1,1,39	98
Figure 7. 36. Oil Saturation Distribution in Fractures	99
Figure 7. 37. Gas Saturation Distribution in Fractures	100
Figure 7. 38. Block 1,1,20; Block 2,1,20 and Block 3,1,20	101
Figure 7. 39. Oil Saturation Values in Matrix for Block 1,1,20; Block 2,1,20 and Block 3,1,20 at Layer 20	102
Figure 7. 40. Oil Saturation Values in Fracture for Block 1,1,20; Block 2,1,20 and Block 3,1,20 at Layer 20	103
Figure 7. 41. Gas Saturation Values in Matrix for Block 1,1,20; Block 2,1,20 and Block 3,1,20 at Layer 20	104
Figure 7. 42. Gas Saturation Values in Matrix for Block 1,1,2; Block 2,1,2 and Block 3,1,2 at Layer 2	104
Figure 7. 43. Radial Grid System with 3 Divisions along the r Direction and 3 Layers along the K- Direction (Down) for Experiment-3	105
Figure 7. 44 .Radial Grid System with 3 Divisions along the r Direction and 3 Layers along the K- Direction (Down) for Experiment-4	105
Figure 7. 45. Simulation Results with Diffusion for CH ₄ Experiment-3	106
Figure 7. 46. Simulation Results without Diffusion for N ₂ Experiment-4	107

CHAPTER 1

INTRODUCTION

There exist many naturally fractured reservoirs throughout the world, which contain large amounts of hydrocarbons and make a significant contribution to the total proven hydrocarbon reserves (Van Golf-Racht; 1982, Saidi, 1987). Naturally fractured reservoirs consist of a matrix system and a fracture network system. Matrix system has a high storage capacity and a low permeability, while fracture network system has a low storage capacity and high permeability (Pirson, 1953; Barenblatt, 1960; Reiss, 1980; Van Golf-Racht, 1982). In a fractured reservoir, matrix elements are separated with fractures, which may be closed and cemented or having flow channels in them, as shown in Figure 1.1 (Reiss, 1980).

In fractured reservoirs, when oil saturated matrix is fully or partially surrounded by gas and/or water in the fracture, displacement process takes place (Van Golf-Racht, 1982). Fractures play a role in the transmission of oil in the matrix to the producing wells with their high permeability and low porosity. Main oil recovery mechanisms in fractured reservoirs are fluid expansion, pore volume contraction, combined effects of gravity forces and capillary forces (i.e. gravity drainage, capillary imbibitions), convection and diffusion (Reiss, 1980).

In fractured reservoirs, during primary production stage, most of the oil is produced from fractures and a lot of oil still remains in the matrix system. Gas injection, which activates gas oil gravity drainage mechanism, is an efficient way of producing oil remaining in the matrix till gravitational and capillary forces become equal. Molecular diffusion also plays an important role in oil recovery in

fractured reservoirs, especially when gravity drainage is not very effective due to low permeability of matrix, high capillary pressure and small sizes of matrix blocks (Kazemi and Jamialahmadi, 2009).

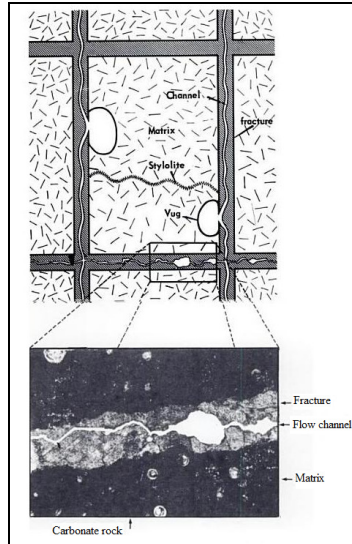


Figure 1. 1. Matrix - Fracture Network System with Flow Channels (Reiss, 1980)

Results of experimental studies carried out with fractured systems, particularly, at the reservoir conditions are key sources to understand the main parameters and processes that affect recovery mechanisms. From this point of view, the main objective in this study is to investigate matrix fracture interaction mechanisms by conducting an experimental study using a fractured sandstone core system. Gas oil gravity drainage and diffusion mechanisms are studied by introducing CO_2 , N_2 and CH_4 gases to the system and obtaining corresponding oil recovery values with time. Effects of type of injected gas, initial gas saturation and diffusion coefficient are investigated. A simulation study is also carried out to compare experimental results and to understand main recovery mechanisms.

CHAPTER 2

THEORY

2.1. Gas Oil Gravity Drainage (GOGD) in Fractured Reservoirs

Gravity drainage is a process that occurs due to the density difference of fluids in the reservoir. Before the discovery of a reservoir, reservoir fluids are originally separated into layers as gas, oil and water with depth. This is an evidence of the effect of the gravity (Muskat, 1981; Cole, 1969). Furthermore, in order to maintain the density equilibrium, reservoir fluids may move through the reservoir rock by gravitational forces acting on them, i.e. gas moves upward, while oil moves downward providing oil production from deeper wells (Calhoun, 1955; Cole, 1969).

Gravity drainage is one of the reservoir drive mechanisms, which provides the natural energy needed for oil production and which could be the reason of significant oil recoveries greater than 80 % of the initial oil in place (Cole, 1969; Ahmed and McKinney, 2005). Oil production by gravity drainage may be originated from a gas cap existing in the reservoir or an expanding gas cap developed with the pressure decline during the production. If there is an expansion of an original gas cap in the reservoir or if there is a gas cap originated from gas injection at the crest of the reservoir, no solution gas from the oil zone will move to the gas cap. The process can be named as “segregation drive without counterflow”. On the other hand, if a counterflow of oil and gas within the oil zone occurs as a result of the density difference between oil and gas, produced oil will be replaced with solution gas, resulting in “segregation drive with

counterflow” (Pirson, 1958). This process does not necessarily include a gas cap occurred originally in the reservoir and generally involve vertical fracture systems and high permeability (Pirson, 1958).

There are several conditions favor gravity drainage such as high formation dips, low oil viscosities, high permeabilities to oil and high gradients of density (Calhoun, 1955; Cole, 1969). For efficient production under gravity drainage drive, considering the dip direction and locating wells at lower depths and limiting producing rates to the gravity drainage rate will be beneficial. Maintaining reservoir pressure by gas injection also results in producing oil more rapidly (Lewis, 1944). Process of oil production under gravity drainage drive in the direction of the reservoir dip in a conventional reservoir is shown in Figure 2.1 (Cole, 1969, Ahmed and McKinney, 2005).

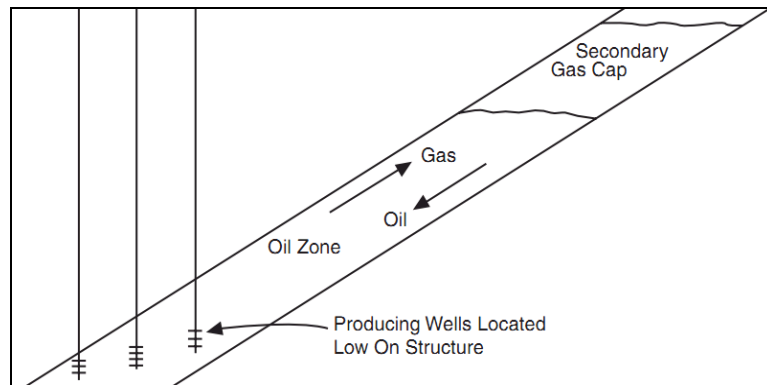


Figure 2. 1. Process of Oil Production under Gravity Drainage Drive in a Conventional Reservoir (Cole, 1969; Ahmed and McKinney, 2005)

Gravity drainage mechanisms in reservoirs may be classified as processes with pressure maintenance provided by gas injection into the gas cap and processes with declining pressure (Hall, 1961). Figure 2.2 shows a cross section of a conventional gravity drainage reservoir with an originally present gas cap and its oil saturation profile at the beginning of the gas oil gravity drainage process. In the constant pressure maintenance gravity drainage, pressure gradient in the oil column, which reaches a stable value after a certain period of time, makes the oil drain downstructure and the location of the gas-oil contact changes as shown in Figure 2.3 (a). Oil is produced due to frontal-type displacement (Hall, 1961). On the other hand, in the declining pressure gravity drainage, there is not gas injection into the gas cap or the amount of the injected gas is not sufficient. With time, pressure declines to the bubble point pressure and free gas moves upward while oil moves downward as shown in Figure 2.3 (b) (Hall, 1961).

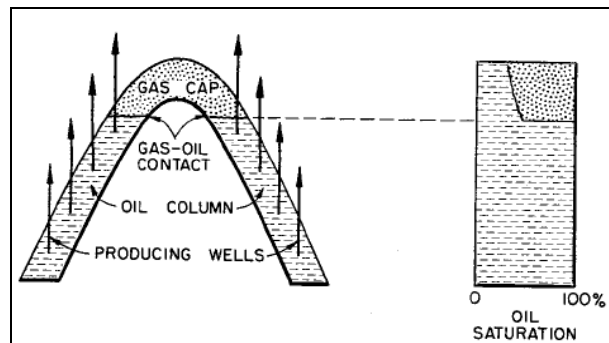


Figure 2. 2. Cross Section of a Conventional Gravity Drainage Reservoir and its Oil Saturation Profile (Hall, 1961)

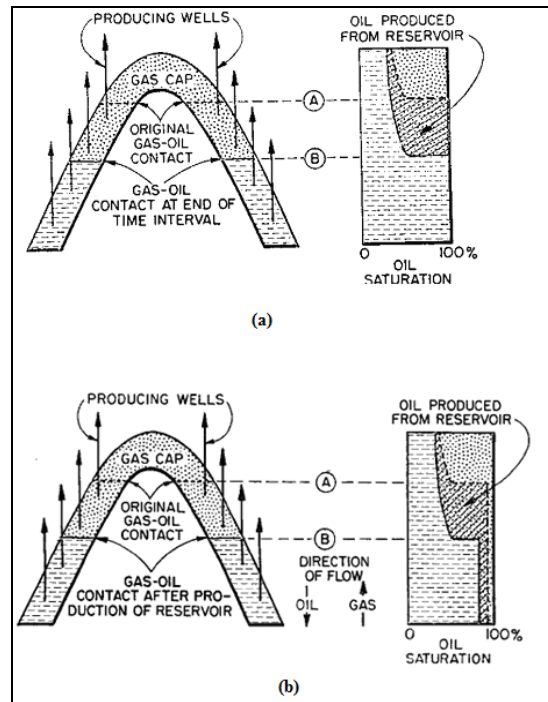


Figure 2. 3. A Conventional Reservoir with (a) Constant Pressure Maintenance Gravity Drainage (b) Declining Pressure Gravity Drainage (Hall, 1961)

Gravity drainage may also be classified as forced gravity drainage, free-fall gravity drainage and simulated gravity drainage (Saidi, 1987; Schechter and Guo, 1996). Forced gravity drainage is a process that occurs due to gas injection into steeply dipping reservoirs with a controlled flow rate. Free-fall gravity drainage, on the other hand, occurs in naturally fractured reservoirs after pressure decline in fractures or gas injection into fractures (Schechter and Guo, 1996). In free-fall gravity drainage, oil production is only obtained by gravity forces and oil production rate may not be economical enough to compensate the expenses of the recovery process and gives rise to the need of enhanced oil recovery activities (Zendehboudi, Mohammadzadeh and Chatzis, 2009). In laboratory applications, if gas is injected from the top of a porous block and oil is produced from the bottom

at a given pressure, the process obtained is free fall gravity drainage. On the other hand, if the top and bottom of the porous medium are connected with a by-pass tube, which includes injected gas, the production mechanism obtained is classified as forced gravity drainage (Saidi, 1987). Simulated gravity drainage is only obtained with centrifuging application at laboratory environment artificially (Schechter and Guo, 1996).

In fractured reservoirs, gas from the fracture network system displaces oil in the matrix surrounded by fractures. In the gas oil gravity drainage mechanism, gravity forces and capillary forces play a significant role. Gas oil gravity drainage occurs when gravity forces exceed capillary forces. Density difference between gas and oil and elevation difference between interfaces of oil and gas in matrix and fracture are significant characteristics that affect gravity drainage process in fractured reservoirs (Sajadian and Danesh, 1998; Zahra and Fariborz, 2009; Zendehboudi, Mohammadzadeh and Chatzis, 2009). Capillary continuity and matrix block height plays important roles in oil recovery by gravity drainage (Fung, 1991, Zahra and Fariborz, 2009).

During gas oil gravity drainage process in fractured reservoirs, different zones occur, namely; a zone where matrix is saturated with oil, while fracture contains gas; an oil rim zone where both matrix and fracture are filled with oil and a zone where fracture is filled with water, while matrix has oil, as shown in Figure 2.4 (Clemens and Wit, 2001). Oil in matrix flows to the oil rim zone and to the fractures, through where it is transmitted to the production wells (Clemens and Wit, 2001). With the decline of reservoir pressure due to production, elevation of the gas oil contact in the fracture moves below the elevation of gas oil contact in the matrix, resulting in an increase in the proportion of matrix zone that is surrounded by gas and resulting in gravity drainage (Sajadian and Danesh, 1998). Figure 2.5 presents the schematic of the fractured reservoir described with different zones in the model DFRAC developed to model recovery mechanisms at

different depths by FRANLAB Company (Reiss, 1980; Reiss et al. 1973). In the model, different zones are simulated with mechanisms of single phase oil expansion, oil and gas expansion with and without two-phase flow below and above bubble point pressure and critical gas saturation in the matrix and gravity drainage where matrix blocks are surrounded by gas in the fracture (Reiss et al. 1973; Reiss, 1980).

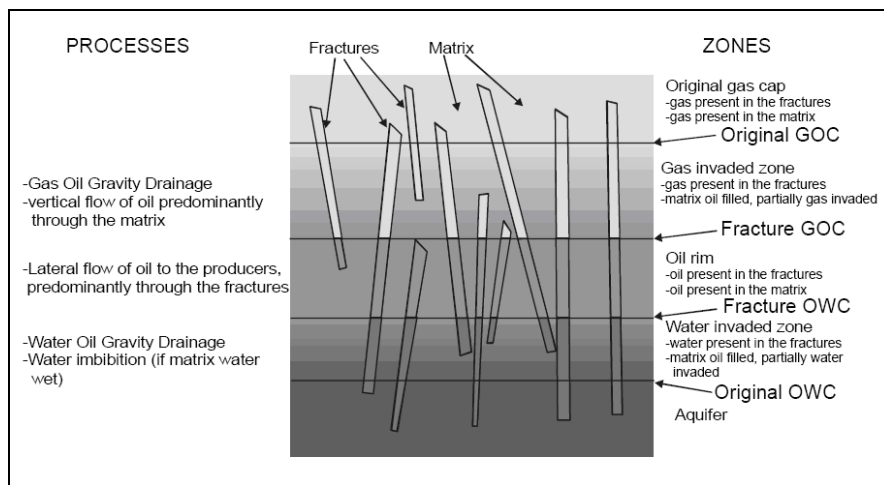


Figure 2. 4. Processes and Zones during Gas Oil Gravity Drainage in Fractured Reservoirs (Clemens and Wit, 2001).

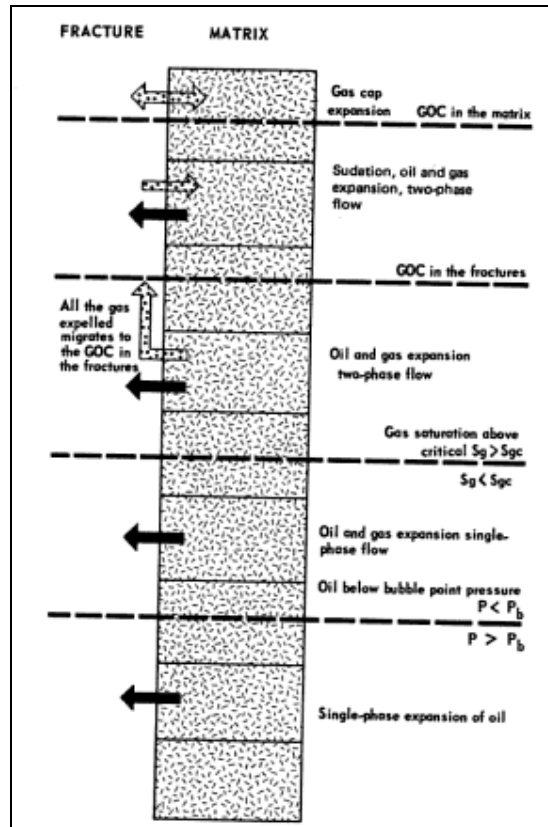


Figure 2. 5. Schematic of the fractured reservoir described in the model DFRAC by FRANLAB Company (Reiss, 1980; Reiss et al. 1973).

2.1.1. Governing Equations of Gas-Oil Gravity Drainage Mechanism

Unlike conventional reservoirs, naturally fractured reservoirs contain different porosity systems of matrix and fracture, in which, matrix has higher storage capacity and low flowing capability, while fractures and fissures have less storage capacity but higher permeability (Pirson, 1953; Barenblatt, 1960; Reiss, 1980; Van Golf-Racht, 1982). In order to understand the main mechanisms dominated between fracture and matrix system, double porosity models are developed to idealize heterogeneous systems of fractures. Warren and Root (1963) developed a

model shown geometrically shown in Figure 2.6, which presents the fracture system as orthogonal, uniform spacing between the identical blocks of the matrix system. In the model, it is assumed that flow is between matrix blocks and fractures through fracture network and there is no flow between matrix blocks, matrix blocks feed fracture continuously. Flow in fractures is unsteady state, while it is quasi-steady state in matrix blocks (Warren and Root, 1963).

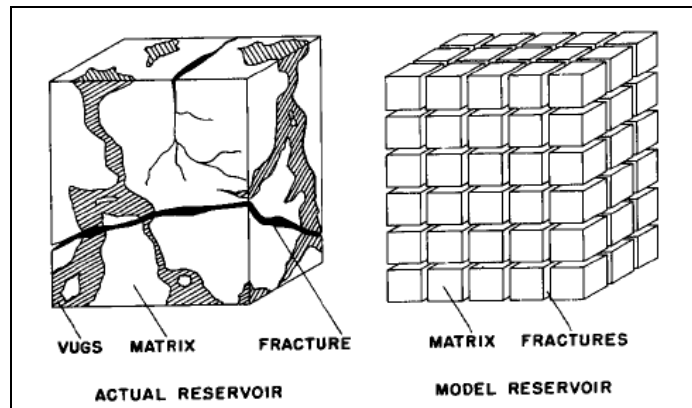


Figure 2. 6. Double Porosity Model Developed by Warren and Root (1963)

In the study of Kazemi et al. (1969), flow equations developed for single phase flow by Warren and Root (1963) are studied further for two phase flow and finite difference solution of these equations are provided. A mass balance on an elemental volume of Warren and Root's model is considered for the flow in fracture and matrix systems, Darcy's law is assumed to be applicable and the following flow equations are presented (Kazemi et al., 1969):

For fracture flow (Kazemi et al., 1969);

$$\begin{aligned} \nabla \cdot \left[\chi_{\alpha f} \rho_{\alpha} \left(\nabla \psi_{\alpha f} - \frac{1}{144} \nabla D_f \right) \right] - \left[T_{\alpha ma} (S_{\alpha ma}) (\psi_{\alpha f} - \psi_{\alpha ma}) \right] \\ + q_{\alpha} \delta (X - X_0) = \frac{1}{5.6146} \frac{\partial}{\partial t} (\phi_f S_{\alpha f} / B_{\alpha f}) \end{aligned} \quad (2.1)$$

For flow in matrix (Kazemi et al., 1969);

$$T_{\alpha ma} (S_{\alpha ma}) \rho_{\alpha} (\psi_{\alpha f} - \psi_{\alpha ma}) = \frac{1}{5.6146} \frac{\partial}{\partial t} (\phi_{ma} S_{ma} / B_{\alpha ma}) \quad (2.2)$$

where

$\chi_{\alpha f}$: mobility coefficient of phase α in fracture, md/cp/ (RB/STB)

ρ : phase density, lb_m/ cu ft

ψ : defined in Equation 2.6, psi/(lb_m/ cu ft)

D: depth measured from datum plane, positive downward, ft

$T_{\alpha ma}$: matrix transmissibility coefficient, md/cp/sq ft (RB/STB)

$S_{\alpha ma}$: saturation of phase α in matrix, fraction

q: flow rate, STB/D

X=(x,y,z)= coordinates of a point

$X_0 = (x_0, y_0, z_0)$ = coordinates of production or injection wells

$\delta (X - X_0)$: Dirac-delta function=1 for X= X_0 , 0 otherwise

t: time, days

ϕ : fracture porosity, fraction of the bulk rock volume

B: formation volume factor, RB/ STB

$S_{\alpha f}$: saturation of phase α in fracture, fraction

α : index, w: wetting phase, nw: nonwetting phase

f: fracture; m. matrix

Mobility coefficient of phase α in fracture, $\chi_{\alpha f}$ (Kazemi et al., 1969);

$$\chi_{\alpha f} = 0.0011271 \left(\frac{k k_{\alpha r}}{\mu_{\alpha} B_{\alpha}} \right)_f \quad (2.3)$$

where

k: absolute permeability, md

k_r : relative permeability

μ : viscosity, cp

Matrix transmissibility coefficient for phase α , $T_{\alpha ma}$ (Kazemi et al., 1969);

$$T_{\alpha ma} (S_{\alpha ma}) = 0.0011271 \left(\frac{k k_{\alpha r}}{\mu_{\alpha} B_{\alpha}} \right)_{ma} \sigma \quad (2.4)$$

where σ is shape factor, ft^{-2} .

Shape factor is described as follows by Warren and Root (1963);

$$\sigma = 4N(N+2) / L^2 \quad (2.5)$$

where N is number of normal sets of fractures.

and,

$$\psi_{\alpha} = \int_{P_o}^P \frac{dP_{\alpha}}{\rho(P_{\alpha})} \quad (2.6)$$

where P is pressure, psi.

Capillary pressure and constraint equations are also presented.

Constraint equations:

$$S_{wf} + S_{nwf} = 1 \quad (2.7)$$

$$S_{wma} + S_{nwma} = 1 \quad (2.8)$$

Capillary pressure equations:

$$P_{nwf} - P_{wf} = P_{cf}(S_{wf}) \quad (2.9)$$

$$P_{nwma} - P_{wma} = P_{cma}(S_{wma}) \quad (2.10)$$

where P_c is capillary pressure, psi.

Considering that $B \propto 1/\rho$ for undersaturated oil and water; following equations are obtained (Kazemi et al., 1969):

For matrix blocks:

$$\begin{aligned} \nabla \cdot [\lambda_{\alpha f} \nabla \Phi_{\alpha f}] - [T_{ama}(S_{ama})(\Phi_{\alpha f} - \Phi_{ama})] \\ + q_{\alpha} \delta(X - X_0) = \frac{1}{5.6146} \{ (S_{\alpha f} / B_{\alpha}) [(\phi_f c_{\phi f} + \phi_f c_{\alpha}) \frac{\partial P_{\alpha f}}{\partial t} + \frac{\phi_f}{B_{\alpha}} \frac{\partial S_{\alpha f}}{\partial t}] \} \end{aligned} \quad (2.11)$$

where Φ : potential, psi; c: compressibility, psi⁻¹

$$\Phi_{\alpha f} = P_{\alpha f} - \rho_{\alpha} D / 144 \quad (2.12)$$

$$\Phi_{ama} = P_{ama} - \rho_{\alpha} D / 144 \quad (2.13)$$

For fracture system:

$$\begin{aligned}
 & T_{\alpha ma} (S_{\alpha ma}) \rho_{\alpha} (\Phi_{\alpha f} - \Phi_{\alpha ma}) \\
 &= \frac{1}{5.6146} \frac{\partial}{\partial t} \{ (S_{\alpha ma} / B_{\alpha}) [(\phi_{ma} c_{\phi ma} + \phi_{ma} c_{\alpha}) \frac{\partial \Phi_{\alpha ma}}{\partial t} + \frac{P_{ma}}{B_{\alpha}} \frac{\partial S_{\alpha ma}}{\partial t}] \}
 \end{aligned} \tag{2.14}$$

Flow equations for matrix and fracture are presented in finite difference form (Kazemi et al., 1976; Thomas et al, 1983; Ladron de Guevara Torres et al., 2007). For 3 phase, 3-D flow, following flow equations are obtained as follows (Thomas et al, 1983):

Fracture flow:

Water:

$$\Delta [\tau_w (\Delta P_w - \gamma_w \Delta D)] + \lambda_w (P_{wm} - P_w) - q_w = \frac{V_b}{\Delta t} \wp (\phi b_w S_w) \tag{2.15}$$

Oil:

$$\Delta [\tau_o (\Delta P_o - \gamma_o \Delta D)] + \lambda_o (P_{om} - P_o) - q_o = \frac{V_b}{\Delta t} \wp (\phi b_o S_o) \tag{2.16}$$

Gas:

$$\begin{aligned}
 & \Delta [\tau_g (\Delta P_g - \gamma_g \Delta D)] + \lambda_g (P_{gm} - P_g) + \Delta [\tau_o R_s (\Delta P_o - \gamma_o \Delta D)] \\
 & + \lambda_o R_s (P_{om} - P_o) - q_g = \frac{V_b}{\Delta t} \wp (\phi b_g S_g + \phi b_o R_s S_o)
 \end{aligned} \tag{2.17}$$

Matrix- Fracture Flow:

Water:

$$-\lambda_w (P_{wm} - P_w) = \frac{V_b}{\Delta t} \wp (\phi b_w S_w)_m \tag{2.18}$$

Oil:

$$-\lambda_o (P_{om} - P_o) = \frac{V_b}{\Delta t} \gamma \rho (\phi b_o S_o)_m \quad (2.19)$$

Gas:

$$-\lambda_g (P_{gm} - P_g) - \lambda_o R_s (P_{om} - P_o) = \frac{V_b}{\Delta t} \gamma \rho (\phi b_g S_g + \phi b_o R_s S_o) \quad (2.20)$$

where

τ : fracture transmissibility, 0.001127 (kA/L) b k_r/μ , STB/D-psi

A: area, sq ft

D: depth measured, ft (positive downward)

L: length, ft

b: 1/B, inverse of formation volume factor, STB/RB or /scf/ RB

γ : specific weight, psi/ ft

λ : matrix-fracture transmissibility, STB/D-psi

V_b : bulk volume, res bbl

ρ : time step difference, $\rho = \rho_{x=x_{n+1}} - \rho_{x=x_n}$

R_s : solution gas oil ratio, scf/ STB

Matrix- fracture transmissibility, λ is defined as;

$$\lambda = 0.001127 \sigma k_r \left(\frac{kV_b}{B\mu} \right)_m \quad (2.21)$$

Also,

$$S_w + S_o + S_g = 1 \quad (2.22)$$

$$P_{cwo} = P_o - P_w \quad (2.23)$$

$$P_{cgo} = P_g - P_o \quad (2.24)$$

2.2. Diffusion in Naturally Fractured Reservoirs

Molecular diffusion is one of the recovery mechanisms of naturally fractured reservoirs, which gains importance especially in small matrix blocks with low permeability (Kazemi and Jamialahmadi, 2009; Chordia and Trivedi, 2010). Molecular diffusion in fractured reservoirs can be described as random motion of molecules due to different concentrations of components in matrix and fracture (da Silva and Belery, 1989; Yanze and Clemens, 2011). Combination of diffusion and convection, which is due to local differences of bulk velocity resulted from medium heterogeneity, is defined as dispersion (da Silva and Belery, 1989).

There are many different aspects of diffusion in fractured reservoirs. Gas in the gas phase or gas in the oil phase in the fracture may diffuse into the oil phase in the matrix as well as into the gas phase in the matrix (Spivak et al., 1989). Efficiency of the diffusion process directly depends on fracture spacing, fracture intensity and diffusion coefficients, which determine the rate of diffusion (Spivak et al., 1989).

In matrix fracture interaction processes, diffusion of gas from saturated fracture to undersaturated matrix block and a pressure gradient across the matrix block may be a reason of matrix fracture flow as well as gravity, capillary and viscous forces. With the addition of diffusion term in the equations, following expression for matrix-fracture interaction can be presented (Thomas et al, 1983):

$$q_{wmf} = \lambda_w (P_{wm} - P_w) + \lambda_w \frac{L_c}{L_B} \Delta P_{wf} \quad (2.22)$$

$$q_{omf} = \lambda_o (P_{om} - P_o) + \lambda_o \frac{L_c}{L_B} \Delta P_{of} \quad (2.23)$$

$$q_{gmf} = \lambda_g (P_{gm} - P_g) + \lambda_g \frac{L_c}{L_B} \Delta P_{gf} + \lambda_o R_s (P_{om} - P_o) + \lambda_o R_s \frac{L_c}{L_B} \Delta P_{of} + \lambda_{gD} (b_o R_{sm} - b_o R_{sf}) \quad (2.24)$$

where

ΔP : pressure drop across matrix block

L_B : distance ΔP acts

L_C : characteristic length for matrix-fracture flow

D : diffusion coefficient

and,

$$\lambda_{gD} = \frac{\sigma V_b S_{gf} D}{5.615} \quad (2.25)$$

Diffusion coefficient can be defined as a measure indicating the speed of penetration of a component's molecules into another component when there is a contact between them (Saidi, 1987). Pressure, temperature, concentration and interfacial tension in between the components have effects on diffusion coefficients. As temperature increases, diffusion coefficient also increases, while an increase in pressure results in a decrease in diffusion coefficient in hydrocarbon systems. In porous media, since there are variable contact areas and longer flow paths for diffusing molecules as well as throats and wide pore areas, there is a decrease in the diffusion coefficient although diffusion process remains the same (Saidi, 1987). To account for these effects, a diffusion coefficient is defined for porous media, namely, effective diffusion coefficient, D_e , which is smaller than diffusion coefficient in pure liquids rather than in porous medium. Effective diffusion coefficient in porous media increases with increasing porosity and decreasing ratio of flow path length to the length of porous media sample

(Domenico and Schwartz, 1998). When velocity is involved in the flow of molecules, effective diffusion coefficients are termed as dispersion coefficients, which are directional properties, such as longitudinal (parallel to the flow direction) and transversal (perpendicular to the flow direction) (Saidi, 1987).

Different experimental studies for the estimation of effective diffusion coefficient are carried out involving direct methods in which compositional analysis is used and indirect methods in which change in some parameters such as rate of solution volume change, pressure drop in a confined cell and level of gas-liquid interface are investigated and a correlation between these changes and diffusion coefficient is made instead of compositional analysis (Chordia and Trivedi, 2010; Hoteit, 2011).

During the diffusion process of gas in the fracture into the matrix, firstly, oil at the matrix-fracture interface becomes fully saturated with gas in the fracture and later on gas in the fracture continuously diffuses across the matrix- fracture contact area with a decreasing dissolved gas concentration profile from the fracture to the centre of the matrix block. As the gas in the fracture diffuses into the oil in the matrix, oil in the matrix swells as it gets more saturated with gas and some of the oil in the matrix expels into the fracture (Sener, 1986). Models describing diffusion process are mostly based on Fick's first law of diffusion (Chordia and Trivedi, 2010; Hoteit, 2011).

In one dimensional flow, diffusion flux J for the molecular diffusion of gas in fracture into oil in matrix by Fick's first law of diffusion, where dispersion is taken as not present in the case (Sener, 1986; Bird, 2002):

$$J = -D_e \frac{\partial C}{\partial x} \quad (2.25)$$

where

J: molecular mass flux; mass flow rate of gas per unit area across which diffusion takes place

D_e : effective diffusion coefficient of gas in matrix porous media

C: concentration of dissolved gas in matrix oil

With the combination of equations of continuity and Fick's first law of diffusion, Fick's second law of diffusion is obtained, which presents the relation between diffusion and concentration change with respect to time (Saidi, 1987; Sharma, 2007):

$$D_e \frac{\partial C}{\partial x^2} = \frac{\partial C}{\partial t} \quad (2.26)$$

where t: time

2.3. Miscibility Considerations

Displacement of a fluid in a reservoir with another fluid may be either an immiscible or a miscible process. If two fluids do not mix in all proportions to form a single phase fluid, these fluids are classified as immiscible. Immiscible fluids exhibit two different phases separated with an interface (Green and Willhite, 1998). In immiscible displacement of oil with gas injection, main recovery mechanisms include reduction in oil viscosity, oil swelling, reduction in interfacial tension, solution gas drive and vaporization and extraction in a limited amount (Lake, 1989). During CO₂ injection into crude oil systems, CO₂ dissolves in oil, resulting in an increase in the liquid volume and causing oil swelling (Simon and Graue, 1965; Holm and Josendal, 1974). Swelling factor, which is defined as the ratio of the volume of oil and dissolved CO₂ to the volume of oil without CO₂ is dependent on dissolved CO₂ amount and size of oil molecules.

Figure 2.7 represents swelling factor values for different dissolved CO₂ mole fraction and oil molecular size (Simon and Graue, 1965). Moreover, CO₂ has a high solubility at certain reservoir pressure values and when CO₂ dissolves in oil, an expansion of about 10 to 60 % of that oil occurs as well as a reduction in the viscosity of oil around 5 to 10 times before (Holm, 1982). Another recovery mechanism is that light components of hydrocarbon are extracted into CO₂ (Holm and Josendal, 1974, Bank et al., 2007).

If two fluids mix in all proportions and remain as a single phase, they are miscible. Some injection fluids that mix directly with reservoir fluids on first contact are called as first-contact miscible. Some injection fluids, on the other hand, form two phases when they mixed with reservoir fluids; including a transition phase ranging from oil to injection fluid composition. This type of miscibility that is occurred due to repeated contact of fluids is called as multiple contact or dynamic miscibility (Stalkup Jr., 1983).

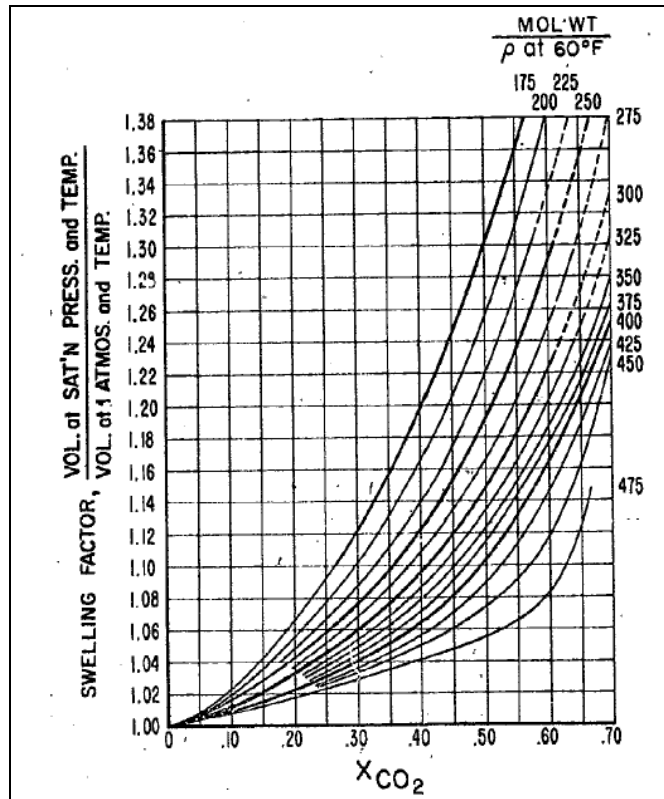


Figure 2. 7. Swelling Factor Values for Different Dissolved CO₂ Mole Fraction and Oil Molecular Size

Miscible displacement is only obtained at pressure values which are greater than a specific pressure value, called Minimum Miscibility Pressure (MMP) (Lake, 1989). Minimum miscibility pressure (MMP) value is obtained by Slim-Tube displacement tests that are conducted with sand packs in very small diameter tubes at constant temperature. Successively increasing pressure values are applied with gas injection into oil saturated sample and recovery values are obtained. From the recovery versus pressure curves, it is observed that there is an increase in the recovery with pressure up to a point and later on stabilization in recovery with pressure is achieved. The pressure value where the slope of the curve

changed sharply is indicated as Minimum Miscibility Pressure (MMP) (Lake, 1989; Latil et al., 1980). Figure 2.8 illustrates an example of the results of a slim tube experiment showing the recovery values at various test pressures at 1.2 pore volume (PV) of CO₂ injection for the test oil and at constant temperature (Yellig and Metcalfe, 1980). In pressure-composition (P-X) diagrams, saturation pressures versus mole fraction of one of the phases are indicated and miscibility relationships can be obtained. Figure 2.9 shows an example of P-X diagrams for CO₂-butane and CO₂-ndecane systems at 71 °C. Critical points designated by letter C on the plot indicate the points where liquid and gas phases are identical (Orr Jr. and Jensen, 1984).

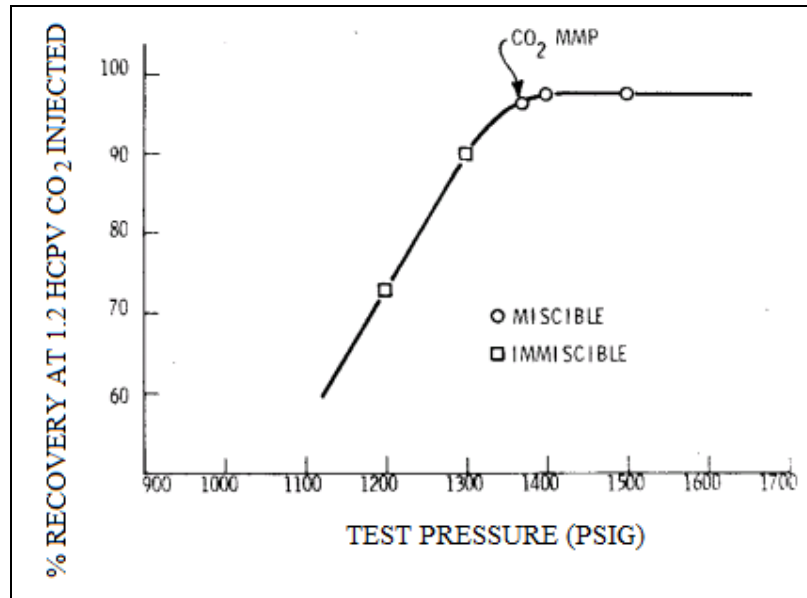


Figure 2. 8. Recovery versus Pressure Curve obtained from Slim-Tube Experiments for MMP Determination (Yellig and Metcalfe, 1980)

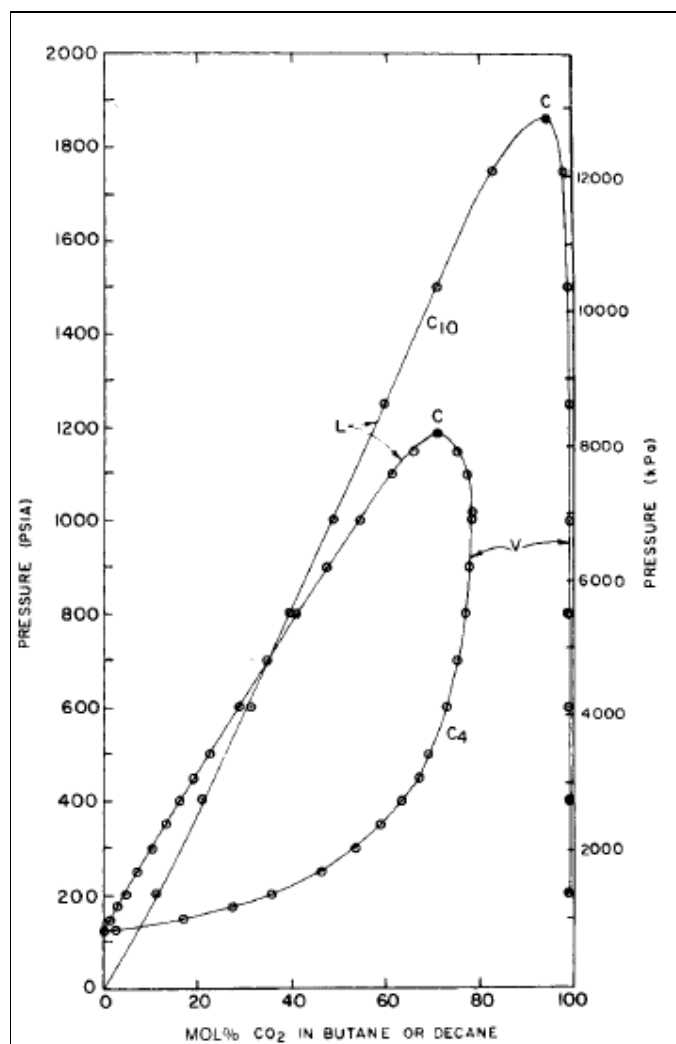


Figure 2. 9. P-X diagrams for CO₂-butane and CO₂-ndecane systems at 71 °C (Orr Jr. and Jensen, 1984)

CHAPTER 3

PREVIOUS EXPERIMENTAL AND SIMULATION WORK

In literature, there are significant studies reported considering matrix-fracture interaction and production mechanisms in fractured reservoirs as well as gas injection processes for the purpose of enhancing oil recovery. These studies include experimental work as well as modeling and numerical simulation studies.

3.1. Experimental Studies Carried Out On Matrix-Fracture Interaction, Gas-Oil Gravity Drainage and Gas Injection Processes

Chatzis et al. (1988) carried out an experimental study to investigate gravity drainage processes during the inert gas injection. Square capillary tubes of different sizes of 500 μ and smaller are used as well as 1.2 m long Berea sandstones in gravity drainage experiments performing air and nitrogen injection. Computerized tomography is used to identify fluid distributions and oil zone and transition zone during inert gas injection gravity drainage. It is concluded that production rate of gravity drainage is both dependent on the capillary diameter and kinematic viscosity of drained fluid. In Berea sandstone experiments, waterflooded core is subjected to nitrogen injection at a rate of 5 psi from the top and 40 % of residual oil is obtained to be produced after 1000 hours.

Denoyelle et al. (1988) studied effectiveness of a fractured carbonate reservoir to apply CO₂ and CO₂- N₂ gases for enhanced oil recovery. Besides, field scale characterization and injection tests, laboratory studies are also conducted. 2 m long, oil saturated sand packs and reservoir cores are used during CO₂, CO₂- N₂

mixture and pure N₂ injection at reservoir pressure and temperature. A higher amount of oil recovery is obtained during CO₂ injection compared to CO₂- N₂ mixture and pure N₂ injection and it is concluded that with continuous CO₂ injection, higher amounts of oil recovery is obtained than waterflood tests carried out with the reservoir cores.

In the study of Gümrah (1988), oil recovery during CO₂, steam and CO₂-steam flooding into limestone linear and three dimensional models is investigated. Effects of injection pressure are considered and recovery and steam front movements are examined. Cyclic and continuous CO₂ injection experiments are performed and cyclic CO₂ injection is considered to be more efficient than continuous CO₂ injection for heavy oil recovery for the conditions of experiments.

Sadaghiani (1992) studied the effects of CO₂ on the physical properties of Garzan crude oil (24 °API) with an experimental study containing a PVT set-up. Properties such as viscosity, density, bubble point pressure, gas-oil ratio, liquid compressibility and formation volume factor are investigated by providing bottom hole conditions combining crude oil with natural gas and different CO₂ concentrations. It is concluded that increase in the formation volume factor, reduction in viscosity and stripping effect are more significant with CO₂ than obtained with natural gas.

The objective of the study of Sumnu et al. (1994) is to study matrix-fracture transfer function for steam injection and experimental design parameters by using fine grid simulation results to develop a 3-D matrix-fracture model. Sumnu et al. (1996) also aim at obtaining fluid transfer between matrix and fracture during continuous and cyclic steam injection. An X-ray transparent plastic core holder is used that contains a rectangular sandstone Boise core and a fracture is formed between the core and the core holder. Thermocouples are used to measure temperature in the fracture and matrix and heat flux sensors are used to determine

heat losses from the system during steam injection. In the steam injection experiments, steam is injected into 100 % water saturated core and effect of different steam injection rates, back pressures and injection temperatures are investigated. Steam saturations in fracture and matrix is obtained by using a CT scanner and it is concluded that there is not steam saturation in the matrix and conduction is dominant in heat transfer.

In the study of Mangalsingh and Jagai (1996), an experimental work is carried out to investigate CO₂ immiscible displacement by using the continuous injection method and water alternating gas (WAG) method. The experimental set-up contains a core holder, an injection system and a production system. Unconsolidated cores are prepared by using Silica sand and sand core is 100 % saturated with water. Then, crude oil is injected and continuous CO₂ injection, water alternate CO₂ injection, waterflood and WAG on waterflooded core methods are applied. Gas production and volumes of oil and water are measured. 16 °API to 29 °API crude oils are used and different CO₂ injection rates are maintained. It is observed that WAG recoveries are higher than recoveries obtained from CO₂ continuous injection.

The study of Sajadian and Danesh (1998) includes an experimental study that is carried out to identify the main parameters affecting the capillary continuity between matrix blocks in reservoir conditions. A stack of a glass beads pack over a dead block and stack of 2 outcrop sandstone cores used. Porous and non-porous spacers of different thickness are artificially constructed. Synthetic oil is employed and air is used as the gas phase. It is stated that there exists a critical fracture thickness, t_{cf}, which is the maximum value of fracture thickness that retains a stable liquid bridge.

In the study of Rangel-German et al. (1999), both an experimental and numerical simulation study is carried out to understand the flow processes in fractured

media. Water-air imbibition and oil-water drainage displacements in fractured sandstones are investigated by using an 8 % NaBr brine solution as wetting phase, and decane as the nonwetting phase. Saturation distributions along the core are obtained by using a Computerized Tomography (CT) scanner and rate and pressure distributions are also determined. Two blocks are placed together in the first core holder design, while in the second design; there is a 1 mm thick spacer to create a fracture. By using a commercial reservoir simulator, experimental results are matched and the effect of fracture relative permeability, matrix-fracture capillary pressure and fracture width is obtained.

Hujun et al. (2000) also investigated oil recovery efficiency of waterflooded naturally fractured reservoirs, followed by gas injection experimentally in their study. In the experiments, actual case of waterflooding and CO₂ gravity drainage in Spraberry trend Area in USA is provided. Effects of permeability, initial water saturation and injection schemes are investigated during the experiments. Gas chromatography is used to analyze the produced samples. Artificially fractured Berea cores and Spraberry core are used along with synthetic brine and dead Spraberry oil in the experiments. Berea cores used are 24.45 cm and 48.74 cm in length and 10.16 cm in diameter. The experimental setup, which is placed in an oven at reservoir temperature of 58.9 °C, consists of a core holder, produced fluids container, back pressure regulator, pump, CO₂ and brine source, and separator. CO₂ gravity drainage process is conducted at reservoir temperature for 38 days after water injection by CO₂ injection vertically from the top. It is concluded that CO₂ gravity drainage after water injection is an efficient method of enhanced oil recovery. It is observed that during CO₂ gravity drainage, produced oil results in increased concentrations of components C₁₁- C₂₀, indicating significant extraction by CO₂. According to the results of the experiments, it is observed that lower initial water saturation before CO₂ injection yields higher oil recovery.

In the experimental study carried at the Petroleum Research Centre at Middle East Technical University (METU) (2001), an artificial fracture is provided by fixing the core at the center of the core holder. A 2 mm fracture is created between the walls of the model and the core. Heat flow sensors are used to measure the heat flow from the core to the fracture and from the steam in the fracture to the core. Moreover, a thermocouple is used to measure the temperature of the steam in the fracture between the surface of the core and the wall of the core holder. There are also inlet and outlet ways to inject steam to the fracture and produce oil and water from the system. The fractured core system is placed on the CT table and a data logger is used to record data.

In the study of Oedai and van Wunnik (2002), the recovery of remaining oil in a sandstone reservoir by an immiscible gas injection that has undergone a waterflood is considered. Gas-oil gravity drainage potential is investigated by using partly oil and water filled plugs. After aging, plugs are waterflooded followed by an oil flood and then drained in air. Dead crude oil is used in the experiments, which are run at atmospheric pressure and 60°C. Gas (air) drainage of aged plugs at connate water saturation (OG experiments), gas drainage of waterflooded plugs (OWG experiments) and gas drainage of oil re-saturated water flooded plugs (OWOG experiments) are performed. After the study, it is concluded that residual oil saturation for GOGD is lower than that is obtained for waterflooding and waterflooding before GOGD also increases the residual oil saturation slightly.

Another study that is investigating the effects of steam injection and together with CO₂ and CH₄ is conducted by Bagci and Gumrah (2004). In the study, effects of simultaneous injection of steam and CO₂ and CH₄ at different flow rates, different injection temperatures and different CO₂-steam ratios are investigated. Heavy oil (12.4 °API) is mixed with unconsolidated limestone and 1-D and 3-D models are used to obtain recovery. Optimum gas/ steam ratios are determined for both of the

models. It is concluded that by gas-steam injection lower residual oil recoveries are obtained than the ones obtained with only steam injection.

Rao et al. (2004) studied gas assisted gravity drainage (GAGD) process and carried out an experimental study with glass bed packs constituting a porosity value of 0.39 and a permeability value of 10 Darcy to identify free fall gravity drainage mechanism. Oil recovery results are obtained and two intervals are observed on the recovery versus time plot in which at first there is a sharp increase in oil production while in the second interval there is 2 phase flow of oil and gas together resulting in a lower oil production rate. In another part of the study, immiscible CO₂ injection is performed to Berea cores of 6 ft to observe GAGD process and it is concluded that highest amount of recovery is obtained during GAGD than continuous injection or water alternating gas (WAG) processes, especially in long core lengths.

Ayatollahi et al. (2005) studied effect of wettability on GOGD process with an experimental study. Experiments are conducted by using water-wet, oil-wet and 50 % water-wet- 50 % oil-wet sand packs, which are waterflooded first. Free fall gravity drainage is provided by opening valves at the top and at the bottom of the system and oil recovery is recorded for a period of 2 months. Highest amount of tertiary oil recovery is obtained in the water-wet sand pack sample after the experiments.

The experimental study of Batemann et al. (2005) aims at obtaining CO₂, pore, water and rock interactions. In the study, a packed reacting material assemblage, which is placed in a pressure vessel, is used. The mineral composition of the assemblage is based on the Utsira sand. The experimental setup contains a syringe pump used to maintain the CO₂ pressure at 180 bar during the experiments. The reactant fluid is first equilibrated with CO₂ and then displaced by the pressuring CO₂. Samples of reactant fluids are used for the chemical analysis. Scanning

electron microscopy (SEM) analysis and surface area analysis are also carried out. The results of the experiments are used in a computer modeling study.

Another experimental study is carried out by Egermann et al (2005), which aims at defining dissolution and precipitation mechanisms during the co-injection of CO₂ and brine in carbonate cores. During the experiments, temperature and pressure ranges where CO₂ will stay in the supercritical phase are provided. As well as NMR and CT techniques, chemical analyses of the producing fluids are used during the study. The experimental setup used can be operated at the reservoir conditions up to 300 bar and 120°C and includes a Hassler type core holder and a pumping system. By the use of the pumping system, CO₂ and brine can be pumped separately or simultaneously. The effect of the change of flow rate and brine composition is investigated.

The study of Kulkarni (2005) focuses on the mechanisms of gas assisted gravity drainage (GAGD) mechanisms. An experimental study is carried out to investigate the effects of different conditions, such as miscible-immiscible flooding, homogeneous and fractured sample and secondary and tertiary injection. In the study, previously proposed analytical models are also investigated and used to describe the mechanisms of GAGD.

Shariatpanahi et al. (2005) investigated the effect of the orientation of fractures during gas injection and waterflooding in 2D porous water-wet micromodels. Different injection rates are applied and air is injected into the system after waterflooding. Besides gas injection, free-fall gravity drainage condition is also investigated, in which lower oil recovery is obtained compared to gas injection tests. It is also concluded that fracture orientation is more significant in during gas injection than waterflooding.

Darvish et al. (2006) carried out an experimental study to determine the efficiency of tertiary CO₂ injection into fractured chalk cores at reservoir conditions. A 2 mm fracture is created by centralizing the core inside a steel tube and providing space between the core and the wall of the tube. The fracture is filled with a sealing material. In the study, the initial reservoir oil is prepared by the combination of stock tank oil with a synthetic gas mixture and components C₅ and C₆ as a liquid mixture. After reservoir oil is injected into the core, the sealing material is removed from the fracture by increasing temperature to the reservoir temperature of 130 °C and melting the material. After the removal of the sealing material, water injection is performed and CO₂ is injected after water injection. During the study, oil and water production and fluid compositions are observed and it is concluded that CO₂ injection after water injection can be used to recover residual oil and an increase in oil recovery by 15% of original oil in place is obtained. Moreover, change in the composition of the produced oil is considered to be an evidence of different production mechanisms in mass transfer between matrix and fracture.

Study of Grigg and Svec (2006) was carried on sandstone and carbonate core samples. During the study, displacement tests were conducted at reservoir conditions of 145 °F and 2200 psig by injecting gas to residual brine saturation with respect to gas followed by brine injection to a residual gas with respect to brine. The experimental set-up used contains a syringe pump and a separator system. The core flooding system is placed into a temperature-controlled air bath. A liquid trap and a vapor trap are included and a wet test meter is used to determine the gas production at the ambient temperature. During the displacement tests, CO₂ saturation in the injected brine at reservoir conditions is changed from 0 % to 90 %.

The objective of the study of Fernø et al. (2007) is to observe the fracture/ matrix transfer and fluid flow in the fractured carbonate rocks. An experimental study is

carried out at various wettability conditions from strongly water-wet to moderately oil-wet with analysis of MRI images. In the experimental study, core plugs are stacked horizontally and a vertical fracture of constant aperture is provided. Fluids are injected with constant pressure or flow rate and the 2D water movement in the flow direction and the 2D saturation development in the fracture, orthogonal to the flow direction are imaged. Effects of different types of fracture widths and various flow rates are also investigated. Tests are conducted on two different outcrop carbonate rocks with different pore structure and level of pore scale heterogeneity. It is concluded that the possibility of forming capillary continuity by liquid bridges is dependent on fracture width. Bridges are likely to form at smaller widths and did not form beyond a critical width.

The study of Karpyn et al. (2007) aims at obtaining the effects of fracture morphology on immiscible fluid transport by continuing an experimental study on Berea sandstone cores with a single artificial longitudinal fracture. Micro-computed tomography (MCT) is used to obtain fluid distributions. A mixture of silicone oil and 30 % by weight of n-decane is used as the oil phase. Continuous oil injection, continuous water injection, simultaneous injection of oil and water, and a static pseudo-segregated state are provided during the experiments. It is concluded that there is a strong correspondence between fluid distributions with fracture geometry and fracture apertures as well as wetting characteristics of the rock. It is obtained that the non-wetting phase (oil) tends to occupy large apertures, while the wetting phase (water) spreads through small cavities.

Another study related to the gas oil gravity drainage concept is the study of Nabipour et al. (2007). In the study, thermally-assisted gas-oil gravity drainage for secondary and tertiary oil recovery is investigated experimentally using a fractured model. In the experimental part of the study, water-wet and oil-wet sand are used to investigate secondary and tertiary recovery. A core holder in a thermal jacket is placed vertically. Sand pack used is 70 cm long and has a 6.5 cm

diameter and the annular space between sand pack and the core holder is considered as a fracture. The model in the study is used for secondary GOGD process. For tertiary GOGD process, injecting several pore volumes of water from the bottom of the model, waterflood residual oil conditions are obtained. After matrix connate water conditions are reached, valves at the top and bottom of the model are opened and air enters from top and oil recovery as a function of time is recorded. Nitrogen is injected into fracture and then core holder is warmed by heating strips in a range between 25 °C to 60 °C. Wettability is also changed by aging the sand packs in crude oil for one month. Water-wet and oil-wet sand packs are used with fractures and without fracture. As a result of the study, it is concluded that thermally-assisted gas–oil gravity drainage process is a good heavy oil recovery alternative and tertiary oil recovery is more effective than secondary thermal recovery process.

Asghari and Torabi (2008) investigated the effects of CO₂ injection into fractured media on oil recovery by conducting both experimental and simulation studies. Both miscible and immiscible conditions are provided during the experiments and an open space around the core is considered as a surrounding fracture. Experiments are conducted by injecting CO₂ directly to the fracture at a range of pressure between 250 psi to 1500 psi at 35 °C by keeping the system at the pressure value for 1 day and measuring the n-decane recovery. Recovery obtained for both miscible and immiscible conditions are recorded and in the simulation part of study, CMG-GEM is used to simulate the results.

In the study of Tian and He (2008), the objective is to study effects of steam-only injection, steam injection with CO₂, steam injection with surfactant and steam injection with CO₂ on oil recovery using a laboratory model and a numerical simulation model. Effect of amount of CO₂ and amount of steam injected, effect of steam quality, steam temperature and effect of surfactant concentration are investigated. It is concluded that as the amount of both amount of steam and CO₂

increased, cumulative oil production is also increased as expected. Also, high recovery factors are obtained with high steam quality, high steam temperature and increasing surfactant concentrations. It is also concluded that simultaneous injection of steam, CO₂ and surfactant result in higher oil recoveries than that of steam injection, steam injection with CO₂ and steam injection with surfactant.

Trivedi and Babadagli (2008) continued an experimental study by performing continuous CO₂ injection into fractured Berea cores, providing different conditions of miscible and also immiscible process. The authors also conducted a simulation study and investigated diffusion coefficients by the comparison of the experimental results with the numerical model developed for matrix-fracture transfer. It is concluded that continuous CO₂ injection at low rates for long times followed by a shutdown results in diffusion process and increases recovery.

Zendehboudi et al. (2009) investigated the controlled gravity drainage in naturally fractured reservoirs. The authors stated that in the gravity drainage process in a fractured medium, overall system drainage is directly affected by the density difference between interacting gas and liquid, as well as the elevation difference between gas-liquid interface through matrix and fracture. In the experimental study, a rectangular porous medium is used as the matrix, which is surrounded vertically by one vertical fracture at each side. A pump is connected to the bottom part for producing liquid at various fixed discharge rates and the top part is open to the atmosphere providing that air is the gas phase. Effect of model height, fracture aperture, matrix permeability, liquid viscosity, well spacing and initial liquid saturation are investigated.

Torabi and Asghari (2010) continued an experimental study with immiscible and miscible injection of CO₂ into Berea cores with a surrounding fracture. Effects of connate water saturation, oil viscosity, injection pressure and matrix permeability are investigated. It is concluded that miscible CO₂ injection results in higher

amount of oil recovery compared with immiscible conditions. Connate water plays an inverse effect on recovery under immiscible conditions, while it is not very effective in the miscible case. It is also concluded that high matrix permeability favors oil recovery under immiscible conditions for the permeability values of the experiment.

3.2. Simulation Studies Carried Out On Matrix-Fracture Interaction, Gas-Oil Gravity Drainage and Gas Injection Processes

Cardwell and Parson (1948) studied the theory behind the gas oil gravity drainage of a sand column vertically placed, which is saturated with liquid. Governing equations of the process when the column is open to the atmosphere at the top and bottom and draining is studied and rate of gravity drainage is estimated.

Study of Nenniger and Storrow (1958) focuses on gravity drainage during the process of flow of liquid out of a packed bed in gravitational and centrifugal force fields. Equations are developed for the processes and experimental results are used to confirm the accuracy of the solution of these equations for different packed beds.

Barenblatt et al. (1960) studied the seepage of liquids in fissured rock and liquid transfer between fissures and pores. Authors presented fundamental equations for systems of uniform liquid in a fissured medium and also for a double porosity system.

Dkystra (1978) studied free fall gravity drainage mechanism by using the approach developed by Cardwell and Parson (1948) and proposed equations for gravity drainage mechanism and recovery. He compared experimental data with the proposed model and showed its reliability and availability to apply for a field

scale application with different examples considering change in the interface of oil and gas.

In the study of Hagoort (1980), gravity drainage is stated to be a recovery process, which is gas/oil displacement in which gravity is the main driving force. It is indicated that gravity drainage may occur in two cases, such as in the primary stages of oil production (gas cap- drive or segregation drive or segregation drive) and also in the other stages where gas supply can be from an external source. In the study, a classical description of immiscible two phase flow is used in a one dimensional vertical gravity drainage system and displacement is described by using the concepts of relative permeability and capillary pressure along with continuity equation and Darcy's law.

In the study of Gilman and Kazemi (1983), a double porosity simulator is developed with the usage of flow equations for matrix and fracture systems. The finite-difference simulator also makes it possible to model a single porosity system, if only equations for fracture are considered. Solution methods for the equations involving initial and boundary conditions and for the case of chemical transport are also presented. Assumptions used in the development of the simulator are verified by using data available including pressure transient test data.

Wu and Pruess (1988) studied the method of "Multiple Interacting Continua (MINC)", which describes matrix blocks with inside subdivisions depending on the distance from the surface of the matrix and its application for naturally fractured reservoirs and concluded that MINC method gives more accurate results compared with double porosity models, although it requires more computational work.

Bech et al. (1991) developed a model describing two phase oil-gas and water-oil systems in a fractured reservoir. Water-oil imbibition equations are described by

diffusion process assuming that diffusion coefficients are constant. Equation of gas oil gravity drainage rate is also presented with the assumption of the presence of equilibrium in the matrix blocks between oil and gas. Developed model is verified with laboratory data and results of a simulator.

In the study of Fung (1991), double porosity models used for describing gas-oil gravity drainage are investigated and a new model is developed including the effects of matrix continuity and reimbibition considering a stack of three blocks. Obtained results are compared with single block simulators and double porosity models as well.

Kazemi et al. (1992) proposed analytical and numerical solutions to Buckley Leverett displacement problem in the case of imbibition in matrix block surrounded with fracture using empirical transfer functions. The authors also presented a comparison between analytical and finite difference solutions and dual porosity simulation equations.

Luan (1994) presented a mathematical model describing gravity drainage mechanisms in naturally fractured reservoirs as a gas displacement process by using equations proposed by Hagoort (1980). He pointed out the importance of time delay during drainage process to reach a capillary pressure equilibrium, which causes a nonequilibrium stage as well as the effect of capillary continuity in a stack of matrix blocks in oil recovery.

Schechter and Guo (1996) reported that in the literature, there are 3 different gravity drainage processes in porous media investigated, namely; forced gravity drainage, simulated gravity drainage and free-fall gravity drainage. The authors developed a mathematical model describing free fall gravity drainage process and criticizing previously stated models based on Darcy's law and film flow theory. They also conducted experiments to investigate the mechanisms of vertical free-

fall gravity drainage from a matrix block in a naturally fractured reservoir. In the experimental part of the study, CO₂ is continuously injected into the annulus between the core holder and core sample at reservoir pressure and temperature, which simulates the fracture and recovery versus time data is recorded. New developed model with the obtained experimental data showed a good accuracy with the previous models of free-fall gravity drainage.

In the study of Darvish et al. (2005), a numerical model is developed that describes an experiment carried out with carbonate core sample having a surrounded fracture around it at reservoir conditions. In the experiment, a melting material is used to provide matrix with oil saturation, later on, the material is melted and fracture is created in the system. A numerical model is created for the gravity drainage experiment and effects of matrix permeability, height of the matrix, diffusion, pressure and type of the gas (CO₂ or hydrocarbon gas) are investigated. It is concluded that using correct diffusion coefficients are very important for obtaining reliable simulation results.

Donato et al. (2006) proposed expressions for the gas oil gravity drainage of a system I which gas is entering from the top into an oil saturated rock column. Effects of gravitational and capillary forces are included in equations describing the process. Moreover, numerical simulation results obtained for oil recovery are compared with the experimental results in literature. Matrix- fracture transfer functions are also presented that are developed for dual porosity and dual permeability models.

Li and Horne (2008) developed a model describing free fall gravity drainage process and derived equations for oil recovery for the process. Experimental and field data are used to verify the model and effects of pore size distribution and entry capillary pressure are investigated.

Alavian and Whitson (2009) modeled an experimental study, in which a chalk core sample with a surrounding fracture is used during first with C_1 -n- C_7 gas, second with CO_2 injection at 220 bar. A compositional simulator is used to describe the model and experimental results are compared with the model. Near-miscible CO_2 injection is obtained to be a main oil recovery mechanism.

Torabi and Asghari (2009) continued a simulation study and modeled a core system with a surrounding fracture during a gas oil gravity drainage process. Simulator CMG WinProp and CMG GEM are used to create PVT model of the system and to describe matrix and fracture transfer mechanisms under miscible and immiscible conditions. Different parameters affecting recovery such as diffusion coefficient and matrix permeability are considered. Diffusion process is obtained to be not very effective and it is concluded that the reason may be the limited time for the process or the nature of the model itself. On the other hand, matrix permeability is found to be a significant parameter influencing recovery.

Jamili et al. (2010) proposed a mathematical model describing matrix-fracture mass transfer including diffusion mechanism in the matrix and in the matrix fracture boundary presenting governing equations. An experimental study of CO_2 injection into fracture system of a chalk core is simulated and a counterflow of oil and gas in the core is indicated. Diffusion and convection mechanisms during recovery are concluded to be significant.

CHAPTER 4

STATEMENT OF PROBLEM

Naturally fractured reservoirs, which consist of a high porous, low permeable matrix and a low porous, high permeable fracture network, contribute to the hydrocarbon reservoir in the world in a great extent. In fractured reservoirs, there still exist high amounts of oil in the matrix system after primary production stage. In order to recover oil remaining in the matrix system, gas injection is a favorable method since it activates gas oil gravity drainage (GOGD) mechanism. Molecular diffusion also plays an important role in oil recovery in fractured reservoirs. Matrix- fracture interaction during all these processes is a key concept that is needed to be fully understood to provide effective oil recovery.

The aim of the study carried out is to investigate matrix-fracture interaction mechanisms in a fractured sandstone core system during gas injection. Effect of the type of gas injected, namely carbon dioxide, methane and nitrogen and effect of initial gas saturation have been investigated in terms of oil recovery. An experimental study has been carried out to differentiate the effective recovery processes such as gas-oil gravity drainage and diffusion. It is also aimed to simulate the experimental results with CMG (Computer Modeling Group Ltd.) WinProp (Microsoft Windows™ based Phase-Behavior and Fluid Property Program) and GEM (Generalized Equation-of-State Model Compositional Reservoir Simulator).

CHAPTER 5

EXPERIMENTAL STUDY

In the experimental part of the study, experiments are carried out by using consolidated Berea sandstone core samples with fracture. Berea cores were cut perpendicular to the bedding plane. The space around the core sample between the wall of the core holder and the core is considered as a surrounding fracture. Experiments are carried out by injecting CO₂, N₂ and CH₄ into the core in a cyclic manner of 1 day closed period under 250 psi followed by a production period of 2 minutes and the pressure, temperature and recovery versus time data is recorded.

5.1. Experimental Setup

During the experiments, an experimental setup that consists of a saturation system, a gas injection system, a core sample cleaning system and a data logger system are used.

The saturation system contains two different high pressure core holders, which are used to saturate the core sample with brine (5 wt % KCl aqueous solution) and n-decane, separately. Properties of synthetic oil n-decane are presented in Appendix A (Merck-Chemicals Web Site, 2011). 5 wt % KCl aqueous solution is chosen to prevent clay swelling, since KCl concentrations between 3-20 wt % prevents clay swelling (Anderson et al. 2010). The system also includes vacuum and ISCO syringe pumps, gas and brine sources. During the saturation of the core sample with brine, a vacuum pump is used to evacuate the core sample and the system, as well as a silica gel container to prevent the vacuum pump to be exposed to the

brine used for saturation. Core sample is kept at 60 bars for 24 hours. The system used for saturating the core with brine is shown in Figure 5.1 and Figure 5.2.

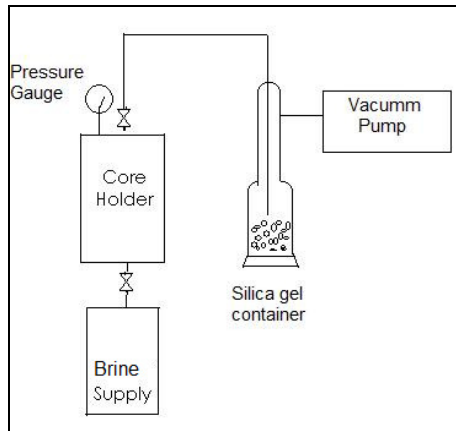


Figure 5.1. Schematic of the System Used For Saturating the Core with Brine

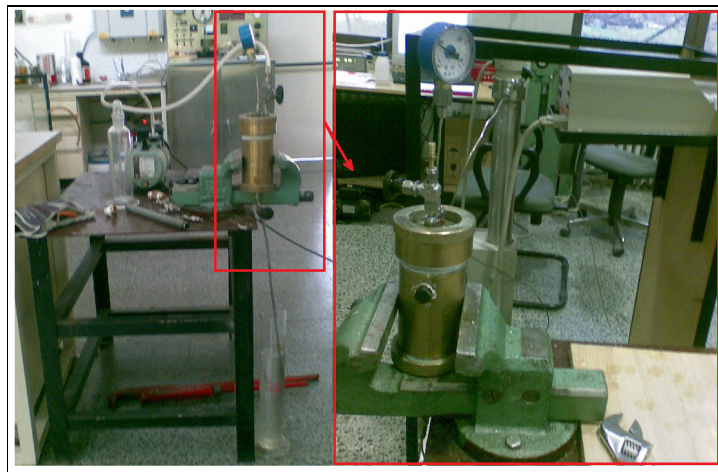


Figure 5.2. Core Holder with its Pressure Gauge Used for Saturating the Core with Brine

Another system is used for saturating the core sample with n-decane after saturating it with brine, which contains a high pressure core holder, an ISCO syringe pump and a vacuum pump as shown in Figure 5.3 and in Figure 5.4. Two pressure transducers are used to record the pressure values at the top and at the bottom of the high pressure core holder, while another transducer is used to record the confining pressure applied.

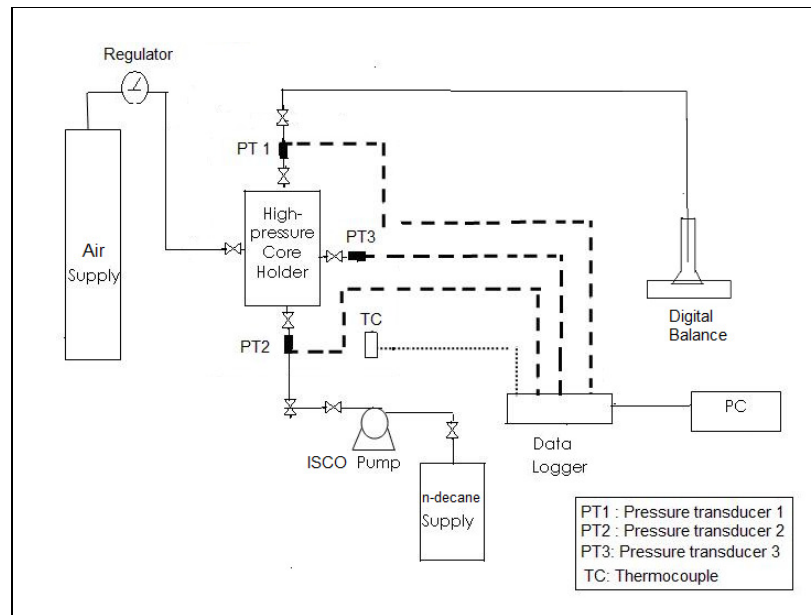


Figure 5. 3. Schematic of the System Used For Saturating the Core with n-decane



Figure 5. 4. Core Holder with its Pressure Transducers Used for Saturating the Core with n-decane

In the experiments, core sample is placed into a high pressure core holder. The inner diameter of the core holder is greater than the diameter of the core sample and a space is created between the inside wall of the core holder and the core sample, which is considered as fracture. The core sample is fixed in between two teflon spacers, which are placed inside the core holder. Fracture width at the top is 1.9 cm and at the bottom is 1.2 cm. In the annulus space around the core, a 0.445 cm wide fracture space is created.

A graduated cylinder is placed at the bottom of the high pressure core holder to collect the produced oil at different time intervals. Pressure transducers are used to record the pressure of each cell, while a thermocouple is used to record the temperature of the system, which is kept constant during the experiments by means of the constant temperature oven. The system used in the experiments is shown in Figure 5.5 and Figure 5. 6.

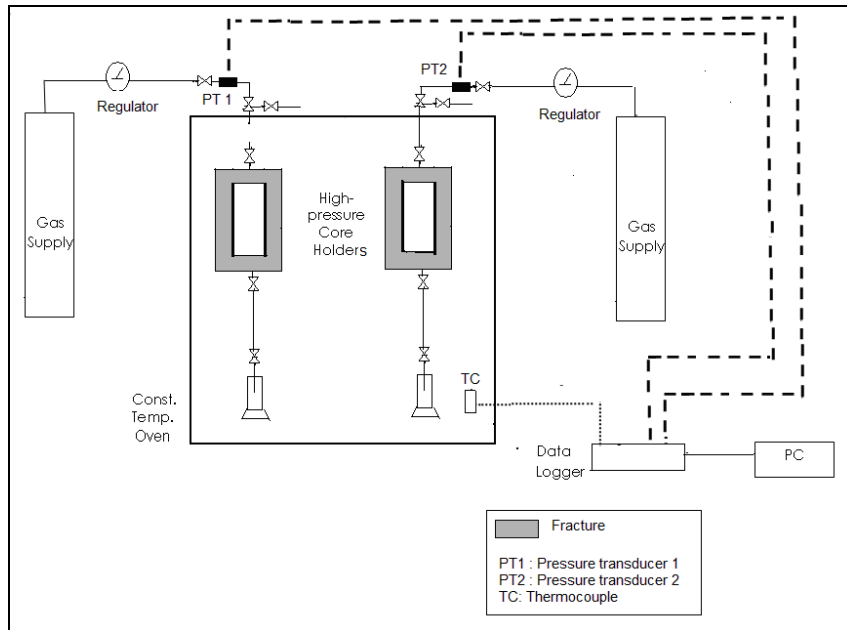


Figure 5. 5. Schematic of the System Used For the Experiments



Figure 5. 6. Core Holders Used for the Experiments

After each experiment, core sample is cleaned by using Toluene Extraction Apparatus shown in Figure 5.7. After the cleaning procedure, core sample is dried at 105 °C in a constant temperature oven.



Figure 5. 7. Core Cleaning Apparatus

Data logging system used during experiments is shown in Figure 5.8. There are different modules on the data logging equipment, namely, modules for temperature measurements, mA and mV output signals. Connections are provided with pressure transducers and the thermocouple. National Instruments LabVIEW Software, which is a graphical programming tool, is used. A flowchart is developed using the software for data recording and visualization (Figure 5.9). Noises obtained during the measuring process are filtered.

A general view of the experimental set-up with its components is shown in Figure 5.10. Equipment used in the set-up and specifications of each equipment is presented in Appendix B.



Figure 5.8. Data Logging System with Different Modules of Temperature and Pressure Measurements

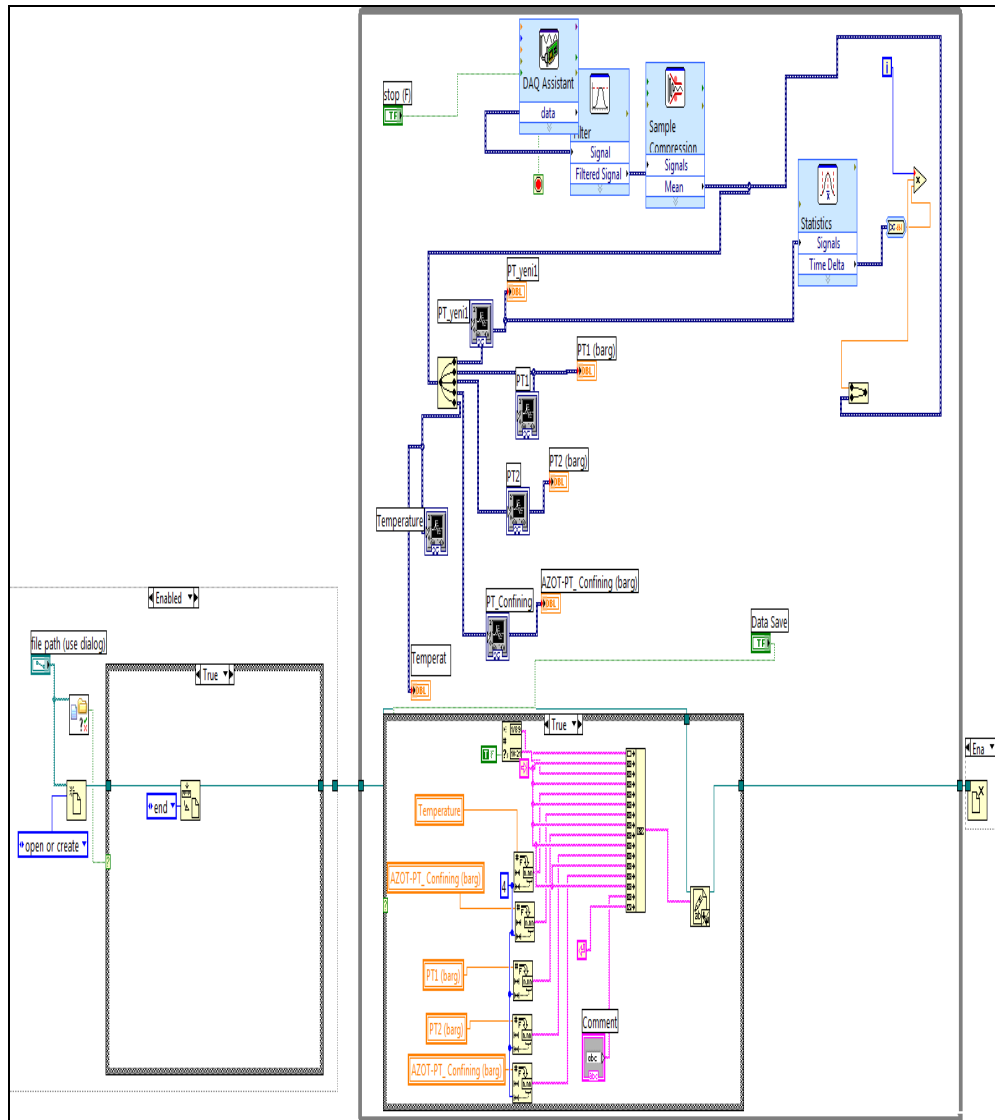


Figure 5.9. Flowchart Developed By LabVIEW Software for Data Logging, Recording and Visualization



Figure 5.10. Experimental Set-up with Its Components

5.2. Experimental Procedure

1. Before each experiment, system is evacuated and core samples are cleaned and dried. Dry weight of the core sample is recorded.
2. Core is saturated with 5 wt % KCl aqueous solution, which is chosen to prevent clay swelling. The core sample is placed into the core holder shown in Figure 5.2 and a vacuum pump is connected to the top of the holder. The core sample and the system are evacuated. While the system is being evacuated from the top, the valve at the bottom of the core holder is opened and brine (5 wt % KCl aqueous solution) is transferred into the holder from the bottom. The system is kept at 60 bar for 24 hours.

3. The brine saturated core sample is placed into the core holder shown in Figure 5.4. The next step is to inject n-decane as synthetic oil from the bottom of the core holder at a rate of 0.1 cc/min until there is no water production is obtained from the top. By this way, connate water conditions are provided.
4. After the saturation process is completed, saturated core is weighed and saturated weight is recorded. Saturated sample is transferred into the core holder shown in Figure 5.6.
5. Before gas injection, the system is kept for 48 hours at reservoir temperature of 70 °C. It is checked whether there will be oil production or not without the effect of the change in the pressure with gas injection.
6. CO₂, N₂ or CH₄ is injected into the core holder from the top. The space between the core sample and the core holder is considered as the fracture space. The system is kept at 250 psi and at 70 °C for a 24 hour-period.
7. The valve at the bottom of the core holder is opened to collect recovered oil. Collected oil is weighed by the use of the digital balance.
8. The valve at the bottom of the core holder is closed and pressure is adjusted again to 250 psi by injecting gas into the holder.
9. Steps 7 and 8 are repeated until the end of the experiment.

CHAPTER 6

EXPERIMENTAL RESULTS AND DISCUSSION

6.1. Core Sample Characterization

During the experimental study, consolidated sandstone samples are used and CO₂, N₂ and CH₄ injection is performed to determine matrix-fracture interaction mechanisms. n-decane is used as the synthetic oil phase.

Before experiments, core sample characterization is carried out. Analysis of mineralogy and petrography by thin section and X-Ray Diffraction (XRD) were conducted at Middle East Technical University (METU) Department of Geological Engineering.

According to the results of the thin section analysis, core sample is classified as sandstone (quartz-arenite) including the abundant mineral of quartz up to 65-70 %. Sample consists of well-compacted, more or less rounded and medium to fine grained mineral and rock fragments with a grain size varying between 0.5-0.2 mm. About 15 % of the grains consist of plagioclases with polysynthetic twinning and about up to 10 % of the grains is K-feldspar represented by both perthite and microcline. Fine flakes present white (muscovite) and dark (biotitic) micas and tourmaline, sphene and zircon minerals are also present. Rounded grains of quartz- and mica-schist, granite and felsic volcanic rock (dacite) make up the rock fragments. The only authigenic mineral observed is the dolomite. There are no water-soluble minerals in the rock (Goncuoglu, 2010).

XRD analyses are performed at METU Department of Geological Engineering with Rigaku Miniflex II instrument by using copper (Cu). Samples are prepared to determine clay and non-clay minerals. To determine non-clay minerals, dried, grinded and sieved (170 mesh size) samples are used for whole rock XRD analyses. Slides prepared from the obtained < 2 μm clay fraction are tested as air dried, as kept in ethylene glycol at 60 °C for 12 hours, as dried at 300 °C for 1 hour and as dried at 550 °C for 1 hour to determine clay minerals. Clay fraction weight percent is also determined. XRD results indicate that the sample includes high amount of quartz and alkaline feldspar as non-clay minerals. It has a clay fraction of 4.13 % containing mainly kaolinite and in less amounts illite and chlorite (Turkmenoglu, 2010). XRD spectrums for each test are presented in Appendix C.

There are 2 Berea sandstone core samples available for the experiments. Core sample E1 has a diameter of 3.81 cm and a length of 11.35 cm, while core sample E2 has a diameter of 3.8 cm and a length of 11.29 cm. Porosity measurements for the core samples are conducted. From the differences between the KCl aqueous solution saturated weight and dry weight of the samples, porosity values are obtained to be 0.20 for core sample E1 and 0.21 for core sample E2. Density of 5 % weight KCl aqueous solution is 1.02 g/cc at 70 °C and 250 psi (TPAO, 2011). Saturated and dry weights of core samples are shown in Table 6.1.

Table 6. 1. KCl Aqueous Solution Saturated and Dry Weights of Core Samples

Core Sample	Dia. (cm)	Length (cm)	Dry Weight (g)	Weight After Saturated with KCl Solution (g)	Bulk Volume (cc)	Porosity (frac.)
E1	3.81	11.35	273.263	299.70	129.40	0.20
E2	3.80	11.29	269.782	296.37	128.04	0.21

Porosity and permeability measurements are also conducted at Turkish Petroleum Corporation (TPAO) on another core sample E3, which is only used for core sample characterization, not in the injection experiments. Core sample E3 has a length of 4.9 cm and a diameter of 3.8 cm. Porosity measurements are conducted using a helium porosimeter and a porosity value of 0.213 is obtained, which is consistent with porosity values obtained at METU Department of Petroleum and Natural Gas Engineering. Permeability measurements are also carried out and an equivalent liquid permeability value of 266 md is obtained. For relative permeability measurements at TPAO, core sample E2 is saturated with 5 wt% KCl aqueous solution under a pressure of 1200 psi for one week. Porosity and permeability measurements under net overburden pressure and capillary pressure tests are also conducted at TPAO. n-decane-brine relative permeability tests are conducted at reservoir temperature of 70 °C, under an overburden pressure of 750 psi and a back pressure of 250 psi. Results of the core sample analysis and capillary pressure, pore size distribution and relative permeability curves obtained are presented in Appendix D (TPAO, 2011).

6.2. Experiments carried out with CO₂, CH₄ and N₂ Injection

Four experiments were carried out to study the matrix-fracture interaction during gas injection into a fractured media. Three different gases, namely carbon dioxide, methane and nitrogen were used to see the effect of different gases on the oil recovery. Among four experiments two of them were run by using carbon dioxide while methane and nitrogen were tested by one test for each. As mentioned above, two core samples (E1 and E2) were utilized to run the tests. Table 6.2 lists the experiments with respect to type of gas used, core sample utilized and the duration of test.

Table 6.2. List of Experiments

Test No	Injected gas	Core Sample	Duration (days)
1	Carbon dioxide	E1	25
2	Carbon dioxide	E2	60
3	Methane	E1	51
4	Nitrogen	E2	35

Before each experiment, cores were saturated with brine and n-decane by using the saturating systems described in Section 5.1. Brine and oil saturations of core samples are calculated by using following formulas:

$$\begin{aligned}
 m_{diff} &= m_{brine} + m_{oil} \\
 &= (V_{brine} \times \rho_{brine}) + (V_{oil} \times \rho_{oil}) \\
 &= [(1 - S_o) \times V_{pore} \times \rho_{brine}] + [S_o \times V_{pore} \times \rho_{oil}]
 \end{aligned} \tag{6.1}$$

$$S_o = \left[(\rho_{brine} \times V_{pore}) - m_{diff} \right] / \left[\rho_{brine} \times V_{pore} - \rho_{oil} \times V_{pore} \right] \tag{6.2}$$

$$S_w = 1 - S_o \tag{6.3}$$

where

S_w : Brine saturation (fraction),

S_o : Oil saturation, (fraction),

V: volume (cc),

ρ : density (g/cc),

m: mass (g),

m_{diff} : Mass Difference between n-decane+ brine Saturated Weight and Dry Core Weight (g)

ρ_{oil} : Density of n-decane at 1 atm and 20 °C (0.73 g/cc) (Merck-Chemicals, 2011),

ρ_{brine} : Density of KCl solution at 1 atm and 20°C (1.02 g/cc) (TPAO, 2011)

Although it was aimed to saturate all the cores with brine and n-decane only (no initial gas saturation), it was found out by applying material balance after brine and oil injection that there must be some gas saturation in the system for all experiments except the first one. Otherwise, for only oil- water system it was not possible to reach reasonable values of saturation. As a result, saturation of brine for Experiments 2, 3 and 4 is assumed to be equal as in the first experiment which was taken as the irreducible water saturation of the core sample. Table 6.3 lists the measured weight of core samples at different stages of core saturation. Calculated initial saturations for each experiment are tabulated in Table 6.4.

Table 6. 3. Weight of Core samples after Brine, n-decane Saturation

Test No	Core Sample	Dry Weight (g)	Weight After Saturated with Brine (g)	Weight after Saturated with Brine and n-decane (g)
1	E1	273.215	299.777	294.96
2	E2	269.782	296.368	286.426
3	E1	273.192	299.620	290.090
4	E2	269.555	296.621	285.064

Table 6. 4. Initial Saturations

Test No	Core Sample	Saturation (fraction)		
		Oil	Brine	Gas
1	E1	0.797	0.203	0
2	E2	0.552	0.203	0.244
3	E1	0.556	0.203	0.241
4	E2	0.495	0.203	0.301

Values reported in Tables 6.3 and 6.4 are used to calculate the Original Oil in Place (cc) for each experiment by utilizing Equation 6.4 and the results are tabulated in Table 6.5.

$$OOIP = \left[m_{diff} - (S_w)(\rho_{brine})(V_{pore}) \right] / \rho_{oil} \quad (6.4)$$

Table 6. 5. Original Oil in Place for each Experiment

Test No	Core Sample	OOIP (cc)
1	E1	21.96
2	E2	15.06
3	E1	15.33
4	E2	13.51

After saturating the core samples and placing them into core holders shown in Figure 5.6, the temperature of constant temperature air bath is set to 70 °C and the system is kept for 48 hours open to the atmosphere by opening the top and bottom valves of the core holder. The aim was to observe any fluid production (oil and water) from the core as the result of fluid expansion due to increase in temperature from ambient to test temperature. Later, gas injection is performed from the top until the system pressure is reached to 250 psi. The space between the core sample and the core holder is considered as the fracture space. Every 24 hours, the valve at the bottom of the core holder is opened to atmosphere for 2 minutes and the recovered oil is collected. After that, the valve at the bottom of the core holder is closed and pressure is adjusted to a value of 250 psi by injecting gas into the holder. Cumulative oil production data of each experiment is presented in Figures 6.1 to 6.4.

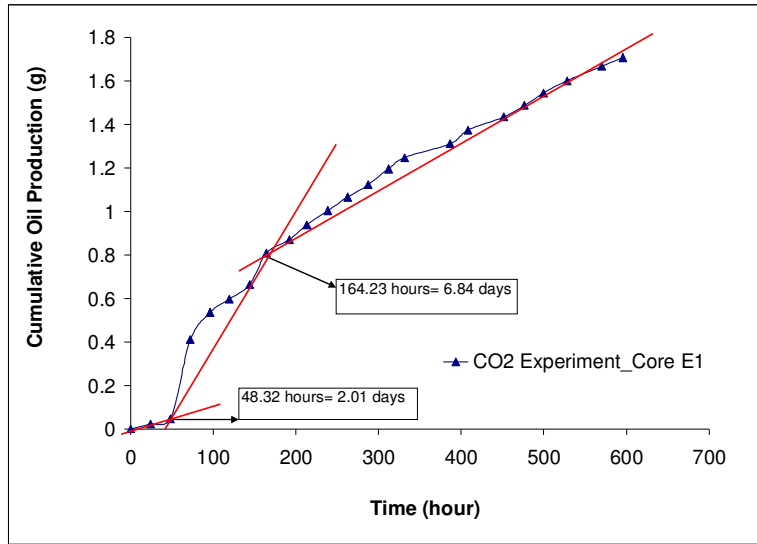


Figure 6.1. Cumulative n-decane production with CO₂ injection- Test-1, Core E1

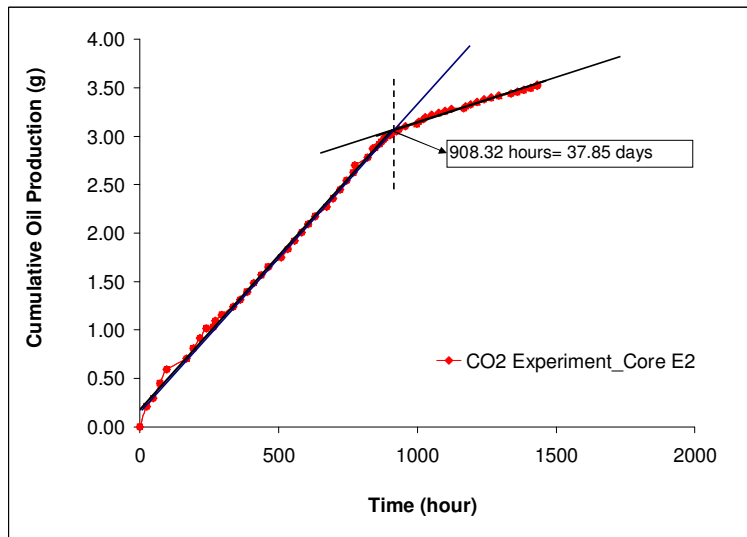


Figure 6. 2. Cumulative n-decane production with CO₂ injection- Test-2, Core E2

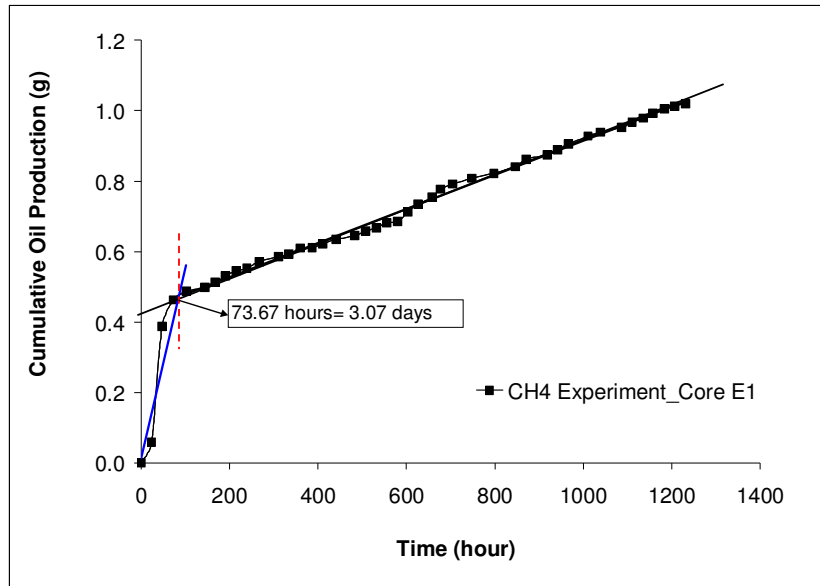


Figure 6. 3. Cumulative n-decane production with CH₄ injection- Test-3, Core E1

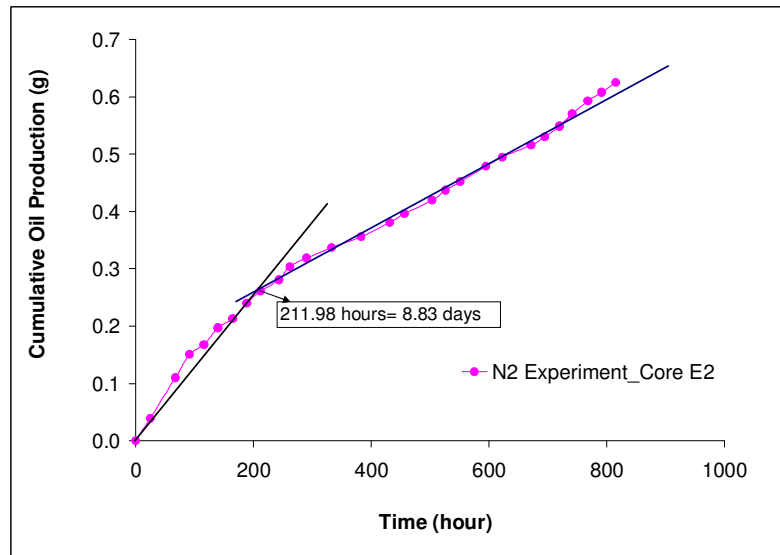


Figure 6. 4. Cumulative n-decane production with N₂ injection- Test-4, Core E2

The common feature of production characteristics of all experiments is that they exhibit specific periods with different productions, which will be analyzed separately.

Test-1: The distinctive feature of this test from all others is that the core is fully saturated with brine and n-decane only, leaving no pore space for gas initially. Therefore, the only available contact area for gas and reservoir fluids is the fracture surface around the core. In that respect, the diffusion should be the effective recovery process at the initial stage of production. This is why the cumulative production of the first few days is very limited for this test. Later, a very steep increase in the production is observed which is slowed down to a steady increase later. The test is ceased at 25th days with no sign of change in the production characteristics of late stage.

Tests 2, 3 and 4: All these three tests were run with an initial gas saturation creating the conditions for the entrance of high pressure gas into pore space at the first glance. Entrance of gas into pore space will increase the effective contact area between gas and reservoir fluids resulting in a more efficient recovery mechanism. This is why those three tests do not show the very limited recovery characteristics of first test at the beginning of test. All tests exhibit relatively higher production increases at the beginning then slowed again as in the case of Test-1.

The absolute cumulative production values expressed in grams are normalized by converting them to recovery factors which makes the comparison easier. Equation 6.5 is used to calculate the Recovery Factor (RF).

$$RF = \frac{(N_p)_{oil}}{[OOIP]} \times 100 \quad (6.5)$$

where

RF: oil recovery factor (%),

$(N_p)_{oil}$: cumulative n-decane production as function of time(cc)

Recovery factors for all tests are plotted in Figures 6.5 to 6.8.

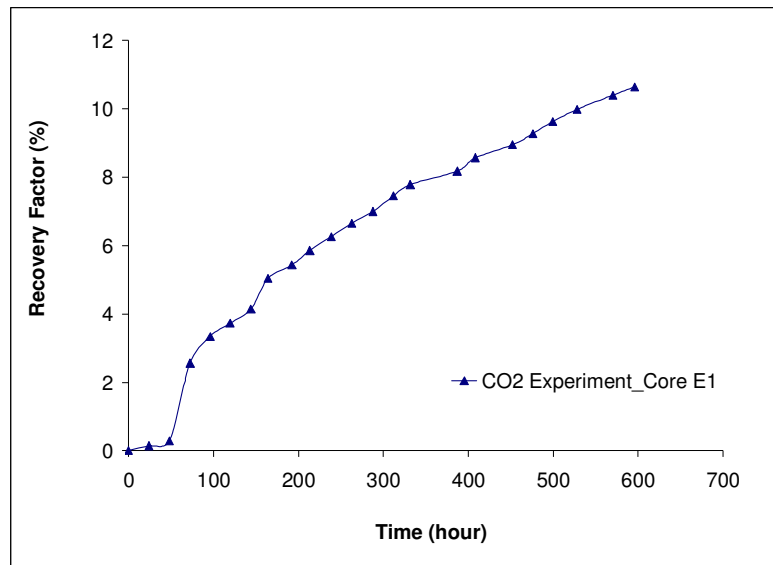


Figure 6. 5. Recovery Factors with CO₂ injection, Test -1, Core E1

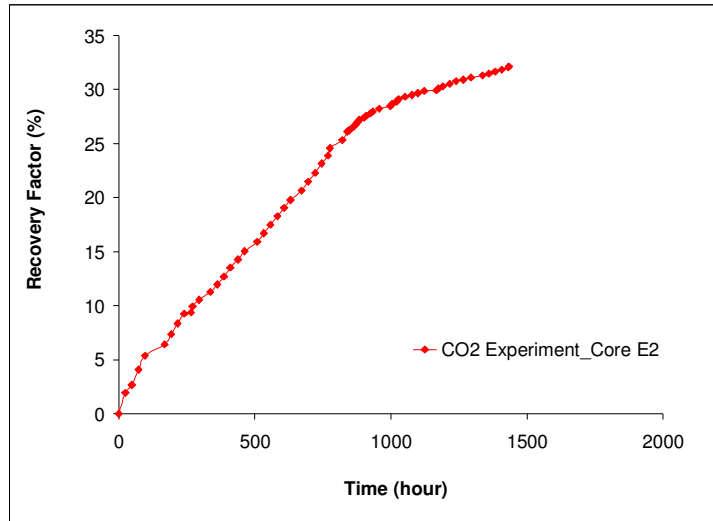


Figure 6. 6. Recovery Factors with CO₂ injection, Test – 2, Core E2

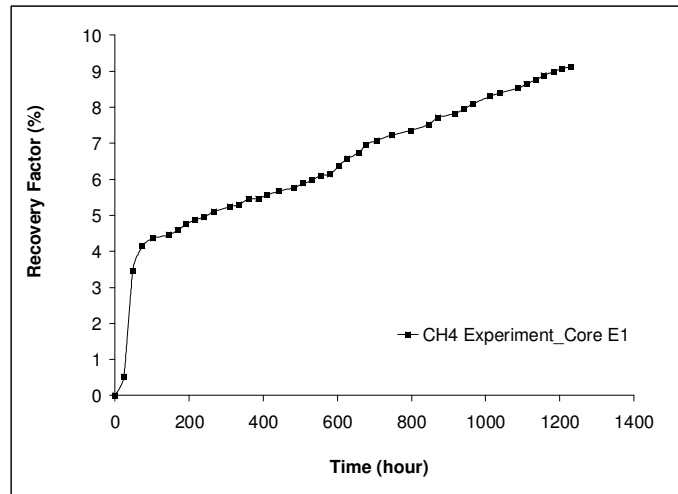


Figure 6. 7. Recovery Factors with CH₄ injection, Test – 3, Core E1

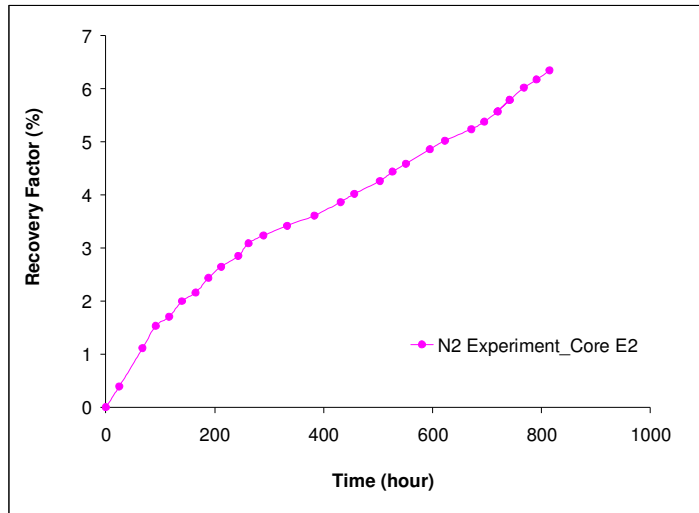


Figure 6. 8. Recovery Factors with N₂ injection, Test – 4, Core E2

Recovery characteristics of tests will be compared first in terms of with and without initial gas saturation (Tests 1 and 2) and type of gas injected (Tests 2, 3 and 4) then the possible recovery mechanisms will be discussed in the following sections.

6.3. Comparison of Experiments carried out with CO₂ Injection

The recovery characteristics of two tests with CO₂ injection is shown in Figure 6.9. The core sample in the first CO₂ test has no initial gas saturation while the second test has a gas saturation of 24.4 %. Comparison of recovery curves of these two tests indicate that the availability of initial gas saturation in the matrix increased the recovery for all times, starting from the first moment. At the 25th day, recovery factor obtained for the CO₂ experiment without initial gas saturation is 11 %, while the recovery factor is 18 % for the CO₂ experiment with initial gas saturation. This is attributed to the fact that the readily available space for CO₂ makes the penetration of CO₂ into the matrix easier. Easy penetration of CO₂ into

matrix results in an increasing efficiency of recovery mechanisms by CO₂ injection, which will be discussed further while comparing the recovery characteristics of tests with different types of gases.

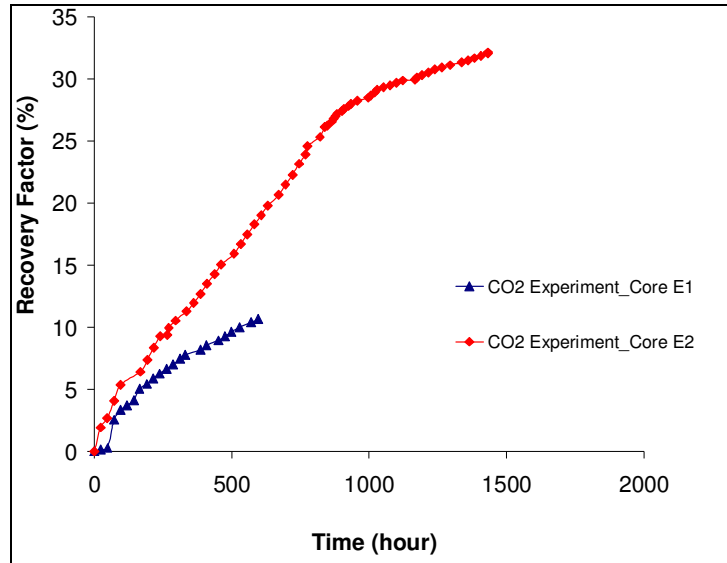


Figure 6. 9. Comparison of Experiments carried out with CO₂ Injection

6.4. Comparison of Recovery Factors Obtained in Tests with CO₂, CH₄ and N₂

Calculated recovery factors for all four tests carried out with CO₂, CH₄ and N₂ are presented in Figure 6.10. Except for the first test, all other experiments have similar initial saturations and their recoveries could be compared. At the 35th day, recovery factor values for CO₂, CH₄ and N₂ that have similar initial saturations could be listed as 25%, 7.5% and 6.3 %, respectively. On the other hand, the

difference of the recovery characteristics of two tests with CO₂ injection should also be investigated.

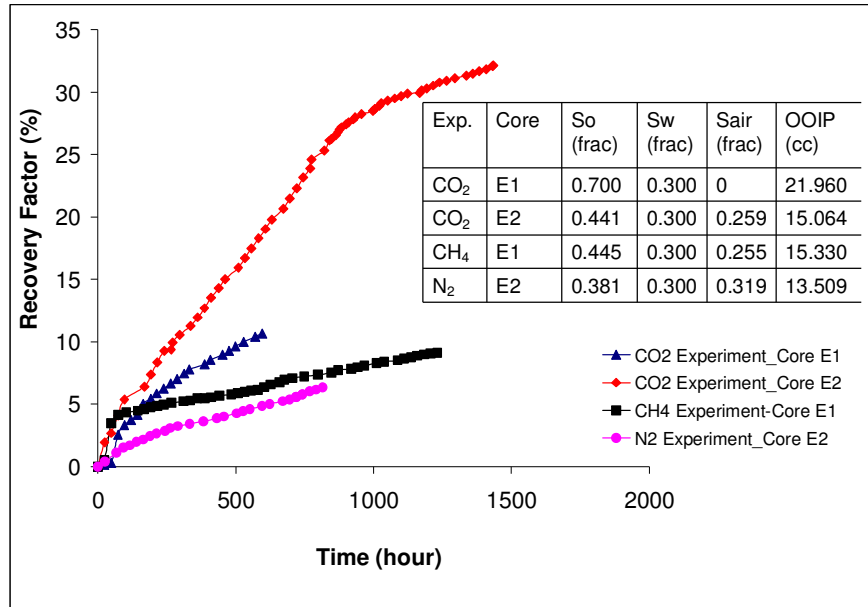


Figure 6. 10. Recovery Factors with CO₂, CH₄ and N₂ injection

During this study, it was aimed to investigate the effect of type of the gas in matrix-fracture interaction. When the recovery plots of tests 2, 3 and 4 are compared, it is observed that highest n-decane recovery is obtained with CO₂ followed by CH₄ and N₂ injection. The main mechanisms that play role during matrix fracture interaction are gas oil gravity drainage (GOGD) and diffusion. Density difference between the gas in the fracture and oil in the matrix is the reason of the gravity drainage process in fractured reservoirs. Table 6.6 shows the density, viscosity and molecular weight values of n-decane and gases used in the

experiments at 250 psi and 70 °C (NIST Chemistry WebBook, 2011). Difference between density of n-decane and CO₂, CH₄ and N₂ are 0.6649, 0.6802 and 0.6729 g/cc, respectively. If these values are taken as the driving force of gravity drainage process, the highest recovery should be expected from CH₄ tests followed by N₂ and CO₂ which does not fit the observations made during the study. The comparison need to be made between the gas saturated oil density and gas densities.

Table 6. 6. Properties of n-decane, CO₂, CH₄ and N₂ at 250 psi and 70 °C (NIST Chemistry WebBook, 2011).

Fluid Properties			
Fluid	Density of fluid at 250 psi and 70 °C (g/cc)	Viscosity of fluid at 250 psi and 70 °C (cp)	Molecular weight (g/mole)
n-decane	0.6931	0.49664	142.2817
CO₂	0.0281	0.017246	44.0095
CH₄	0.0099	0.012796	16.0425
N₂	0.0169	0.020056	28.0134

Solubility of gas in oil plays a significant role in oil recovery. As gas phase dissolves in the oil, an increase in the liquid volume occurs and it results in oil swelling as well as a reduction in the viscosity of oil (Simon and Graue, 1965; Holm and Josendal, 1974). Solubility (mole fraction in liquid phase) of CO₂, CH₄ and N₂ in n-decane at 70 °C and 250 psi are 0.14, 0.07 and 0.026, respectively

(Reamer and Sage, 1963; Beaudin and Kohn, 1967; Srivastan, 1992; Azarnoosh and McKetta, 1963) (Appendix E). CO₂ has the highest solubility in n-decane at the conditions of experiment, compared with the solubilities of CH₄ and N₂ in n-decane and as a result, the highest value of the n-decane recovery is obtained in the CO₂ injection experiment.

One significant change in the oil properties is that as the oil becomes more saturated with CO₂, oil density increases (Holm and Josendal, 1974). Density and viscosity of n-decane - CO₂ mixtures with different CO₂ mole fractions above bubble point pressure in the study of Culllck and Mathls (1984) are shown in Table F.1 in Appendix F. As it is indicated in Table F.1, as mole fraction of CO₂ in n-decane-CO₂ mixture increases, density of mixture increases, while viscosity of the mixture decreases. One of the reasons that CO₂ injection resulted in the highest recovery may be this increase in the oil density, which may cause a more efficient gas oil gravity drainage mechanism due to higher density difference between oil and gas phases. In addition decrease in the viscosity of oil cause also higher recovery.

Another effective mechanism of CO₂ injection would be the expansion of water as CO₂ dissolves in water. Although the cores were saturated with water at irreducible water saturation, the expansion of water will help the additional recovery of oil.

Change in the density and viscosity of n-decane- CH₄ mixtures as function of methane mole fraction is given in Table F. 2 of Appendix F (Agilio and Padua, 2004). It is seen from Table F.2 that density values of the mixture decrease as CH₄ mole fraction increases. Moreover, viscosity of n-decane - CH₄ mixture also decreases with increasing mole fraction of CH₄. Although the decrease in oil viscosity as CH₄ dissolves in oil favors the recovery of oil, the decrease in the density of oil weakens the effectiveness of gravity drainage mechanism.

Consequently, higher n-decane recovery obtained in the CO₂ experiment compared to the CH₄ experiment may be resulted from the density increase and corresponding increase in the density difference between matrix and fracture fluids in the CO₂ experiment, which is not obtained in CH₄ experiment.

After completing the comparison of CO₂ and CH₄ experiments in terms of gravity drainage mechanism which is based on data from literature, the comparison for N₂ experiment will be done based on n-decane- CO₂, CH₄ and N₂ mixture densities which are calculated by using Peng Robinson Equation of State (Peng and Robinson, 1976) since no data were found in the literature for n-decane – N₂ mixtures.

Density of n-decane, as well as density of CO₂, CH₄ and N₂- n-decane mixtures are calculated by using Peng Robinson equation (Appendix G) and the results are tabulated in Table 6.7. As it is seen from Table 6.7, investigating density difference between mixture and CO₂, CH₄ and N₂ density values, the greatest density difference is obtained between CO₂ and CO₂- n-decane mixture, which may be considered as the reason of a more effective gas oil gravity drainage process and consequently, higher n-decane recovery compared with CH₄ and N₂ experiments. As the density difference increases, n-decane recovery also increases in the experiments, respectively, highest in CO₂ experiments, later in the CH₄ experiment and lowest in the N₂ experiment.

Table 6. 7. Mixture and Component Densities Calculated with Peng-Robinson Equation of State (Peng and Robinson, 1976)

	Mole Frac. of CO ₂ , CH ₄ or N ₂ Component	Calculated Binary Interaction Coefficients, k _{ij} (Varotsis et al., 1986)	Calculated Density at 250 psi and 70 °C with Peng-Robinson EOS (Peng and Robinson, 1976) (g/cc)	Density Difference between Mixture and CO ₂ , CH ₄ or N ₂ (g/cc)
n-decane	0	-	0.651	-
CO₂	1	-	0.0283	-
CH₄	1	-	0.0099	-
N₂	1	-	0.0174	-
n-decane-CO₂ Mixture	0.14	0.1155	0.680	0.6517
n-decane-CH₄ Mixture	0.07	0.0431	0.655	0.6451
n-decane-N₂ Mixture	0.03	0.1370	0.654	0.6370

Another significant factor that affects n-decane recovery is the diffusion. CO₂, CH₄ and N₂ diffusion coefficients in n-decane are reported to be in a range between 10⁻⁴ and 10⁻⁵ cm²/sec (Renner, 1988; Killie et al., 1991). Diffusion coefficients for CO₂, CH₄ and N₂ in n-decane for consolidated porous media at the experimental conditions are determined by using the following empirical equation (Renner, 1988):

$$D_{ij} = 10^{-9} \mu_j^{-0.4562} M_i^{-0.6898} V_i^{-1.706} P^{-1.831} T^{4.524} \quad (6.5)$$

where

D_{ij} : gas i diffusion coefficient in liquid j; m^2/sec ,

μ_j : liquid viscosity that diffusion takes part in, cp

$\mu_{n\text{-decane}} = 0.49664$ cp at 250 psia and 70 °C (NIST Chemistry WebBook, 2011);

M_i : molecular weight of gas diffused, g/gmol;

V_i : gas molar volume, cc/gmol;

P: pressure, psia,

T: temperature, °K.

Calculated diffusion coefficients are tabulated in Table 6.8. As it is seen from Table 6.8, the highest value of diffusion coefficient in n-decane belongs to CH₄, which is greater than values of CO₂ and N₂. Greatest density difference between gas and mixture density is obtained in CO₂ experiments and although the diffusion coefficient of CH₄ is greater, gravity drainage mechanism may be concluded to be more dominant compared with the diffusion effect on n-decane recovery, resulting in a highest recovery in CO₂ experiments than CH₄ experiment. The greater n-decane recovery in the CH₄ experiment compared to the N₂ experiment may be both due to higher density difference between gas and mixture and higher diffusion coefficient obtained in the CH₄ experiment.

Table 6.8. Diffusion coefficients for CO₂ and CH₄ in n-decane at 250 psia, 70 °C

Gas	Density of gas (g/cc) (NIST Chemistry WebBook, 2011)	Molar volume of gas (cc/g-mol)	Calculated D_{ij} (10^{-5} cm ² /sec) (Renner, 1988)
CO ₂	0.0281	1564	4.321
CH ₄	0.0099	1623	8.147
N ₂	0.0169	1658	5.343

CHAPTER 7

SIMULATION RESULTS AND DISCUSSION

In the simulation part of the study, CMG (Computer Modeling Group Ltd.) WinProp (Microsoft Windows™ based Phase-Behavior and Fluid Property Program) and GEM (Generalized Equation-of-State Model Compositional Reservoir Simulator) are used to simulate the results.

CMG WinProp is used for modeling phase behavior of reservoir fluids as well as properties and compositional variations of them and their interaction with injected fluids, from lab scale to field scale. WinProp can be used to determine the minimum miscibility pressure (MMP) for given oil and for a given solvent composition at particular temperature (WinProp, 2007). In this study, miscibility pressures for n-decane and injected gas system is obtained by using CMG WinProp.

CMG GEM is an equation-of-state compositional reservoir simulator, which can be used for modeling recovery processes where the fluid composition affects recovery. GEM provides a range of dual porosity/dual permeability techniques for modelling naturally fractured formations including gas phase diffusion. Matrix-fracture transfer in fractured reservoir systems can be modelled including gas-oil gravity drainage concepts by using these dual porosity/dual permeability techniques of GEM (GEM, 2007). In this study, core-scale simulation of experimental results is conducted using GEM.

7.1. CMG (Computer Modeling Group Ltd.) WinProp (Microsoft Windows™ based Phase-Behavior and Fluid Property Program)

In order to determine the miscibility conditions of the system for CO₂, CH₄ and N₂ at reservoir temperature of 70 °C and test temperature of 250 psi, CMG WinProp Program is used. Program makes it available to determine characteristics of systems step by step as shown in Figure 7.1.

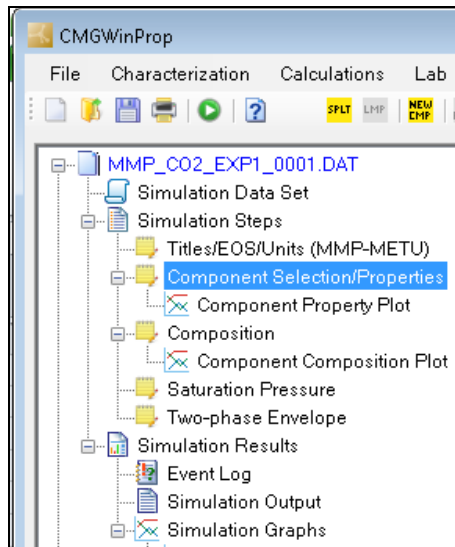


Figure 7. 1. CMG WinProp Steps for Modelling Phase Behavior of Reservoir Fluids

The first step is defining each component, which are n-decane and injected gas (CO₂, CH₄ or N₂) in this case, from the library of the program as shown Figure 7.2. In order to include the composition data for n-decane and injected gas, oil,

gas and brine saturations are used and mole fractions of n-decane and injected gas are determined, which are shown in Table 7.1.

Table 7. 1. Mole Fractions of n-Decane and Injected Gas (CO₂, CH₄ or N₂)

Exp.	Core	S_{CO2} (frac.)	S_{brine} (frac.)	S_{n-decane} (frac.)	Pore Vol. (cc)	n-decane Mole Frac.	CO₂ Mole Frac.
CO ₂ Exp-1	E1	0	0.203	0.797	27.562	1.000	0
CO ₂ Exp-2	E2	0.245	0.203	0.552	27.273	0.945	0.055
Exp.	Core	S_{CH4} (frac.)	S_{brine} (frac.)	S_{n-decane} (frac.)	Pore Vol. (cc)	n-decane Mole Frac.	CH₄ Mole Frac.
CH ₄	E1	0.241	0.203	0.556	27.562	0.933	0.067
Exp.	Core	S_{N2} (frac.)	S_{brine} (frac.)	S_{n-decane} (frac.)	Pore Vol. (cc)	n-decane Mole Frac.	N₂ Mole Frac.
N ₂	E2	0.302	0.203	0.495	27.273	0.917	0.083

Since the program does not make it possible to enter a 0 composition value, primary composition of gas component is specified as 0.001, while secondary composition of injected gas is entered as 1.00. Primary composition of n-decane is 0.999 and secondary composition of n-decane is 0 (Figure 7.3).

Component		Int. Coef.	Viscosity	Aqueous Phase					
Comments									
No. of components: 2 <input type="checkbox"/> Use temperature-dependent volume shifts									
No.	Component	HC	Pc (atm)	Tc (K)	Acentric fact.	Mol. weight	Vol. shift	Z (Rackett)	
1	CO2	3	72.8	304.2	0.225	44.01	0.000000E+000	0.2736	
2	NC10	1	20.8	617.6	0.49	142.286	0.000000E+000	0.2503	

Figure 7. 2. CMG WinProp Component Selection

Comments		
Enter the composition in mass fraction or percent. Normally, "Primary" corresponds to the reservoir fluid and "Secondary" corresponds to the injection fluid (if applicable). Blanks will be replaced by zeros.		
Component	Primary	Secondary
CO2	0.001	1.0
NC10	0.999	0.000000E+000
Sum	1.0	1.0

Normalize Composition

Figure 7. 3. CMG WinProp- Composition

For the two-phase envelope construction, ranges for pressure and temperature values can be specified (Figure 7.4). By using CMG (Computer Modeling Group Ltd.) WinProp, P-T diagram with different constant volume fraction vapor phase lines (quality lines) are constructed. As an example, for different primary CO₂ compositions (0.01-0.9) P-T phase boundaries for n-decane- CO₂ system are constructed as shown in Figure 7.5.

Specification Construction Controls Feed/K-values/Output level/Stability

Comments

Envelope Type

X-Y Phase Envelope Pseudo-Ternary Phase Envelope

X-Y Phase Envelope

Y-Axis

Pressure Temperature

Min. Pressure (psia) 0

Max. Pressure (psia) 14895.95

X-Axis

Temperature Composition

Min. secondary mole frac.: 0

Max. secondary mole frac.: 0.98

Min. mole frac. step size: 0.03

Max. mole frac. step size: 0.15

Pressure/Temperature Specification

Pressure (psia)

Unknown User input 14.696

Temperature (deg F)

158.0

Min. vapor mole frac. -10.0

Max. vapor mole frac. 10.0

Figure 7. 4. CMG WinProp Two-Phase Envelope Construction

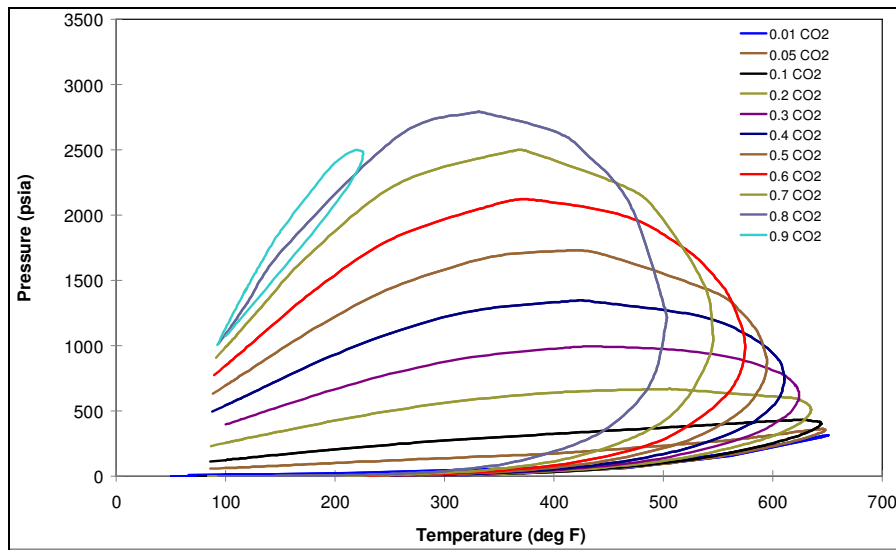


Figure 7. 5. P-T Phase Boundaries for n-decane- CO₂ System for Different Primary CO₂ compositions (0.01-0.9)

P-T Diagrams with primarily 0.001 mole fraction of CO₂ (Experiment-1), 0.055 mole fraction of CO₂ (Experiment-2), 0.067 mole fraction of CH₄ (Experiment-3) and 0.083 mole fraction of N₂ (Experiment-4) are also constructed and presented in Figure 7.6- 7.9.

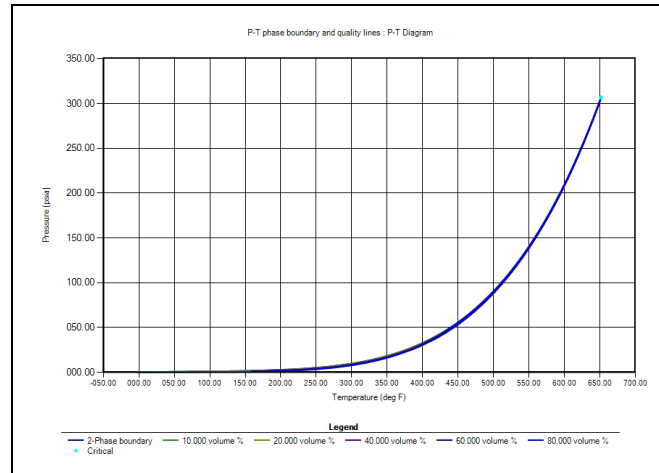


Figure 7. 6. P-T Diagram with primarily 0.001 mole fraction of CO₂ (Exp-1)

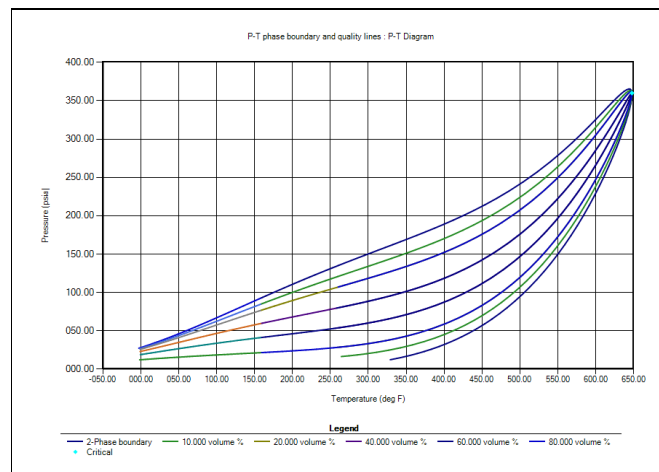


Figure 7. 7. P-T Diagram with primarily 0.055 mole fraction of CO₂ (Exp-2)

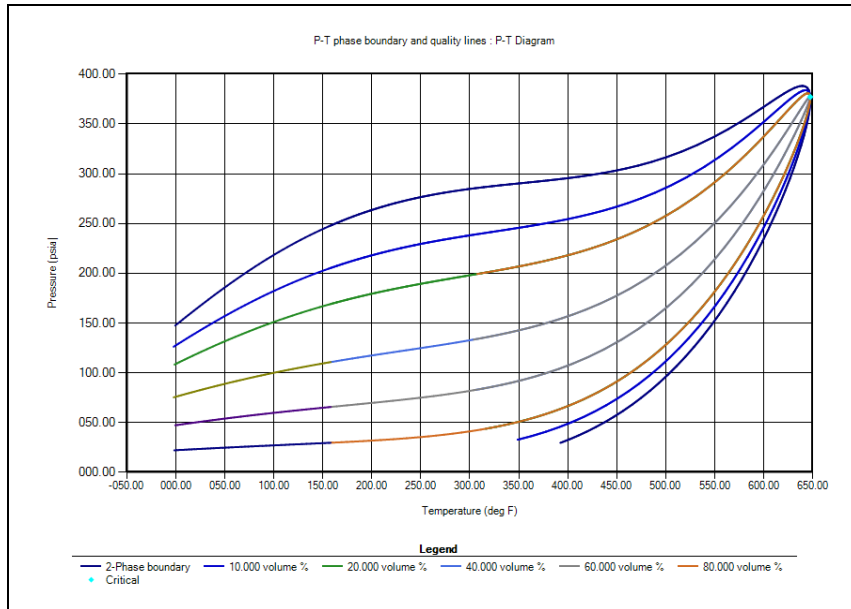


Figure 7. 8. P-T Diagrams with primarily 0.067 mole fraction of CH₄ (Exp-3)

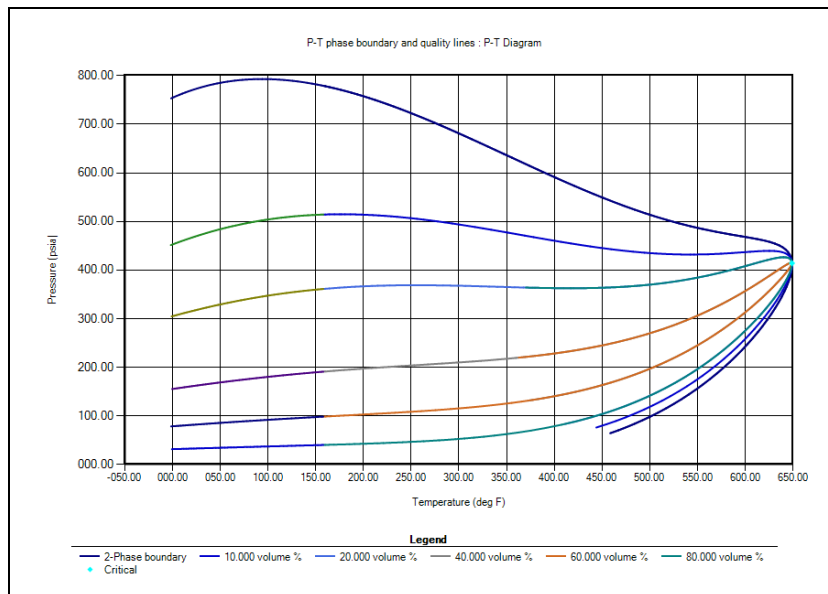


Figure 7. 9. P-T Diagrams with primarily 0.083 mole fraction of N₂ (Exp-4)

P-X diagrams for n-decane and CO₂, CH₄ and N₂ system are constructed (Figure 7. 10- 7.13). As shown in Figure 7. 9- 7.10, the critical point that liquid and vapor phases become identical is obtained to be at 1976.18 psia for CO₂- ndecane system in Experiment-1 and 1976.25 psia for CO₂- ndecane system in Experiment-2. For the CH₄ experiment, minimum miscibility pressure reaches to 5971.68 psia, while it is 39412.9 psia for the N₂ experiment. These results indicate that the experimental conditions of 250 psia and 70° C correspond to immiscible conditions. A PVT Model for n-decane and CO₂, CH₄ and N₂ systems is also created by WinProp to use in data preparation in CMG Builder.

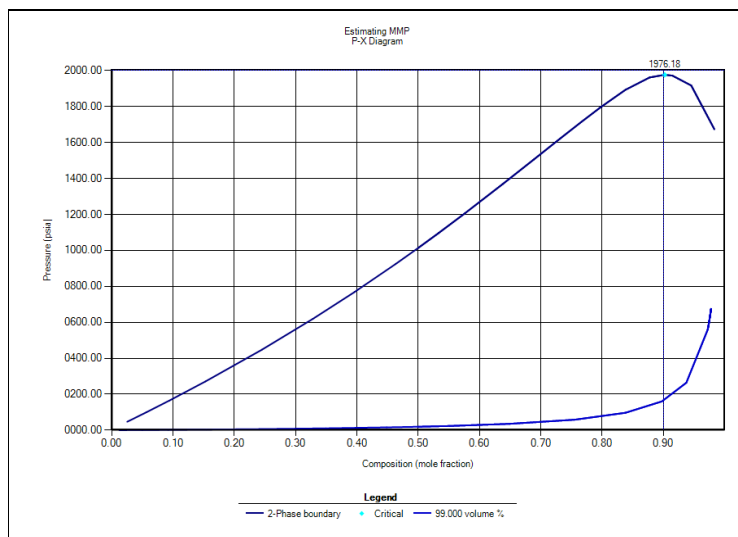


Figure 7. 10. P-X diagram for n-decane and CO₂ system with primarily 0.001 mole fraction of CO₂ (Exp-1)

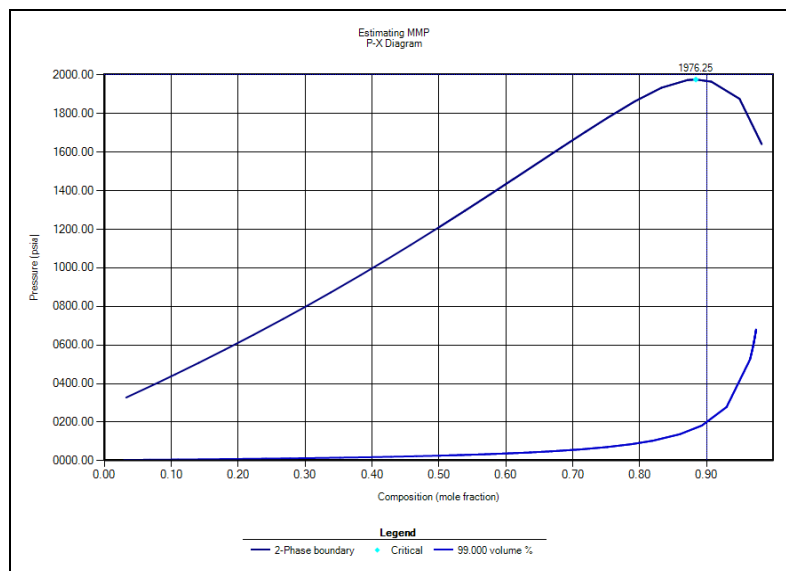


Figure 7. 11. P-X diagram for n-decane and CO₂ system with primarily 0.055 mole fraction of CO₂ (Exp-2)

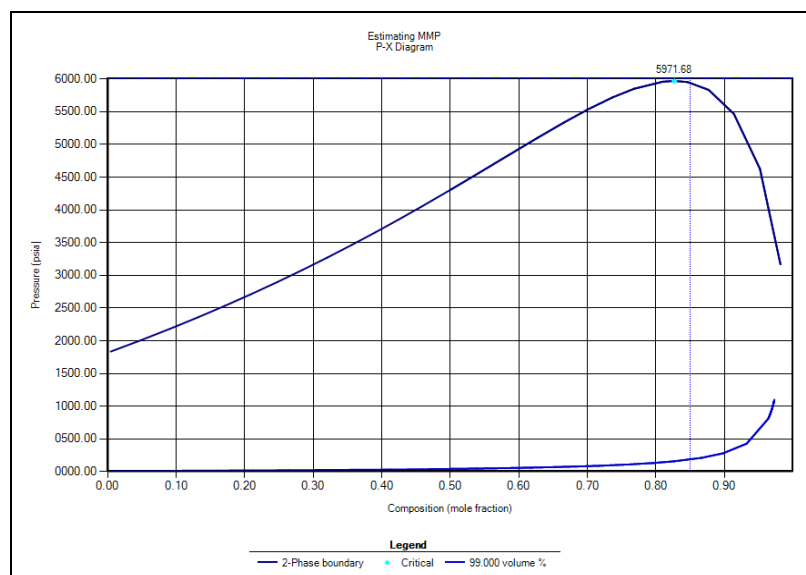


Figure 7. 12. P-X diagram for n-decane and CH₄ system with primarily 0.067 mole fraction of CH₄ (Exp-3)

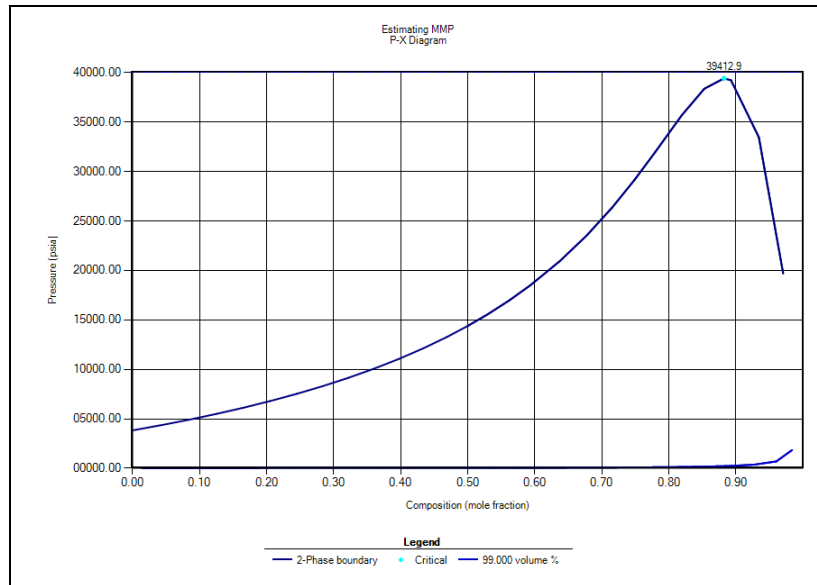


Figure 7. 13. P-X diagram for n-decane and N₂ system with primarily 0.083 mole fraction of N₂ (Exp-4)

7.2. Data Preparation by using CMG Builder for CMG GEM (Generalized Equation-of-State Model Compositional Reservoir Simulator)

CMG Builder is used to describe the core system for CMG GEM modeling. First of all, simulator settings for CMG GEM are defined as shown in Figure 7.14 and a double-porosity model is chosen to describe the fracture system surrounding core sample, which is the space created between the core sample and inside diameter of the core holder.

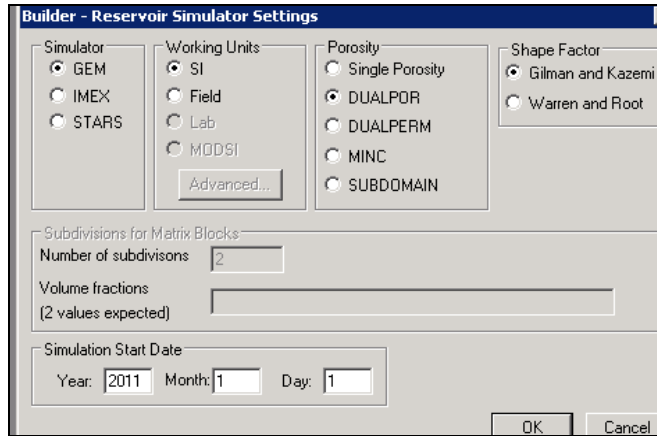


Figure 7. 14. Reservoir Simulation Settings for CMG GEM

To describe the core sample system, a radial grid system is created with different number of divisions along the r direction and layers along the k- direction (down). The outer block width in the r direction is greater than the other equally divided block widths in the r direction, which is designated as the fracture space as shown in Figure 7.15. 3 D view of a grid system with 20 Divisions in the r Direction is shown in Figure 7.16.

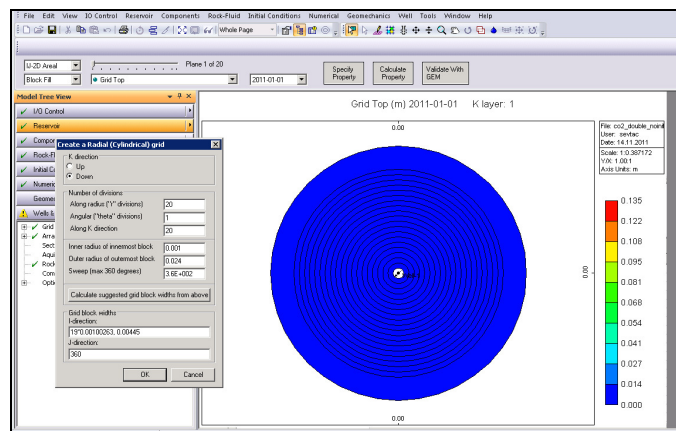


Figure 7. 15. Radial Grid System Created with 20 Divisions in the r Direction

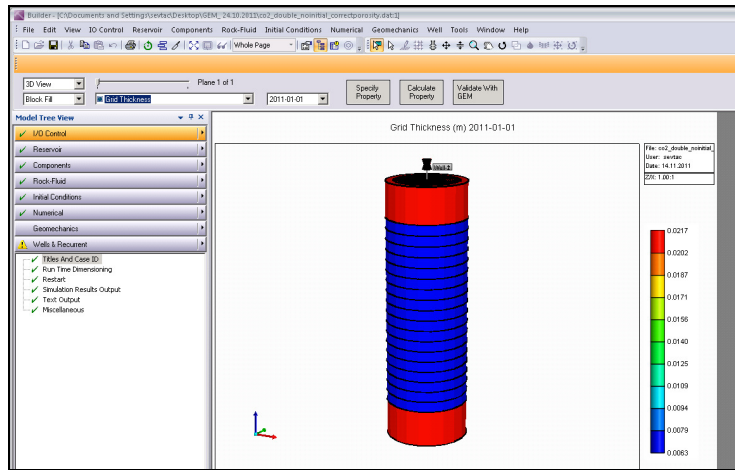


Figure 7. 16. 3 D View of the Radial Grid System with 20 layers along the k-direction

Layers along the k direction are specified by entering grid block thickness values as shown in Figure 7.17. The top and the bottom layers have greater thicknesses, which are indicating the top and bottom parts of the fracture.

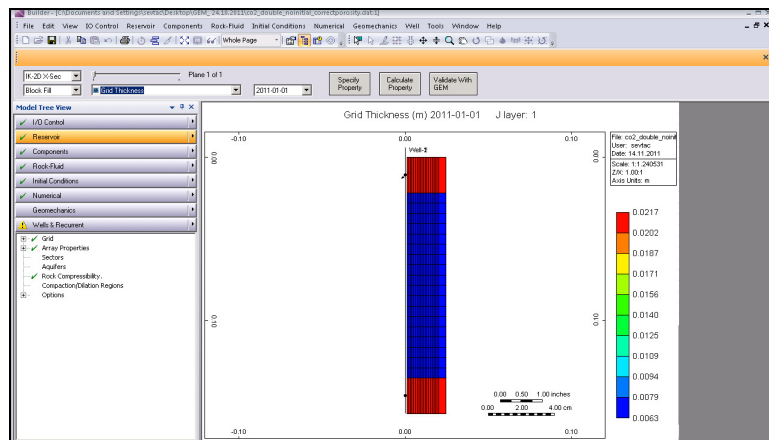


Figure 7. 17. Layers along the k Direction in the Grid System

As the next step, properties such as porosity, permeability, fracture porosity, fracture permeability and reservoir temperature are defined in the program (Figure 7.18). Matrix porosity is taken as 0.2, while fracture porosity is taken as 0.99. Matrix permeability in i, j and k direction are specified as 266 md. On the other hand, fracture permeability is taken to be 1330 md, which is 5 times the matrix permeability value.

Global composition value of gas phase (CO_2 , CH_4 or N_2) is taken as primary mole fraction of gas (0.001 mole fraction of CO_2 (Experiment-1), 0.055 mole fraction of CO_2 (Experiment-2), 0.067 mole fraction of CH_4 (Experiment-3) and 0.083 mole fraction of N_2 (Experiment-4)) in the fracture, while it is taken to be 0 in the matrix blocks. Global composition of n-decane in the fracture, on the other hand, is taken to be 0.

Pressure is specified as 250 psi, both in matrix and fracture blocks. Temperature is specified as 70 °C for both matrix and fracture blocks. Fracture spacing in all i, j, k direction are taken to be 0.00001 m. By specifying different fracture and matrix properties such as permeability and porosity, it is planned to describe the core sample system with its surrounding fracture system. Figure 7.19 shows different values of permeability in i direction for matrix and fracture blocks and Figure 7.20 presents changes in permeability values in different layers in the areal view.

General Property Specification							
Edit Specification							
Go To Property: Grid Thickness		Use Regions / Sectors					
UNITS:	Porosity	Porosity - Fracture	Permeability I	Permeability J	Permeability K	Permeability I - Fracture	Permeability,
SPECIFIED:	X	X	md	md	md	md	
HAS VALUES:	X	X	X	X	X	X	X
Whole Grid							
Layer 1	0.2	0.99	266	266	266	26600	26600
Layer 2	0.2	0.99	266	266	266	26600	26600
Layer 3	0.2	0.99	266	266	266	26600	26600
Layer 4	0.2	0.99	266	266	266	26600	26600
Layer 5	0.2	0.99	266	266	266	26600	26600
Layer 6	0.2	0.99	266	266	266	26600	26600
Layer 7	0.2	0.99	266	266	266	26600	26600
Layer 8	0.2	0.99	266	266	266	26600	26600
Layer 9	0.2	0.99	266	266	266	26600	26600
Layer 10	0.2	0.99	266	266	266	26600	26600
Layer 11	0.2	0.99	266	266	266	26600	26600
Layer 12	0.2	0.99	266	266	266	26600	26600
Layer 13	0.2	0.99	266	266	266	26600	26600
Layer 14	0.2	0.99	266	266	266	26600	26600
Layer 15	0.2	0.99	266	266	266	26600	26600
Layer 16	0.2	0.99	266	266	266	26600	26600
Layer 17	0.2	0.99	266	266	266	26600	26600
Layer 18	0.2	0.99	266	266	266	26600	26600
Layer 19	0.2	0.99	266	266	266	26600	26600
Layer 20	0.2	0.99	266	266	266	26600	26600

Figure 7. 18. Property Specification

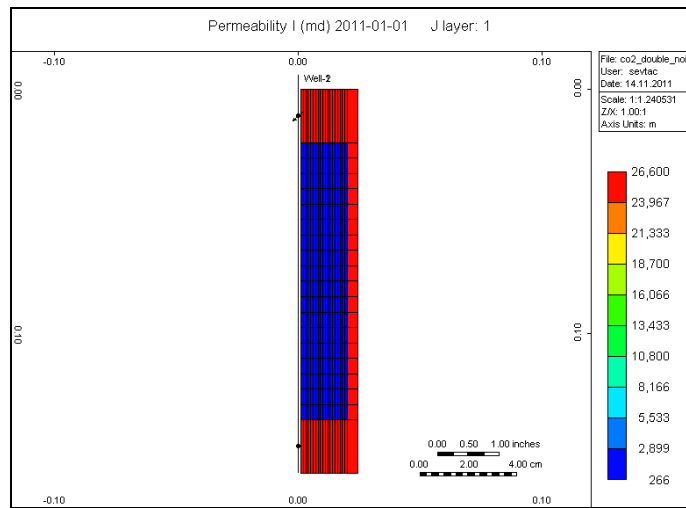


Figure 7. 19. Permeability in i Direction for Matrix and Fracture Blocks

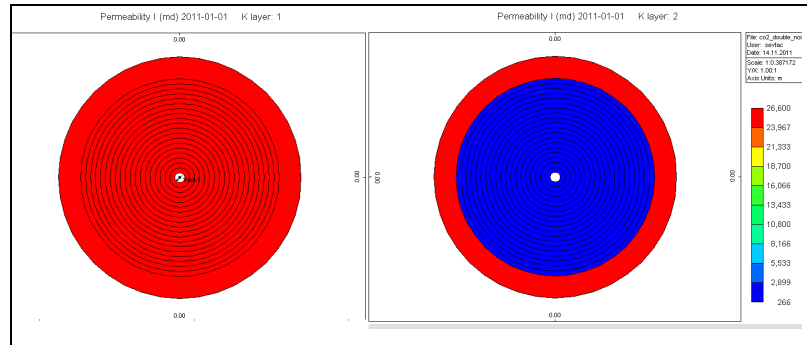


Figure 7. 20. Changes in Permeability Values in Different Layers in the Areal View

WinProp Generated PVT Model and the relative permeability values of n-decane and brine system determined at TPAO (2011) are imported into the CMG Builder. Figure 7.21 shows relative permeability curve constructed by the program.

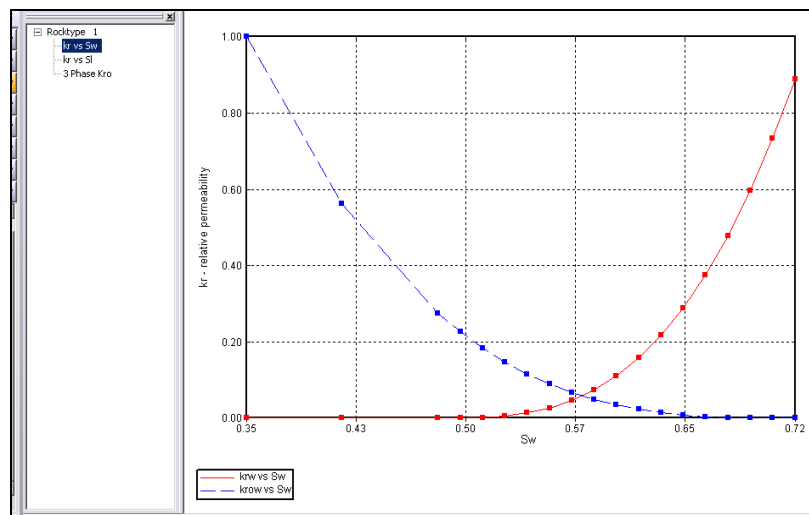


Figure 7. 21. Relative Permeability Curve constructed by the CMG Builder

User specified option of CMG Builder is used to define initial conditions. Pressure, water saturation and global composition values are specified for each grid block (Figure 7.22).

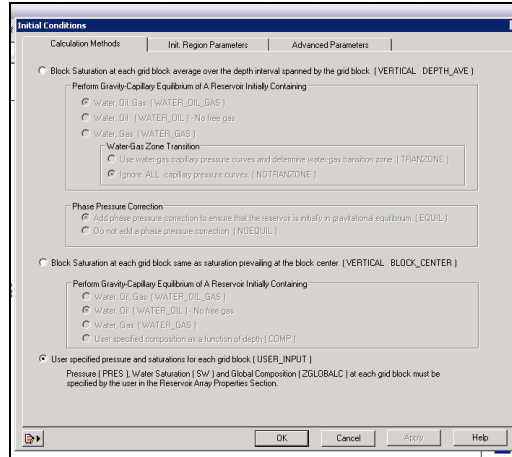


Figure 7. 22. User specified Initial Conditions

Wells are also added to the system, one injection well is at the top grid block, while a production well is at the bottom grid block. Well constraints are also specified. For the injection well, the maximum bottom hole pressure is set to be 250 psi, while for the production well it is specified as 14.7 psi. Well events are adjusted for 1 day shut-in and later on for 2 minutes open periods, since the system is kept at a pressure of 250 psi for 1 day and then production period is started for 2 minutes during the experiments (Figure 7.23).

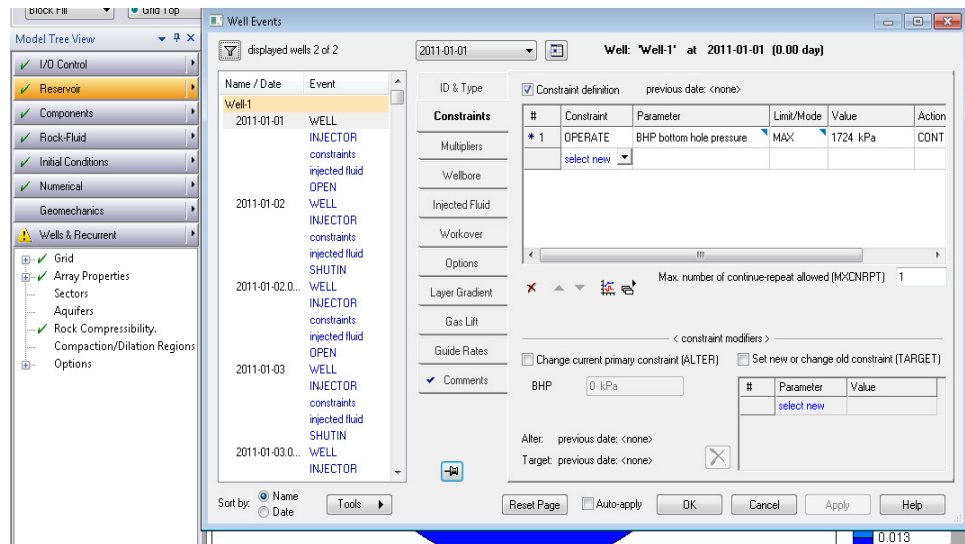


Figure 7. 23. Well Constraints and Well Events Specified

7.3. Results of Simulation Study carried out with CO₂, CH₄ and N₂ Injection Experiments

For the simulation of the CO₂ experiment carried out without initial CO₂ saturation, a radial grid system is created with 3 divisions along the r direction and 3 layers along the k- direction (down). The outer block width in the r direction is defined as the fracture space as shown in Figure 7.24.

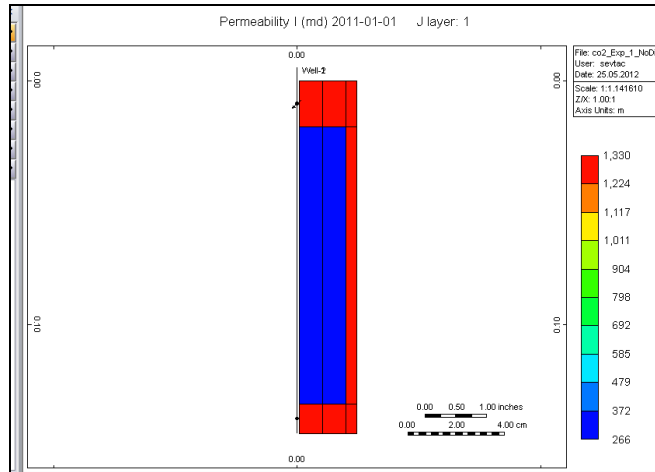


Figure 7. 24. Radial Grid System with 3 Divisions along the r Direction and 3 Layers along the K- Direction (Down) for Experiment-1

After running CMG GEM with the data file prepared by using CMG Builder, n-decane recovery values are obtained. n-decane recovery values obtained after the simulation are presented and compared with experimental results in Figure 7.25. As it is seen from Figure 7.25, simulation results of n-decane recovery without diffusion process continue at lower values than experimental results after around 7 days.

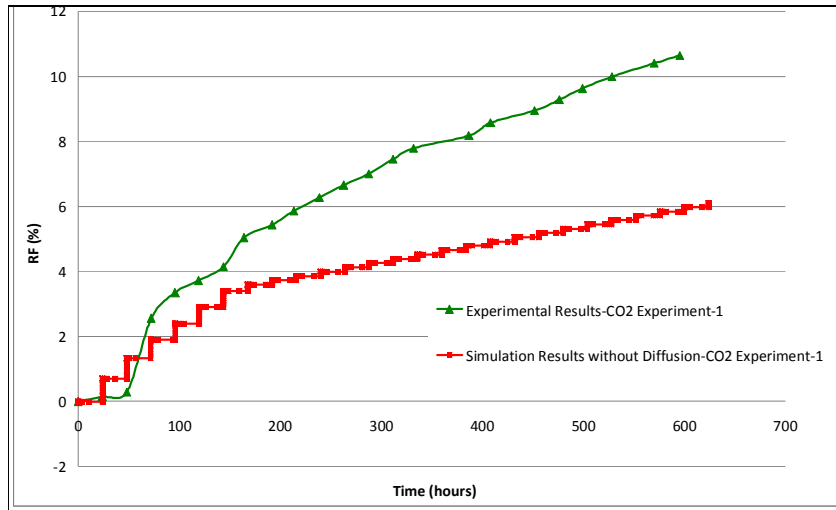


Figure 7. 25. Simulation Results without Diffusion for CO₂ Experiment-1

After obtaining n-decane recovery simulation results without diffusion for the CO₂ Experiment-1, effect of diffusion on the recovery mechanisms are studied by including gas phase matrix- fracture diffusion coefficient during data preparation with CMG Builder (Figure 7.26).

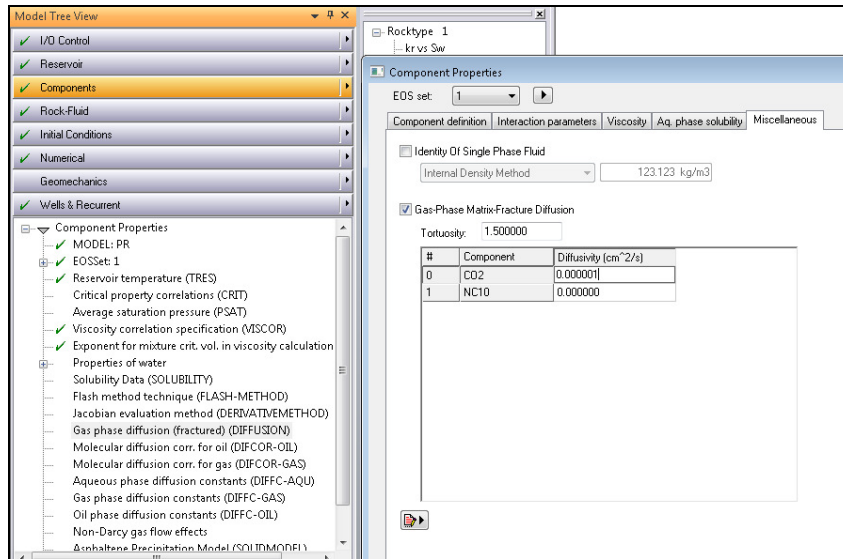


Figure 7. 26. Defining Gas Phase Matrix- Fracture Diffusion Coefficient in CMG Builder

n-decane recovery simulation results for diffusion process with CO₂ matrix-fracture diffusion coefficient of 10⁻⁶ cm²/sec and 10⁻⁵ cm²/sec are obtained and shown in Figure 7.27. As it is seen from Figure 7.26, simulation results with diffusion, especially, the case for diffusion coefficient D= 10⁻⁶ cm²/sec fits very well to the experimental results. The input file prepared for modeling CO₂ experiment-1 with diffusion (D= 10⁻⁶ cm²/sec) is included in Appendix H.

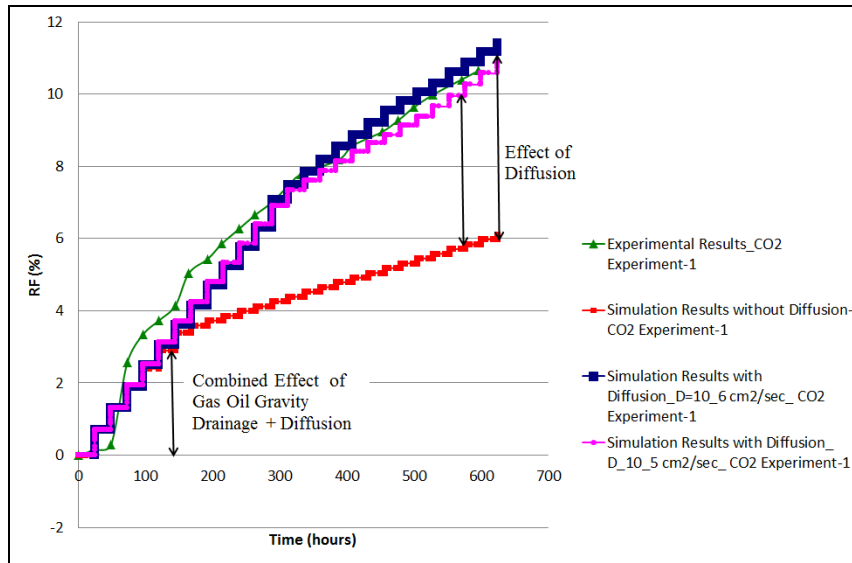


Figure 7.27. Simulation Results with Diffusion for CO₂ Experiment-1

As it is seen from Figure 7.27, experimental results of recovery show higher values than simulation results for the model without diffusion. In Experiment-1, there is no initial free gas space since the core sample is fully saturated with n-decane and brine. Experimental results follow a similar trend with model results with diffusion, indicating that the dominant recovery mechanism in Experiment-1 is diffusion from the initial stages to the end of the production.

When simulation results are investigated, it is seen from Figure 7.27 that up to a specific point recovery values are following the same trend for diffusion and no diffusion cases, which is the result of the combined effect of gas oil gravity drainage and diffusion. After a point, recovery values for different diffusion coefficient cases gradually increase. The difference between simulation results of diffusion and no diffusion cases corresponds to the effect of diffusion, which is significant for the model.

For the simulation of the CO₂ experiment carried out with initial CO₂ saturation, a radial grid system is created with 3 divisions along the r direction and 40 layers along the k- direction. The surrounding blocks are defined as the fracture space as shown in Figure 7.28.

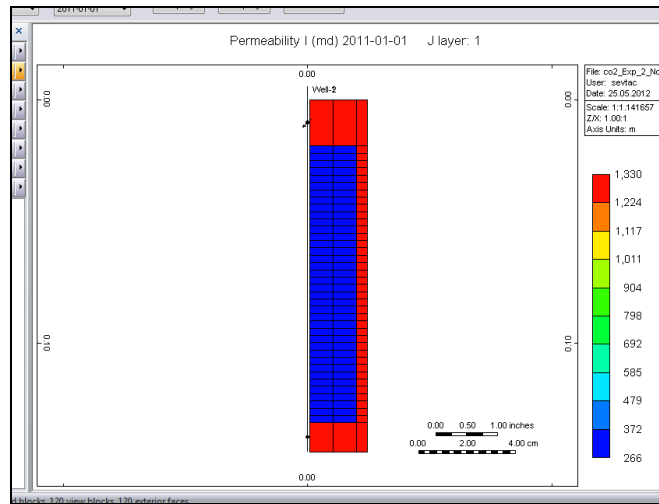


Figure 7. 28. Radial Grid System with 3 Divisions along the r Direction and 3 Layers along the K- Direction (Down) for Experiment-2

n-decane recovery values are obtained after running CMG GEM program and results obtained are shown in Figure 7.29. Effect of diffusion is also investigated by applying diffusion coefficient values of 10^{-6} cm²/sec and 10^{-5} cm²/sec. As it is seen in Figure 7.29, simulation results of recovery factors with diffusion reaches higher values than without diffusion case, although no much difference could be observed between the values of diffusion coefficient values of 10^{-6} cm²/sec and 10^{-5} cm²/sec.

Unlike Experiment-1, there is initial gas saturation in Experiment-2 carried with CO₂ injection. The existence of free gas space promotes the entrance of gas from the fracture into the matrix, as a result, recovery obtained from gas oil gravity drainage mechanisms become significant along with diffusion processes. As it is seen from Figure 7.29, n-decane recovery factor values from experimental study follow the same trend with simulation results till around 1063 hours.

Since there is initial gas saturation, the existence of free gas space promotes the entrance of gas from the fracture into the matrix. As a result, recovery obtained from gas oil gravity drainage mechanisms become significant until the time of 908 hours. After 908 hours, the dominant effect of gas oil gravity drainage starts to decrease and diffusion becomes to be more effective in the recovery process at the final stages of production, which can be indicated with a decrease in the rate of change of recovery. The reason for this decrease can be explained by the changes in the saturations of the reservoir fluids and relative permeability effect. Oil and gas saturation in fractures, which are spaced with a fracture spacing of 1×10^{-5} m in between matrix at 884, 908 and 932 hours is shown in Figure 7.30. As shown in Figure 7.30, oil saturation in fractures increases from Block 1,1,5 to Block 1,1,7 and then a region with constant oil saturation is observed till Block 1,1,30. It shows that there is a gas cap region at the uppermost blocks from Block 1,1,5 to Block 1,1,7. Also, at the lower blocks (Block 1,1,38 –Block 1,1,39) gas saturation in fracture is high. On the other hand, oil saturation in fractures in Blocks 1,1,7 and 1,1,38 is higher, showing that oil is accumulated within these Blocks, which have higher gas saturation in fracture. This results in a decrease in oil recovery at the final stages of production.

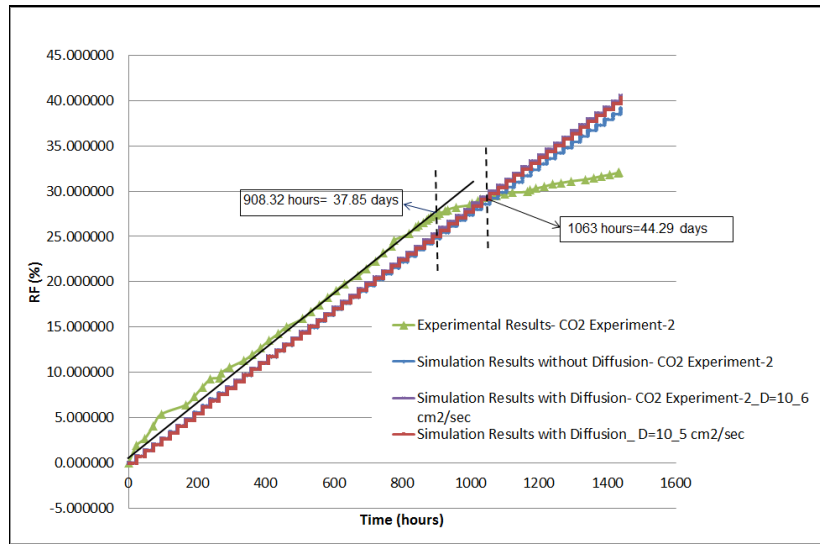


Figure 7. 29. Simulation Results with Diffusion for CO₂ Experiment-2

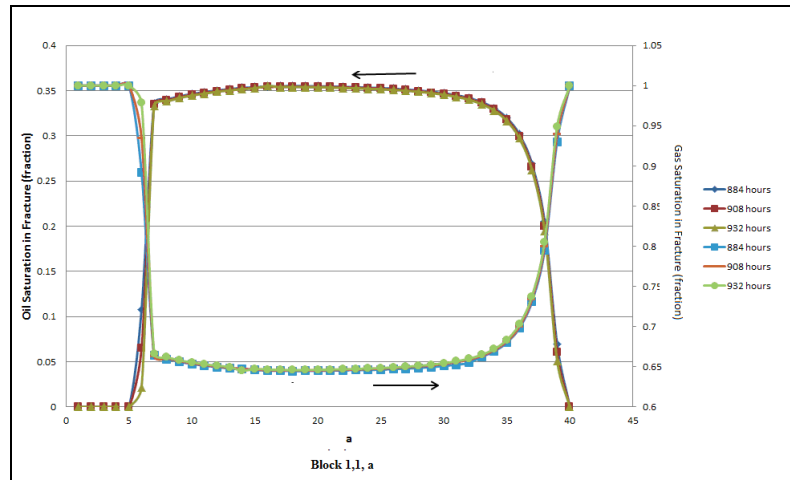


Figure 7. 30. Oil and Gas Saturation in Fractures with a Spacing of 1×10^{-5} m in Matrix at 884, 908 and 932 hours

For Experiment-2, oil and gas saturation distributions in matrix and fracture are also investigated. Oil saturation values in matrix and in fracture for 3 different blocks, namely, Block 1,1,2; Block 1,1,20 and Block 1,1,39 (Figure 7.31) are obtained in order to observe the change along the matrix vertically. Oil saturation values in matrix and in fracture are tabulated in Table 7.2 and shown in Figure 7.32 and 7.33. As shown in Figure 7.32, at the beginning of the simulation, there is a sharp decrease in the oil saturation in matrix and the highest decrease in oil saturation is observed in Block 1,1,2, which is the nearest block to the gas injection well Well-1.

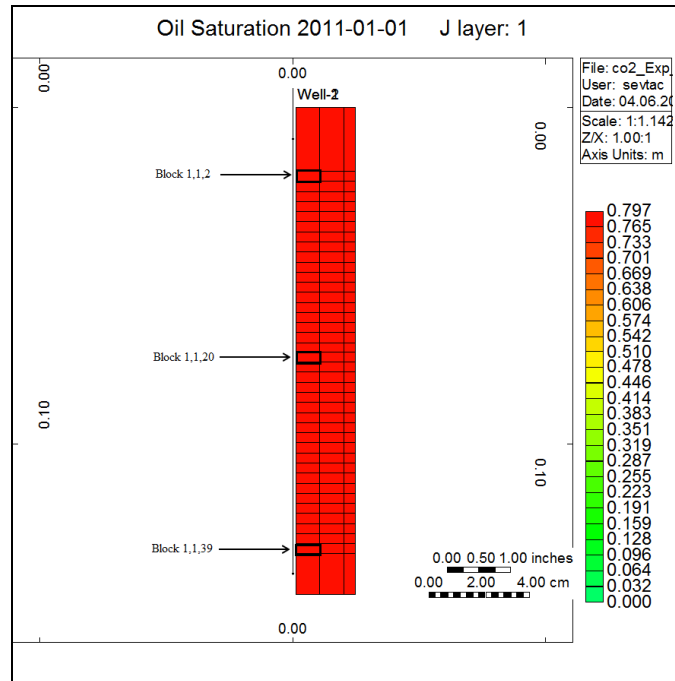


Figure 7. 31. Block 1,1,2; Block 1,1,20 and Block 1,1,39

Table 7. 2. Oil Saturation Values in Matrix and in Fracture

Time	Block 1,1,2		Block 1,1,20		Block 1,1,39	
	Oil Saturation (Matrix)	Oil Saturation (Fracture)	Oil Saturation (Matrix)	Oil Saturation (Fracture)	Oil Saturation (Matrix)	Oil Saturation (Fracture)
01.01.2011	0.797	0	0.797	0	0.797	0
02.01.2011	0.3515	0.3784	0.3515	0.3756	0.3515	0.3756
10.01.2011	0.3508	0	0.3514	0.3711	0.3514	0.3111
20.01.2011	0.3452	0	0.3514	0.3646	0.3514	0.2186
30.01.2011	0.3391	0	0.3514	0.3586	0.3514	0.1259
10.02.2011	0.3324	0	0.3514	0.3519	0.3514	0.0227
20.02.2011	0.3264	0	0.3514	0.3460	0.3514	0.0004
02.03.2011	0.3203	0	0.3514	0.3402	0.3514	0.0003

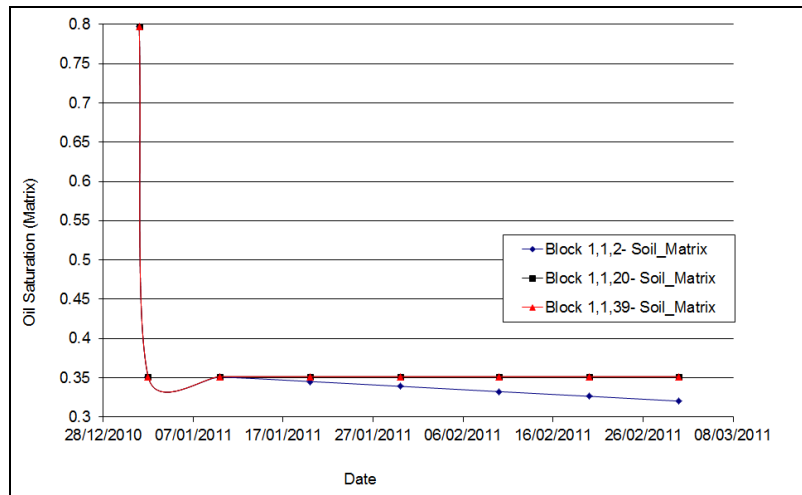


Figure 7. 32. Oil Saturation Values in Matrix for Block 1,1, 2; Block 1,1,20 and Block 1,1,39

Oil saturation changes in fractures, which are spaced with a fracture spacing of 1×10^{-5} m in between matrix blocks are shown in Figure 7.33. Oil saturation values sharply increase at the start of the simulation, however, they decrease during the simulation period for Block 1,1,2; Block 1,1,20 and Block 1,1,39. It indicates that as a result of gas oil gravity drainage process with the start of the gas injection, oil in the matrix blocks migrates into the fractures from the matrix and later on moves downward.

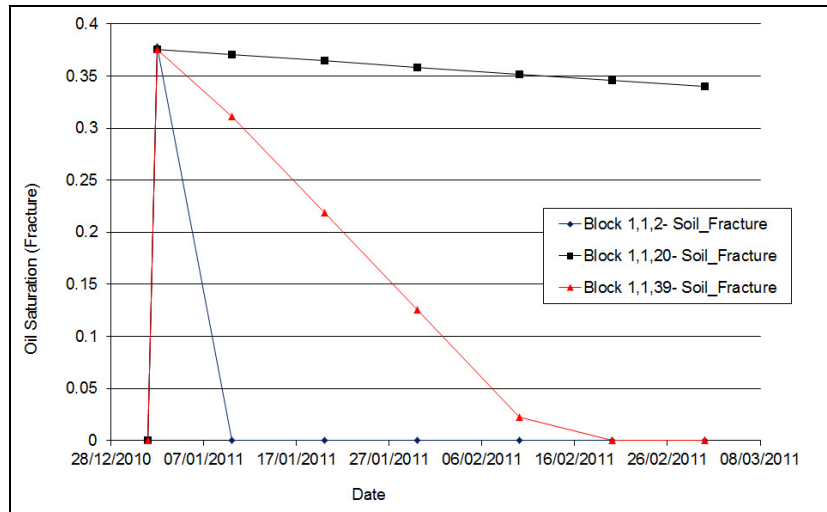


Figure 7. 33. Oil Saturation Values in Fracture for Block 1,1,2; Block 1,1,20 and Block 1,1,39

Gas saturation values in matrix and in fracture are tabulated in Table 7.3 and shown in Figure 7.34 and 7.35 for Block 1,1,2; Block 1,1,20 and Block 1,1,39. As shown in Figure 7.34, gas saturation values in matrix increases as the block gets close to the gas injection well Well-1. After a sharp increase in the gas saturation in the matrix at the beginning of the simulation, gas saturation values follows a constant value trend.

Table 7. 3. Gas Saturation Values in Matrix and in Fracture

Time	Block 1,1,2		Block 1,1,20		Block 1,1,39	
	Gas Saturation (Matrix)	Gas Saturation (Fracture)	Gas Saturation (Matrix)	Gas Saturation (Fracture)	Gas Saturation (Matrix)	Gas Saturation (Fracture)
01.01.2011	0	1	0	1	0	1
02.01.2011	0.4455	0.6216	0.4455	0.6216	0.4455	0.6244
10.01.2011	0.4462	1	0.4456	0.6289	0.4456	0.6889
20.01.2011	0.4518	1	0.4456	0.6352	0.4456	0.7814
30.01.2011	0.4579	1	0.4456	0.6414	0.4456	0.8741
10.02.2011	0.4646	1	0.4456	0.6481	0.4456	0.9773
20.02.2011	0.4706	1	0.4456	0.654	0.4456	0.9996
02.03.2011	0.4767	1	0.4456	0.6598	0.4456	0.9997

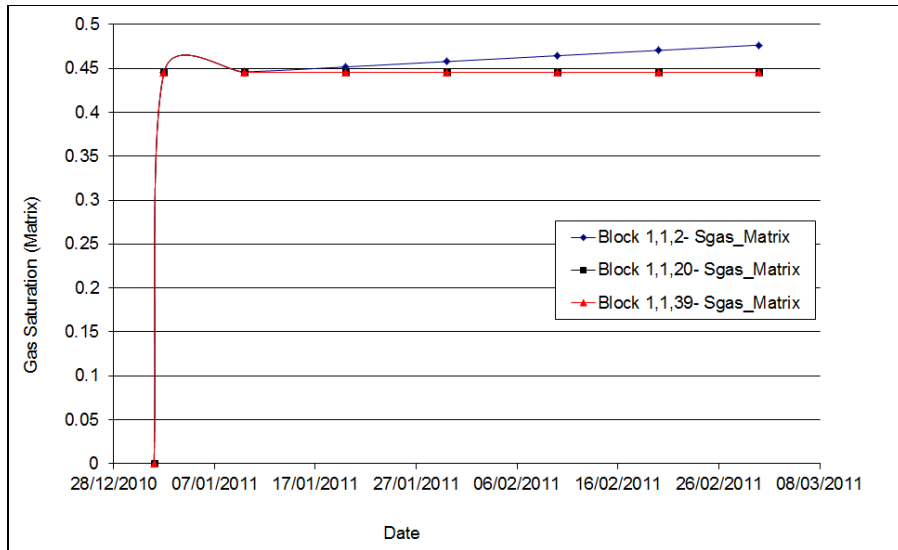


Figure 7. 34. Gas Saturation Values in Matrix for Block 1,1,2; Block 1,1,20 and Block 1,1,39

When gas saturation values in fracture for Block 1,1,2; Block 1,1,20 and Block 1,1,39 are investigated, it is seen that there is a higher increase in the gas saturation in fracture than in matrix as expected (Figure 7.35). A sharp decrease followed by a sharp increase in gas saturation in fracture is observed for Block 1,1,2 at the initial stages of the simulation. A slower but still high amount of gas saturation increase is seen for Block 1,1,39, while a slower rate of gas saturation increase is obtained for Block 1,1,20, which is at the middle of the core system.

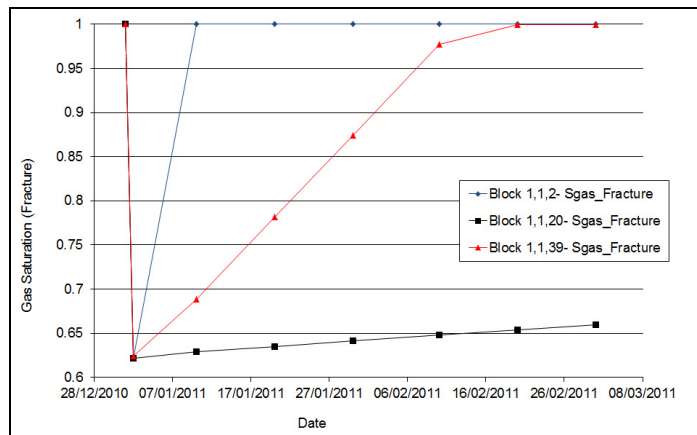


Figure 7. 35. Gas Saturation Values in Fracture for Block 1,1,2; Block 1,1,20 and Block 1,1,39

Figure 7.36 and Figure 7.37 shows changes of oil and gas saturation in fractures, which are spaced with a fracture spacing of 1×10^{-5} m in between matrix blocks for different time steps during the simulation. As time passes, oil saturation in fractures in the uppermost blocks decreases, while gas saturation in fractures in the uppermost blocks increases (Figure 7.36, Figure 7.37). A gas cap is formed in the uppermost blocks which gives rise to oil recovery resulted from gas oil gravity drainage mechanism.

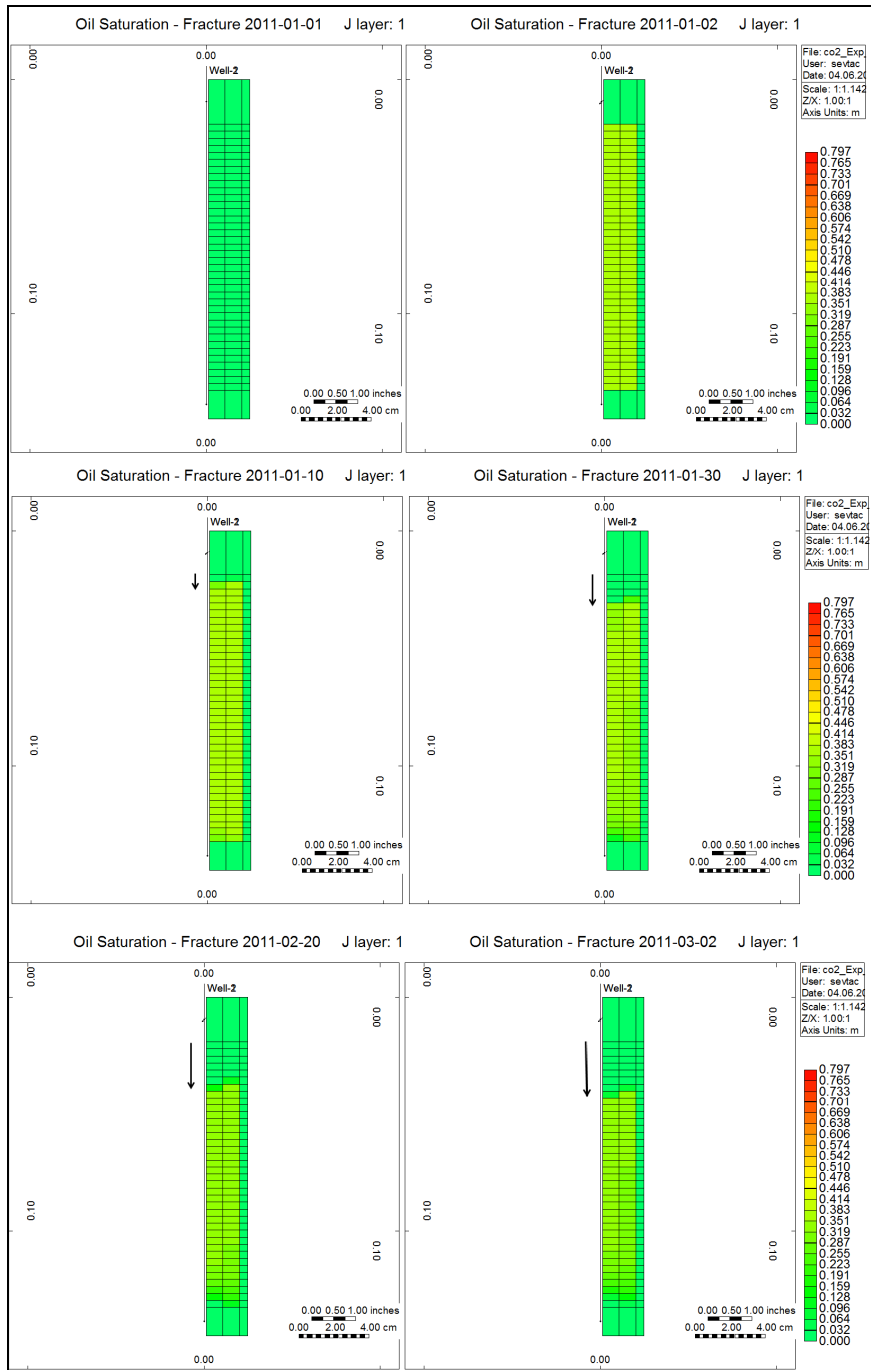


Figure 7. 36. Oil Saturation Distribution in Fractures

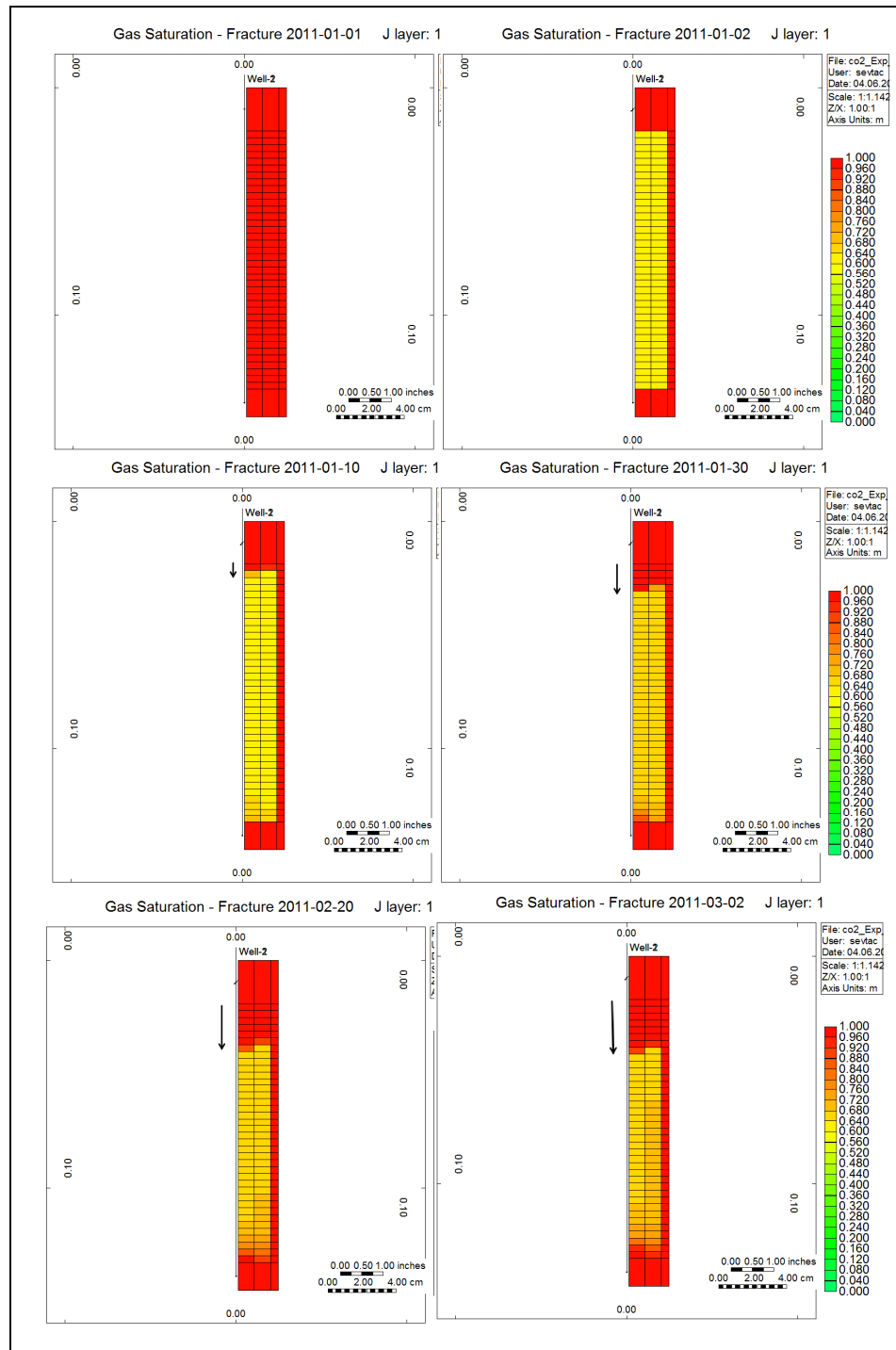


Figure 7. 37. Gas Saturation Distribution in Fractures

Change in oil and gas saturations in radial direction is also investigated at Layers 20 for 3 different blocks, namely, Block 1,1,20; Block 2,1,20 and Block 3,1,20 (Figure 7.38).

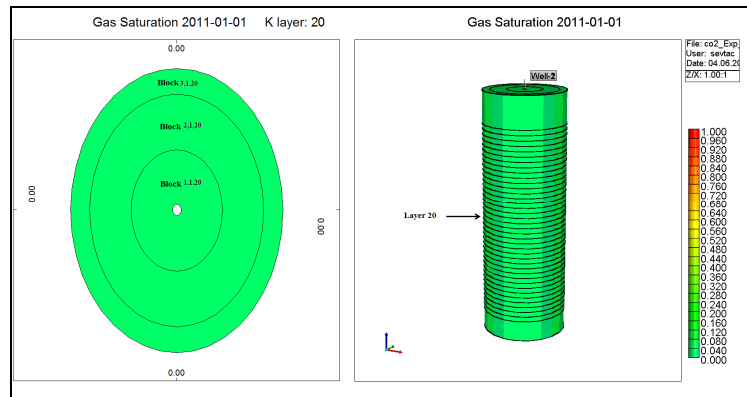


Figure 7. 38. Block 1,1,20; Block 2,1,20 and Block 3,1,20

Oil saturation in matrix decreases suddenly at the start of the simulation with the effect of gas injection. As the time passes the highest amount of oil saturation in matrix is observed for the Block 1,1,20 (Figure 7.39), which is the innermost block with the longest distance from the surrounding fracture.

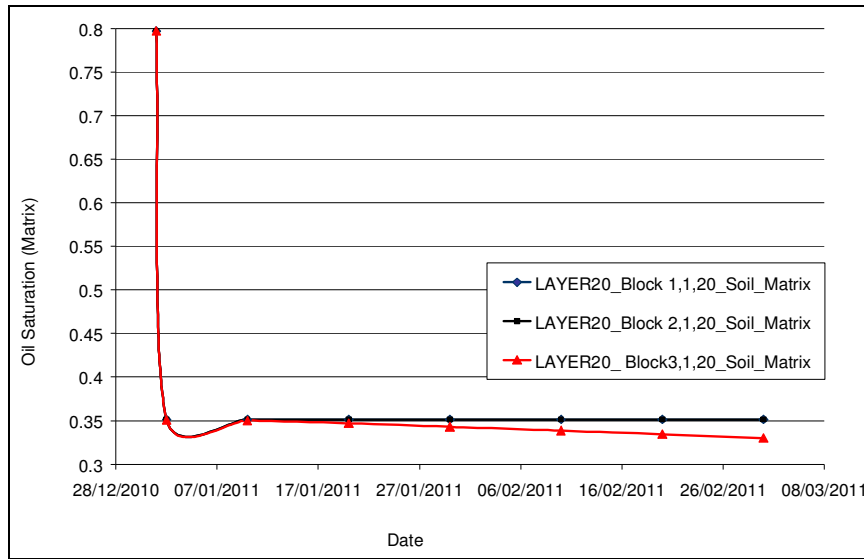


Figure 7. 39. Oil Saturation Values in Matrix for Block 1,1,20; Block 2,1,20 and Block 3,1,20 at Layer 20

When oil saturation in fracture is investigated, it is seen that the highest oil saturation is again obtained in the innermost Block 1,1,20 (Figure 7.40). The outermost Block 3,1,20, has the lowest oil saturation in fracture, since it may provide a flow path from matrix to the surrounding fracture for oil production.

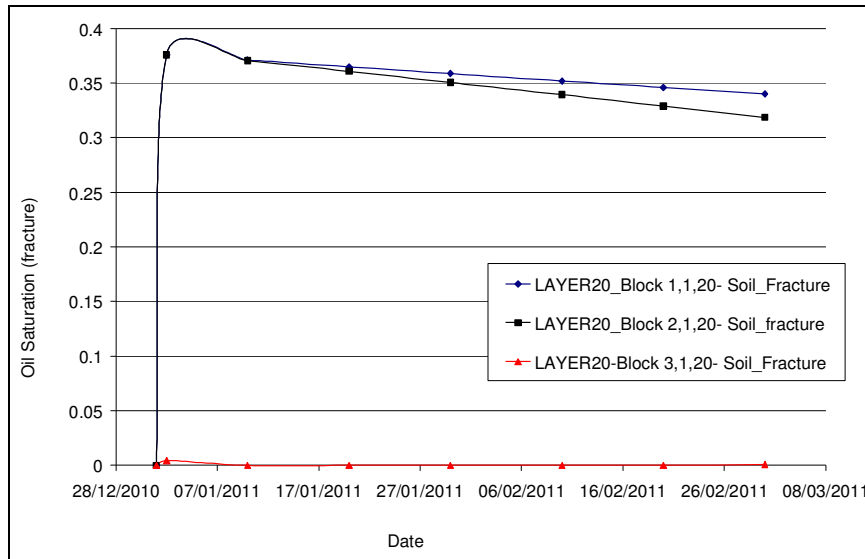


Figure 7. 40. Oil Saturation Values in Fracture for Block 1,1,20; Block 2,1,20 and Block 3,1,20 at Layer 20

Change in gas saturation in matrix and fracture for Block 1,1,20; Block 2,1,20 and Block 3,1,20 at Layer 20 is shown in Figure 7.41 and 7.42. It is indicated that there is sharp increase in gas saturation in matrix at the beginning of the simulation with gas injection. Gas saturation in fracture for the outermost Block 3,1,20 has a value of around 1 for all the stages of simulation as a result of that it is the closest block to the surrounding fracture that is full of gas.

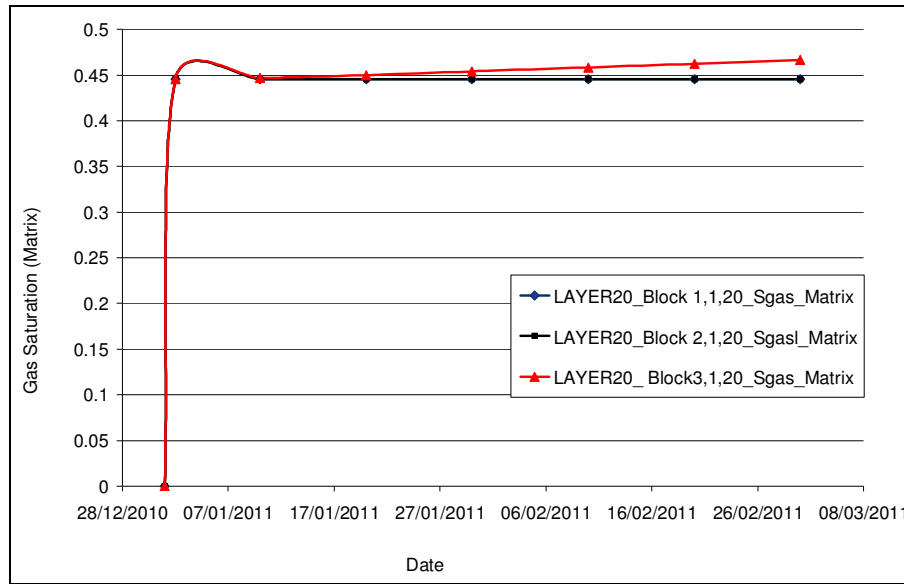


Figure 7. 41. Gas Saturation Values in Matrix for Block 1,1,20; Block 2,1,20 and Block 3,1,20 at Layer 20

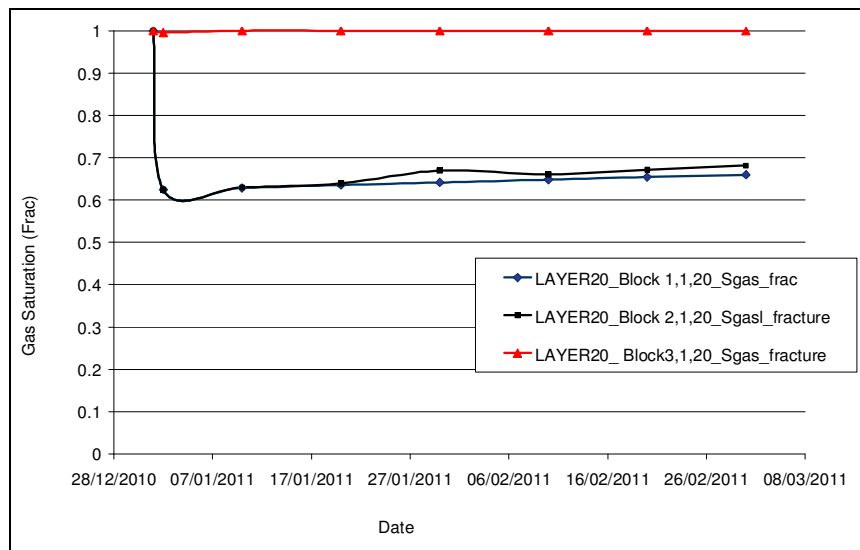


Figure 7. 42. Gas Saturation Values in Matrix for Block 1,1,2; Block 2,1,2 and Block 3,1,2 at Layer 2

For the simulation of the CH₄ experiment and N₂ experiment, radial grid systems are created with 3 divisions along the r direction and 3 layers along the k-direction as shown in Figure 7.43 and Figure 7.44.

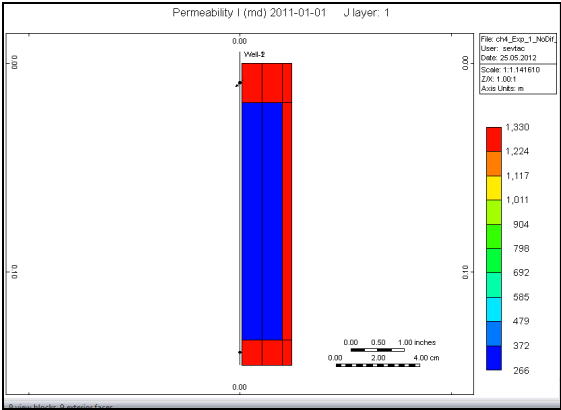


Figure 7. 43. Radial Grid System with 3 Divisions along the r Direction and 3 Layers along the K- Direction (Down) for Experiment-3

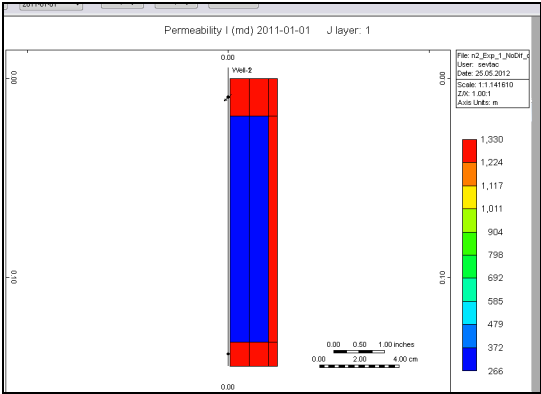


Figure 7. 44 .Radial Grid System with 3 Divisions along the r Direction and 3 Layers along the K- Direction (Down) for Experiment-4

n-decane recovery values are obtained after running CMG GEM program are shown in Figure 7.45 and Figure 7.46. Experimental results and simulation results without diffusion matches very well, including the sudden increase in the recovery at the beginning of the experiments in both CH₄ experiment and N₂ experiment. As in the Experiment-2, there is free space for gas initially and gravity drainage mechanism in the recovery is more pronounced, especially in the early stages of production showing a sharp increase in the recovery. n-decane recovery results for simulation increases as the diffusion coefficient value increases from 10⁻⁶ cm²/sec to 10⁻⁵ cm²/sec.

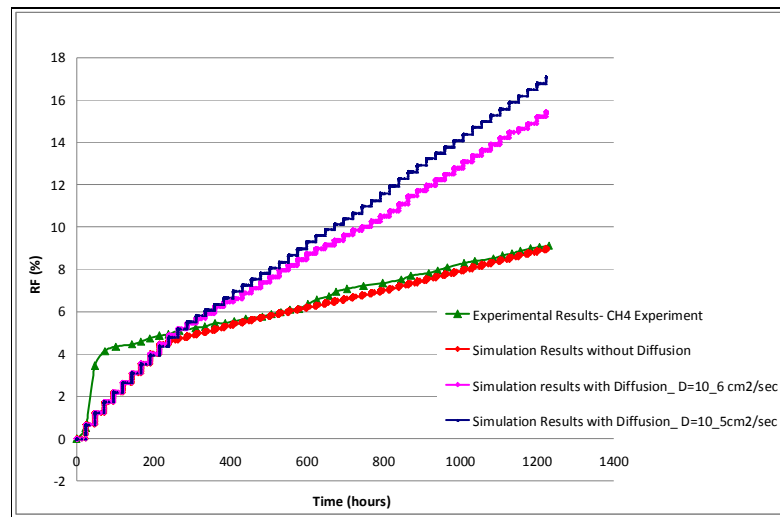


Figure 7. 45. Simulation Results with Diffusion for CH₄ Experiment-3

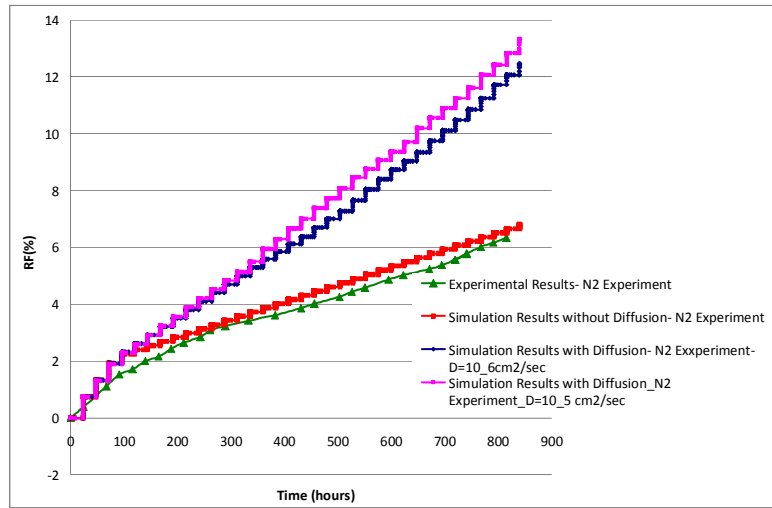


Figure 7. 46. Simulation Results without Diffusion for N₂ Experiment-4

CHAPTER 8

CONCLUSION

In this study, an experimental and modeling work is carried out to investigate matrix-fracture interaction mechanisms by the means of CO₂, CH₄ and N₂ and injection. The following concluding remarks are obtained:

- In the CO₂ injection test conducted with fully n-decane and brine saturated Berea sandstone core without initial gas saturation, the only available contact area for gas and reservoir fluids is the fracture surface. In that respect, diffusion should be the effective recovery process at the initial stage of production. For this reason, cumulative production of the first few days is very limited for the test.
- In the tests that run with an initial gas saturation, the entrance of high pressure gas into pore space is promoted. Entrance of gas into pore space will increase the effective contact area between gas and reservoir fluids and it results in a more efficient recovery mechanism.
- Recovery characteristics of Tests 2, 3 and 4 that have similar initial saturations are investigated in terms of the type of gas injected. It is observed that highest n-decane recovery is obtained with CO₂ followed by CH₄ and N₂ injection. The effective parameters for the difference in recovery with different gases are:

- Effect of solubility of CO₂, CH₄ and N₂ in n-decane at the conditions of the experiments: As gas phase dissolves in the oil, an increase in the liquid volume occurs and it results in oil swelling as well as a reduction in the viscosity of oil. CO₂ has the highest solubility in n-decane at the conditions of experiments compared with the solubilities of CH₄ and N₂ in n-decane. The highest value of the n-decane recovery is obtained in the CO₂ experiment.
 - As the oil becomes more saturated with CO₂, oil density increases which may cause a more efficient gas oil gravity drainage mechanism due to higher density difference between oil and gas phases.
 - Density and viscosity of n-decane- CH₄ mixture decrease as CH₄ mole fraction increases. Although the decrease in oil viscosity as CH₄ dissolves in oil favors the recovery of oil, the decrease in the density of oil weakens the effectiveness of gravity drainage mechanism. Consequently, higher n-decane recovery obtained in the CO₂ experiment compared to the CH₄ experiment may be resulted from the increase in oil density and corresponding increase in the density difference between matrix and fracture fluids in the CO₂ experiment, which is not obtained with CH₄.
 - Calculated densities of n-decane- CO₂, CH₄ and N₂ mixtures show that the smallest density difference is between n-decane-N₂ mixture and N₂ which may result with the least effective gas oil gravity drainage.
- Although the highest value of diffusion coefficient in n-decane belongs to CH₄ higher density difference of n-decane-CO₂ mixture with CO₂ gas should compensate for the diffusion effect resulting in a higher recovery in CO₂ experiments than CH₄ experiment.

- The higher n-decane recovery in the CH₄ experiment compared to the N₂ experiment may be both due to higher density difference between gas and mixture and higher diffusion coefficient obtained in the CH₄ experiment, concluded from the laboratory study.
- Simulation results for the CO₂ experiment carried out without initial CO₂ saturation indicates that the dominant recovery mechanism in the CO₂ experiment carried out without initial CO₂ saturation is diffusion from the initial stages to the end of the production.
- Results of simulation for the CO₂ experiment carried out with initial CO₂ saturation show that the dominant effect of gas oil gravity drainage starts to decrease and diffusion becomes to be more effective in the recovery process at the final stages of production, which can be indicated with a decrease in the rate of change of recovery.
- Investigation of oil and gas saturation distributions in matrix and fracture indicates an immediate and a sharp decrease in the oil saturation in matrix and of which the highest decrease in oil saturation is observed in the nearest block to the gas injection well Well-1.
- Oil saturation changes in fractures, which are spaced with a fracture spacing of 1×10^{-5} m in between matrix blocks show that oil in the matrix blocks migrates into the fractures in the matrix and later on moves downward along fracture as a result of gas oil gravity drainage process with the start of the gas injection.
- As time passes during the simulation, oil saturation in fractures, which are spaced with a fracture spacing of 1×10^{-5} m in between matrix blocks, in the uppermost blocks decreases, while gas saturation in fractures in the uppermost blocks increases. A gas cap is formed in the uppermost blocks,

which gives rise to oil recovery resulted from gas oil gravity drainage mechanism.

- When change in oil and gas saturations in r direction is investigated, it is obtained that oil saturation in matrix decreases suddenly at the start of the simulation with the effect of gas injection. As the time passes the highest amount of oil saturation in matrix is observed within the innermost block with the longest distance from the surrounding fracture.

CHAPTER 9

RECOMMENDATIONS

Recommendations for the following studies include the investigation of the effect of fracture width on the oil recovery during matrix-fracture interaction processes.

Experiments at various reservoir temperature and pressure values may be performed to investigate the corresponding effects of the conditions. Miscible recovery conditions with higher pressures could be obtained to investigate the effect of miscibility on the recovery mechanisms in fractured reservoirs.

Moreover, experiments of longer period of time may be performed to obtain the effect of diffusion process more effectively and to observe the required time interval for the completion of oil recovery.

REFERENCES

- Agilio, F. A.; Padua, A. H. Viscosity and density of mixtures of methane and n-decane from 298 to 393 K and up to 75 MPa. *Fluid Phase Equilibria*. **2004**, 216, 235-244.
- Ahmed, T.; McKinney, K. D. *Advanced Reservoir Engineering*; Gulf Professional Publishing, Elsevier: USA, 2005; pp 296-298.
- Alavian, S. A. and Whitson, C. H. Modeling CO₂ Injection in a Fractured Chalk Experiment. *SPE/ EAGE Reservoir Characterization and Simulation Conference held in Abu Dhabi, UAE, SPE 125362*. **2009**, 1-10.
- Anderson et al. Clay Swelling- A Challenge in the Oilfield. *Earth Science Reviews*. **2010**, 98, 201–216.
- Asghari, K. and Torabi, F. Effect of Miscible and Immiscible CO₂ Flooding on Gravity Drainage: Experimental and Simulation Results. *SPE 110587*. **2008**, 1-9.
- Ayatollahi, S.; Boukadi, F.; Wadhai, M.; Maamari, R. and Bemani, A. Investigation of Thermal Gas-Oil Gravity Drainage (GOGD) in Fractured Carbonate Reservoirs. *SPE 93585*. **2005**, 1-6.
- Azarnoosh, A.; McKetta, J. J. Nitrogen-n-Decane System in the Two-Phase Region. *Journal of Chemical and Engineering Data*. **1963**, Vol. 8, No. 4, 494-496.
- Barenblatt, G. I.; Zheltov, Iu. P. and Kochina, I. N. Basic Concepts in the Theory of Seepage of Homogeneous Liquids in Fissured Rocks (Strata). *Journal of Applied Mathematics and Mechanics*. **1960**, Vol. 24, Issue 5, 1286-1303.
- Batemann, K. et al. Large- Scale Column Experiment: Study of CO₂, Porewater, Rock Reactions and Model Test Case. *Oil & Gas Science and Technology– Rev. IFP*. **2005**, Vol. 60, No. 1, 161-175.
- Bagci, S. and Gumrah, F. Effects of CO₂ and CH₄ Addition to Steam on Recovery of West Kozluca Heavy Oil. *Thermal Operations and Heavy Oil Symposium and Western Regional Meeting held in Bakersfield, California, USA, SPE 86953*. **2004**, 1-13.

Bank, G. C.; Riestenberg, D. And Koperna, G. J. CO₂- Enhanced Oil Recovery Potential of the Appalachian Basin. *SPE Eastern Regional Meeting held in Lexington, Kentuck, USA, SPE 11282*. **2007**, 1-11.

Beaudoin, M. J. and Kohn, J. P. Multiphase and Volumetric Equilibria of the Methane-n-Decane Binary System at Temperatures between -36° and 150 °C. *Journal of Chemical and Engineering Data*. **1967**, Vol. 12, No.2, 189-161.

Bech, N.; Jensen, O. K. and Nielsen, B. Modeling of Gravity- Imbibition and Gravity-Drainage Processes: Analytic and Numerical Solutions. *SPE 18428*. **1991**, 129- 136.

Bird, R. B.; Stewart, W. E. and Lightfoot, E. N. *Transport Phenomena*, 2nd ed.;John Wiley & Sons, Inc.: USA, 2002; Chapter 17.

Cardwell, Jr., W. T.; Parsons, R. L. Gravity Drainage Theory. *Petroleum Technology, TP 2464*. **1948**, 199-215.

Calhoun, J. C. Jr. *Fundamentals of Reservoir Engineering*; University of Oklahoma Press: USA, 1955; pp 300-313.

Chatzis, I.; Kantzas, A. and Dullien, F. A.L. On the Investigation of Gravity-Assisted Inert Gas Injection Using Micromodels, Long Berea Sandstone Cores, and Computer-Assisted Tomography. *SPE 18284*. **1988**, 223-234.

Chordia, M.; Trivedi, J. J. Diffusion in Naturally Fractured Reservoirs- A Review. *SPE Asia Pacific Oil & Gas Conference and Exhibition held in Brisbane, Queensland, Australia, SPE 134589*. **2010**, 1-32.

Clemens, T.; Wit, K. The Effect of Fracture Spacing on Gas/Oil Gravity Drainage in Naturally Fractured Reservoirs. *SPE Annual Technical Conference and Exhibition held in New Orleans, Louisiana, SPE 71507*. **2001**, 1-7.

Cole, F. W. *Reservoir Engineering Manual*; Gulf Publishing Company: Houston, 1969; Chapter 7.

Culllck, A. S. and Mathls M. L. Densities and Viscosities of Mixtures of Carbon Dioxide and n-Decane from 310 to 403 K and 7 to 30 MPa. *Journal of Chemical and Engineering Data*. **1984**, Vol. 29, No. 4, 393-396.

da Silva, F. V.; Belery, P. Molecular Diffusion in Naturally Fractured Reservoirs: A Decisive Recovery Mechanism. 64th Annual Technical Conference and Exhibition of SPE held in San Antonio, TX, *SPE 19672*. **1989**, 429-442.

Darvish, G. R.; Lindeberg, E.; Holt, T. and Utne, S. A. Laboratory Experiments of Tertiary CO₂ Injection into a Fractured Core. *SPE/DOE Symposium on Improved Oil Recovery held in Tulsa, Oklahoma, U.S.A, SPE 99649*. **2006**, 1-7.

Denoyelle, L.; Bardon, C. and Couve de Murville. Interpretation of a CO₂/ N₂ Injection Field Test in a Moderately Fractured Carbonate Reservoir. *SPE 14942*. **1988**, 220-226.

Domenico, P. A.; Schwartz, F. W. *Physical and Chemical Hydrogeology*, 2nd ed.; John Wiley & Sons, Inc.: New York, 1998; Chapter 10.

Donato, G. D.; Tavassoli, Z. and Blunt, M. J. Analytical and Numerical Analysis of Oil Recovery by Gravity Drainage. *Journal of Petroleum Science and Engineering*. **2006**, 54, 55-69.

Dykstra, H. The Prediction of Oil Recovery by Gravity Drainage. *SPE 6548*. **1978**, 818-830.

Egermann, P.; Bazin, B. and Vizika, O. An Experimental Investigation of Reaction-Transport Phenomena During CO₂ Injection. 14th *SPE Middle East Oil & Gas Show and Conference held in Bahrain, SPE 93674*. **2005**, 1-10.

Fung, L. S.-K. Simulation of Block-to-Block Processes in naturally Fractured Reservoirs. *SPE 20019*. **1991**, 477-484.

Fernø, M. A. et al. Impacts from Fractures on Oil Recovery Mechanisms in Carbonate Rocks at Oil-Wet and Water-Wet Conditions- Visualizing Fluid Flow across Fractures with MRI. *International Oil Conference and Exhibition in Mexico held in Veracruz, Mexico, SPE 108699*. **2007**, 1-8.

GEM User's Guide, Advanced Compositional Reservoir Simulator, Version 2007, Computer Modelling Group.

Gilman, J. R. and Kazemi, H. Improvements in Simulation of Naturally Fractured Reservoirs. *SPE 10511*. **1983**, 695-707.

Green, D. W. and Willhite, G. P. *Enhanced Oil Recovery*. Henry L. Doherty Memorial Fund of AIME, Society of Petroleum Engineers: Richardson, Texas, 1998; Chapter 6.

Grigg, R. B.; Svec, R. K. CO₂ Transport Mechanisms in CO₂/ Brine Coreflooding. *SPE Annual Technical Conference and Exhibition held in San Antonio, Texas, SPE 103228*. **2006**, 1-10.

- Goncuoglu, M. C. Geology-Geophysics Research Center Minerological-Petrographic Analyses Report 10-03-09-583. 2010.
- Gümrah, F. The Use of Steam-CO₂ Process in Linear and Three Dimensional Unconsolidated Limestone Models for Heavy Oil Recovery. Ph.D. Thesis, Middle East Technical University, Petroleum and Natural Gas Engineering, June 1988.
- Hagoort, J. Oil Recovery by Gravity Drainage. *Society of Petroleum Engineers Journal*. **1980**, 139-150.
- Hall, H. N. Analysis of Gravity Drainage. *SPE 1517-G*. **1961**, 927-936.
- Holm, L. W. CO₂ Flooding: Its Time Has Come. *SPE 11592*. **1982**, 2739-2745.
- Holm, L. W. and Josendal, V. A. Mechanisms of Oil Displacement by carbon Dioxide. *Journal of Petroleum Technology, SPE 4736-PA*. **1974**, Vol. 26, No. 12, 1427-1438.
- Hoteit, H. Proper Modeling of Diffusion in Fractured Reservoirs. *The SPE Reservoir Simulation Symposium held in The Woodlands, Texas, USA, SPE 141937*. **2011**, 1-22.
- Hujun L.; Putra, E.; Schechter, D. S. and Grigg, R. B. Experimental Investigation of CO₂ Gravity Drainage in a Fractured System. *SPE Asia Pacific Oil and Gas Conference and Exhibition held in Brisbane, Australia, SPE 64510*. **2000**, 16–18.
- Jamili, A.; Willhite, G. P. and Green, D. W. Modeling Gas- Phase Mass Transfer Between Fracture and Matrix in Naturally Fractured Reservoirs. *SPE Western Regional Meeting held in Anaheim, California, USA, SPE 132622*. **2010**, 1-13.
- Johnson, E. F.; Bossler, D. P. and Naumann, V. O. Calculation of Relative Permeability from Displacement Experiment. *SPE 1023-G*. **1959**, 370-372.
- Karpyn, Z. T.; Grader, A. S and Halleck, P. M. Visualization of Fluid Occupancy in a Rough Fracture Using Micro-Tomography. *Journal of Colloid and Interface Science*. **2007**, 307, 181–187.
- Kazemi et al. Numerical Simulation of Water-Oil Flow in Naturally Fractured Reservoirs. *SPE 5719*. **1976**, 317-326.
- Kazemi, H.; Gilman J. R. and Elsharkawy, A. M. Analytical and Numerical Solution of Oil Recovery From Fractured Reservoirs with Emprical Transfer Functions. *SPE 19849*. **1992**, 219-227.
- Kazemi, A.; Jamialahmadi, M. The Effect of Oil and Gas Molecular Diffusion in Production of fractured Reservoir During Gravity Drainage Mechanism by CO₂

Injection. *SPE EUROPEEC/ EAGE Annual Conference and Exhibition held in Amsterdam, The Netherlands, SPE 120894*. **2009**, 1-12.

Killie, S. et al. High-Pressure Diffusion Measurements by Mach- Zehnder Interferometry. *AIChE Journal*. **1991**, Vol. 37, No.1, 142-146.

Klinkenberg, L. J. The Permeability of Porous Media to Liquids and Gases. *Drilling and Production Practice, American Petroleum Inst.* **1941**, 200–213.

Kulkarni, M. M. Multiphase Mechanisms and Fluid Dynamics in Gas Injection Enhanced Oil Recovery Processes. PhD Dissertation, Craft and Hawkins Department of Petroleum Engineering, 2005.

Ladron de Guevara Torres, J. E.; Rodriguez-da la Garza, F.; Galindo-Nava, A. Gravity Drainage and Oil Reinfiltration Modeling in Naturally Fractured Reservoir Simulation. *SPE International Oil Conference and Exhibition held in Veracruz, Mexico, SPE 108681*. **2007**, 27–30.

Lake, L. W. *Enhanced Oil Recovery*; Prentice-Hall, Inc.: United States of America, 1989; Chapter 7.

Latil, M; Bardon, C.; Burger, J. and Sourieau, P. *Enhanced Oil Recovery*; Gulf Publishing Company: Houston, Texas, 1980; Chapter 4.

Lewis, J. O. Gravity Drainage in Oil Fields. *Petroleum Transactions, AIME, SPE 944133-G*. **1944**, 155, 133-154.

Li, K. and Horne, R. N. Modeling of Oil Production by Gravity Drainage. *Journal of Petroleum Science and Engineering*. **2008**, 60, 161- 169.

Luan, Z. Some Theoretical Aspects of Gravity Drainage in Naturally Fractured Reservoirs. *69th Annual Technical Conference and Exhibition of SPE held in New Orleans, Louisiana, SPE 28641*. **1994**, 357-366.

Mangalsingh, D. and Jagai, T. A laboratory Investigation of the Carbon Dioxide Immiscible Process. *The Fourth Latin American and Caribbean Petroleum Engineering Conference held in Port-of-Spain, Trinidad & Tobago, SPE 36134*. 1996, 591-601.

McCain, Jr. W. D. *The Properties of Petroleum Fluids*, 2nd ed.; PennWell Publishing Company: Tulsa, Oklahoma, 1990; Appendix A.

METU, Middle East Technical University, Petroleum Research Centre, Batu Raman Sahası Buhar Enjeksiyonu Laboratuvar Araştırması, in Turkish, supported by Turkish Petroleum Corporation, 2001-2002.

Merck-Chemicals Web Site. http://www.merck-chemicals.com/united-kingdom/n-decane/MDA_CHEM-803405/p_Ijqb.s1LvKMAAAEWd.EfVhTI
(accessed November 2011)

Muskat, M. *Physical Principles of Oil Production*, 2nd ed., Reprint of 1949 ed; International Human Resources Development Corporation: Boston, 1981; Chapter 10.

Nabipour, M. et al. Laboratory Investigation of Thermally-Assisted Gas-Oil Gravity Drainage for Secondary and Tertiary Oil Recovery in Fractured Models. *Journal of Petroleum Science and Engineering*. **2007**. 55, 74-82.

Nenniger, Jr. E.; Storrow, J. A. Drainage of packed Beds in Gravitational and centrifugal-force Fields. *A. I. Ch.E. Journal*. **1958**. Vol.4, No.3, 305-316.

NIST Chemistry WebBook. National Institute of Standards and Technology, Agency of the U.S. Department of Commerce.
<http://webbook.nist.gov/chemistry/name-ser.html>
(accessed November 2011)

Oedai, S. and van Wunnik, J. Experimental Investigation of the Gas-oil Drainage Performance of Water Flooded Rock. *Shell, SCA2002-04*. **2002**. 1-12.

Orr Jr., F. M. and Jensen, C. M. Interpretation of Pressure- Composition Phase Diagrams for CO₂/ Crude Oil Systems. *SPE 11125-PA*. **1984**. Vol. 24, No. 5, 485-497.

Peng, D. and Robinson, D. B. A New Two-Constant Equation of State. *Ind. Eng. Chem., Fundam.* **1976**, Vol. 12, No. 1, 59-64.

Pirson, S. J. Performance of Fractured Oil Reservoirs. *AAPG Bulletin*. **1953**. Vol. 37, Issue 2, 232-244.

Pirson, S. J. *Oil Reservoir Engineering*; McGraw-Hill Book Company, Inc: USA, 1958; pp 658-693.

Rangel-German, E.; Akin, S. and Castanier, L. Multiphase-Flow Properties of Fractured Porous Media. *SPE Western Regional Meeting held in Anchorage, Alaska, SPE 54591*. **1999**, 1-14.

Rao, D. N.; Ayirala, S. C., Kulkarni, M. M. and Sharma, A. P. Development of Gas Assisted Gravity Drainage (GAGD) Process for Improved Light Oil Recovery. *SPE/ DOE Fourteenth Symposium on Improved Oil Recovery held in Tulsa, Oklahoma, U.S.A.* **2004**, 1-12.

Reamer, H. H.; Sage, B. H. Phase Equilibria in Hydrocarbon Systems. Volumetric and Phase Behaviour of the n-Decane- CO₂ System. *Journal of Chemical and Engineering Data*. **1963**, Vol. 8, No.4, 508-513.

Reiss, L. H. *The Reservoir Engineering Aspects of Fractured Formations*; Gulf Publishing Company: Houston, Texas, 1980; pp 1-108.

Reiss, L. H.; Bossie-Codreanu, D. N. and Lefebvre Du Prey, E. J. Flow in Fissured Reservoirs. *American Institute of Mining, Metallurgical and Petroleum Engineers, SPE 4343*. **1973**. 1-16.

Renner, T. A. Measurement and Correlation of Diffusion Coefficients for CO₂ and Rich- Gas Applications. **1988**. 517-523.

Shariatpanahi, S. F. et al. Visualization Experiments on Immiscible Gas and Water Injection by Using 2D-Fractured Glass Micromodels. *SPE 93537*. **2005**, 1-9.

Sadaghiani, V. R. Determination of the Effects of Carbon-dioxide on the Physical Characteristics of Garzan Crude Oil. M.S. Thesis, Middle East Technical University, Petroleum and Natural Gas Engineering, March 1992.

Saidi, A. M. *Reservoir Engineering of Fractured Reservoirs- Fundamental and Practical Aspects*; TOTAL Edition Presse, Paris, 1987; pp 499-684.

Sajadian, V. A.; Danesh, A. Laboratory Studies of Gravity Drainage Mechanism in Fractured Carbonate Reservoir- Capillary Continuity. *SPE 49497*. **1998**, 267-274.

Schechter, D. S.; Guo, B. Mathematical Modeling of Gravity Drainage After Gas Injection into Fractured Reservoirs. *SPE Improved Oil Recovery Symposium held in Tulsa, Oklahoma, SPE/DOE 35170*. **1996**, 23-35.

Sener, I. Relative Diffusion Flux: A Practical Concept for Characterizing Fracture to Matrix Gas Transfer—Application to Fractured Reservoir Model. *61st Annual Technical Conference and Exhibition of the Society of Petroleum Engineers held in NewOrleans, LA, SPE 15522*. **1986**, 1-12.

Sharma, K. R. *Principles of Mass Transfer*; Prentice-Hall of India Private Limited, New Delhi, 2007; Chapter 1.

Simon, R. and Graue, D.J. Generalized Correlations for Predicting Solubility, Swelling and Viscosity Behavior of CO₂ -Crude Oil Systems. *Journal of Petroleum Technology, SPE 917-PA*. **1965**, Vol. 17, No. 1, 102-106.

Spivak, A.; Karaoguz, D. and Issever, K. Simulation of Immiscible CO₂ Injection in a Fractured Carbonate Reservoir, Batı Raman Field, Turkey. *SPE California Regional Meeting held in Bakersfield, California, SPE 18765*. **1989**, 170-192.

Srivastan, S; Darwish, N. A.; Gasem, K. A. M. and Rabinson, Jr. R. L. Solubility of Methane in Hexane, Decane, and Dodecane at Temperatures from 311 to 423 K and Pressures to 10.4 Mpa. *Journal of Chemical and Engineering Data*. **1992**, Vol. 37, No. 4, 516-520.

Stalkup Jr., F. I. *Miscible Displacement*; Henry L. Doherty Memorial Fund of AIME, Society of Petroleum Engineers of AIME: 1983; pp 1-30.

Sumnu, M. D.; Aziz, K.; Brigham W. E and Castanier, L. M. Use of Simulators in the Design of an Experiment for Steam Injection into a Fractured System. *SPE/DOE Tenth Symposium on Improved Oil Recovery held in Tulsa, Oklahoma, USA, SPE/DOE 27742*. **1994**, 49-60.

Sumnu, M. D.; Brigham W. E.; Aziz, K. and Castanier, L. M. An Experimental and Numerical Study on Steam Injection in Fractured Systems. *SPE/DOE Tenth Symposium on Improved Oil Recovery held in Tulsa, Oklahoma, SPE/DOE 35459*. **1996**, 591-601.

Thomas, L. K.; Dixon, T. N. and Pierson, R. G. Fractured Reservoir Simulation. *Society of Petroleum Engineers Journal, SPE 9305*. **1983**, 42-54.

Tian, S. and He, S. Investigating the Effect of Steam, CO₂, and surfactant on the Recovery of Heavy Oil Reservoirs. *SPE International Thermal Operations and Heavy Oil Symposium held in Calgary, Alberta, Canada, SPE/PS/CHOA 117394*. **2008**, 1-12.

Torabi, F. and Asghari, K. Effect of Connate Water Saturation, Oil Viscosity and Matrix Permeability on Rate of Gravity Drainage During Immiscible and Miscible Displacement Tests in matrix-Fracture Experimental Model. *Journal of Canadian Petroleum Technology*. **2010**, Vol.49, No. 11, 61-67.

Torabi, F. and Asghari, K. Simulation of Oil Recovery by Gravity Drainage Mechanism during Immiscible and Miscible CO₂ Injection. 8th World Congress of Chemical Engineering, **2009**, 1-6.

Trivedi, J. J. and Babadagli, T. Experimental Analysis of CO₂- Sequestration Efficiency During Oil Recovery in Naturally Fractured Reservoirs. *SPE Eastern Regional/ AAPG Eastern Section Joint Meeting held in Pittsburg, Pennsylvania, USA, SPE 117607*. **2008**, 1-16.

TPAO Research Center Core Analysis Report 3578. 2011.

Turkmenoglu, A. S. Geology-Geophysics Research Center Quantative Clay Mineral Analyses Report 10-03-09-584. 2010.

Warren, J. E. and Root, P. J. The Behaviour of Naturally Fractured Reservoirs. *Society of Petroleum Engineers Journal, SPE 426*. **1963**, Vol.3, No.3, 245-255.

WinProp User's Guide, Version 2007, Computer Modelling Group.

Wu, Y. and Pruess, K. A Multiple Porosity Method for Simulation of Naturally Fractured Petroleum Reservoirs. *SPE 15129*. **1988**, 327-336.

Van Golf-Racht, T. D. *Fundamentals of Fractured Reservoir Engineering*; Elsevier Scientific Publishing Company: The Netherlands, 1982; pp 465-640.

Varotsis, N., Stewart, G., Todd, A. C. and Clancy M.: Phase Behavior of Systems Comprising North Sea Reservoir Fluids and Injection Gases. *Journal of Petroleum Technology*. **1986**, 1221-1233.

Yanze, Y.; Clemens, T. The Role of Diffusion for Non-Miscible Gas Injection into a Fractured Reservoir. *SPE EUROPEC/ EAGE Annual Conference and Exhibition held in Vienna, Austria, SPE 142724*. **2011**, 1-18.

Yellig, W. F. and Metcalfe, R.S. Determination and Prediction of CO₂ Minimum Miscibility Pressures. *Journal of Petroleum Technology, SPE 7477*. **1980**, Vol. 32, No. 1, 160-168.

Zahra, R.; Fariborz, R. Sensitivity Analysis of Cumulative Oil Production and Production Rate on B Lock Heights and Capillary Continuity for an Iranian Carbonated Fractured Reservoir. *Iran. J. Chem. Chem. Eng.*. **2009**, Vol. 28, No.3, 15-23.

Zendehboudi, S.; Mohammadzadeh, O.; Chatzis, I. Experimental Study of Controlled Gravity drainage in Fractured Porous Media. *Proceedings of the Canadian International Petroleum Conference, Paper 2009-186*. **2009**, 1-27.

APPENDIX A

SPECIFICATIONS OF N-DECANE

Table A. 1. Specifications of n-decane (Merck-Chemicals, 2011)

n-decane	
Hill Formula	C ₁₀ H ₂₂
Chemical formula	CH ₃ (CH ₂) ₈ CH ₃
HS Code	2901 10 00
EC number	204-686-4
Molar mass	142.28 g/mol
CAS number	124-18-5
Chemical and Physical Data	
Ignition temperature	208 °C
Solubility	0.00005 g/l (25 °C)
Saturation concentration (air)	11 g/m ³ (20 °C) Air
Melting point	-30 °C
Molar mass	142.28 g/mol
Density	0.73 g/cm ³ (20 °C)
Boiling point	174 °C
Vapor pressure	1 hPa (16 °C)
Explosion limit	0.7 - 5.4 %(V)
Flash point	51 °C
Viscosity kinematic	< - 7 mm ² /s (40 °C)

Table A. 1. Specifications of n-decane (Continued) (Merck-Chemicals Site, 2011)

Safety Information according to GHS	
Hazard Statement(s)	H226: Flammable liquid and vapour. H304: May be fatal if swallowed&enters airways.
Precautionary Statement(s)	P210: Keep away from heat. P260: Do not breathe vapour. P262: Do not get in eyes, on skin, or on clothing. P301 + P310: IF SWALLOWED: Immediately call a POISON CENTER or doctor/ physician. P331: Do NOT induce vomiting.
Hazard Pictogram(s)	
Storage class	3 Flammable Liquids
WGK	WGK 3 highly water endangering
Disposal	1 Strongly contaminated halogen-free organic solvents: container A.
R Phrase	R 10-65 Flammable.Harmful: may cause lung damage if swallowed.
S Phrase	S 23-24-62 Do not breathe vapour.Avoid contact with skin.If swallowed, do not induce vomiting: seek medical advice immediately and show this container or label.
Categories of danger	flammable, harmful
Hazard Symbol	 Harmful

Table A. 1. Specifications of n-decane (continued) (Merck-Chemicals Web Site, 2011)

Transport information	
Declaration (railroad and road) ADR, RID	UN 2247 n-Decan, 3, III
Declaration (transport by sea) IMDG-Code	UN 2247 N-DECANE, 3, III
Declaration (transport by air) IATA- DGR	UN 2247 N-DECANE, 3, III
Toxicological data	
LD 50 oral	LD50 rat > 5000 mg/kg
LD 50 dermal	LD50 rat > 2000 mg/kg

APPENDIX B

SPECIFICATIONS OF THE EQUIPMENT USED IN THE EXPERIMENTAL SET-UP

Table B. 1. Specifications of the Equipment Used in the Experimental Set-Up

Equipment	Specifications
Core Holder used in the brine saturation system	Trademark: Manufactured at the Department of Petroleum & Natural Gas Eng. at METU Material: Brass Inner diameter: 6 cm Length: 15 cm
Core Holder used in the n-decane saturation system	Trademark: TEMCO Material: Stainless Steel Inner Diameter: 3.81 cm Length: 19 cm
Core Holders (× 2) used in the gas injection system	Trademark: EPS Core Systems Design Pressure: 11,000 psig Design Temperature: 50 °C Inner Diameter: 4.7 cm Length: 15.8 cm
Thermocouple	Trademark: Elimko, Turkey R/T 1×Pt-100

Table B. 1. Specifications of the Equipment Used in the Experimental Set-Up
(Continued)

Equipment	Specifications
<p>Pressure Transducer (× 3) used in the saturation system</p>	<p>Trademark: GEMS Sensors, England Supply: 7- 35 Vdc Output: 4-20 mA Range: 25 barg</p>
	<p>(× 2) Trademark: GEMS Sensors, England Range: 25 barg Output. 0-40 mV</p>
<p>Pressure Transducer (× 2) used in the gas injection system</p>	<p>Trademark: GEMS Sensors, England Supply: 7- 35 Vdc Output: 4- 20 mA Pressure Range: 0- 100 bar G</p>
	<p>Trademark: GEMS Sensors, England Supply: 7- 35 Vdc Output: 4- 20 mA Pressure Range: 60 bar G</p>
<p>Data Logger and Controller used in the saturation system</p>	<p>Trademark: Elimko, Turkey Model: E- 680 Voltage: 220 V Data Transfer: RS485 Mod Bus Data Analysis: Software by Elimko, Turkey</p>

Table B. 1. Specifications of the Equipment Used in the Experimental Set-Up
(Continued)

Equipment	Specifications
<p style="text-align: center;">Data Logger and Controller used in the gas injection system</p>	<p>Trademark: National Instruments (NI) Device: SCC-68 I/O Connector Block with 4 SCC Signal Conditioning Slots for DAQ Modules: SCC-AI06 Isolated Analog Input Module SCC- CI20 Current Input Module SCC-TC02 Thermocouple Module SCC-RTD01 RTD Input Module Data Analysis: LabVIEW (Laboratory Virtual Instrument Engineering Workbench) Graphical Programming Language by NI</p>
<p style="text-align: center;">Digital Precision Balance</p>	<p>Trademark: Precisa Model: Serie 320XB Weighting Range:320 g Readibility: 1 mg Linearity: 1.5 mg Size (W/ D/ H): 210/ 340/ 150 mm Balance Pan: Chrome nickel steel, 135× 135 mm Data Analysis: BALINT Software by Precisa Instruments AG</p>

Table B. 1. Specifications of the Equipment Used in the Experimental Set-Up
(Continued)

Equipment	Specifications
Syringe Pumps and Pump Controllers	Trademark: ISCO Model. 500 D Cylinder Capacity: 507.38 ml Flow Range: 0.001- 204 ml/min Pressure Range: 10-3,750 psi
	Trademark: ISCO Model. 260 D Cylinder Capacity: 266.05 ml Flow Range: 0.001 - 107 ml/min Pressure Range: 0-7,500 psi
Constant Temperature Oven	Trademark: Despatch Temperature Range: 10-400 °C
Vacuum Pump	Trademark: Javac, England Model: DS40 Voltage: 220 V/ 50 Hz Type: Single stage high vacuum

APPENDIX C

RESULTS OF XRD ANALYSIS

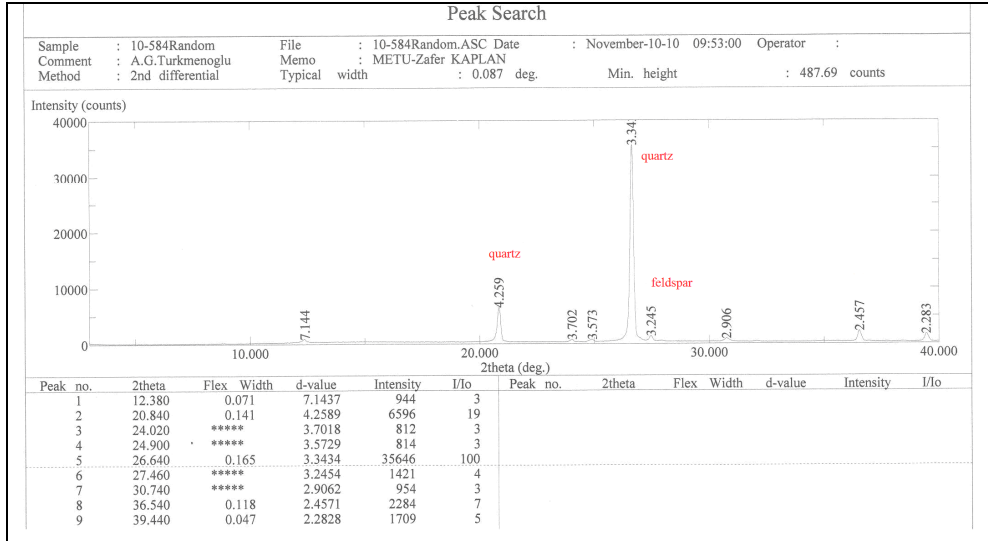


Figure C. 1. XRD Spectrum of Grinded Sample for Identification of Minerals
 Except From Clay (Turkmenoglu, 2010)

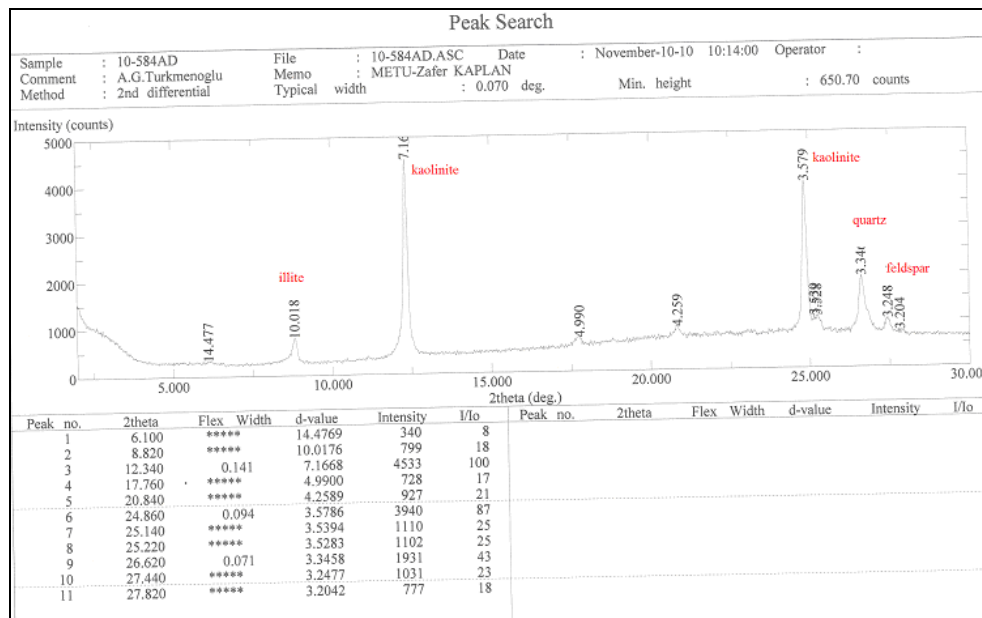


Figure C. 2. XRD Spectrum of Air Dried Sample (Turkmenoglu, 2010)

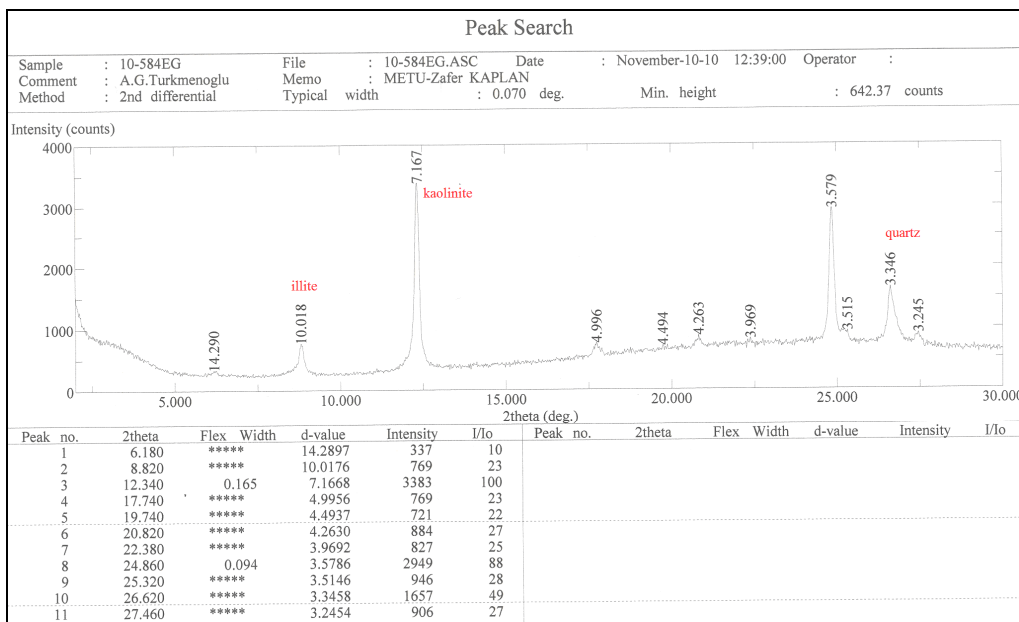


Figure C. 3. XRD Spectrum of Sample kept in Ethylene Glycol at 60 °C for 12 hours (Turkmenoglu, 2010)

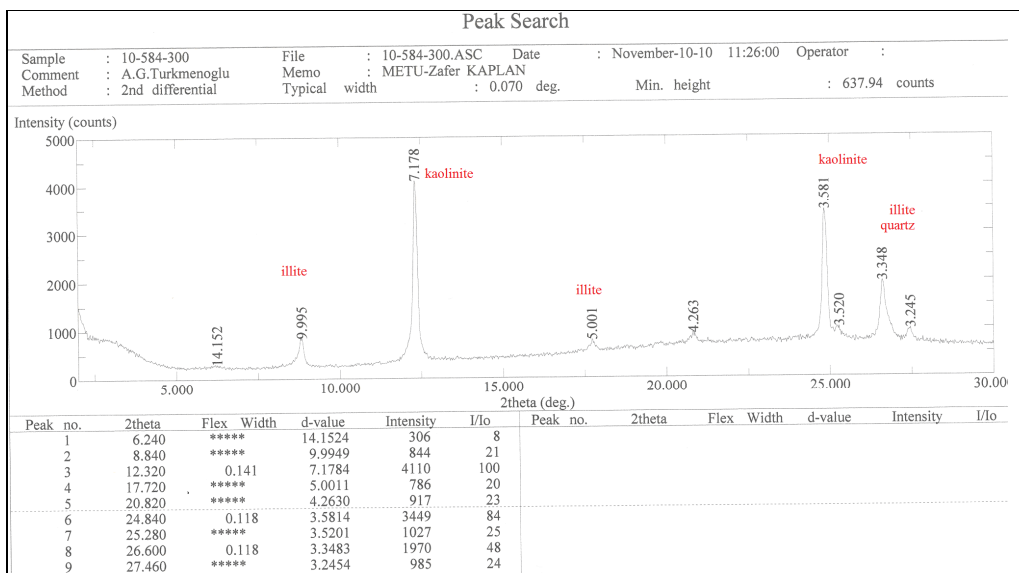


Figure C. 4. XRD Spectrum of Sample Dried at 300 °C for 1 hour (Turkmenoglu, 2010)

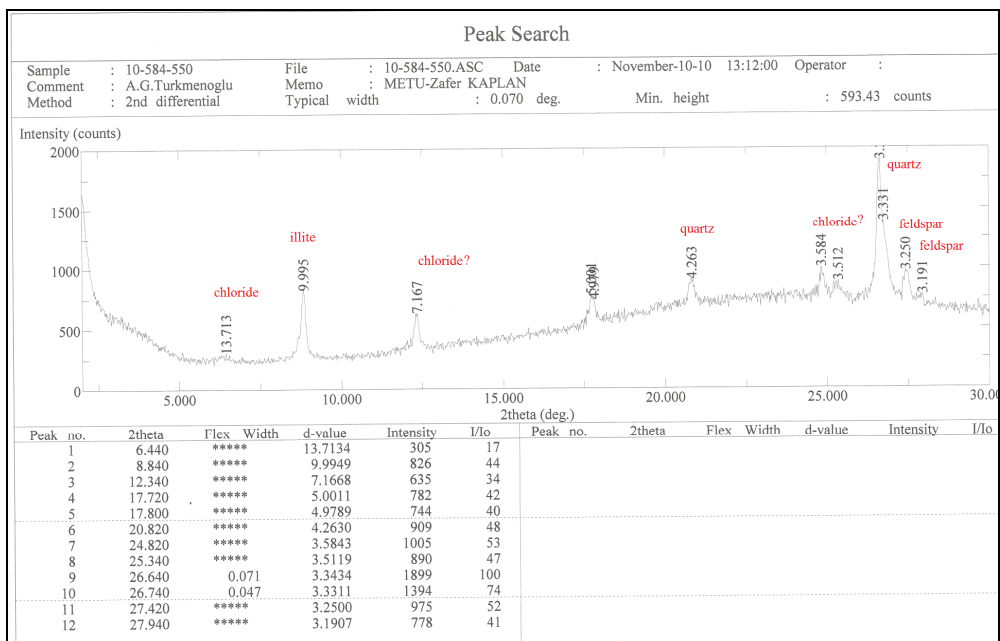


Figure C. 5. XRD Spectrum of Sample Dried at 550 °C for 1 hour (Turkmenoglu, 2010)

APPENDIX D

RESULTS OF CORE ANALYSIS CARRIED OUT AT TPAO

Porosity and permeability measurements of core samples are conducted at Turkish Petroleum Corporation (TPAO). For measurements, first of all, available core sample E3, which has a length of 4.9 cm and a diameter of 3.8 cm, is cleaned by being kept in alcohol under vacuum. Cleaned samples are dried at 70 °C in a temperature controlled oven and weighted. A porosity value of 0.213 is obtained.

Permeability measurements are also carried out by placing the core sample into a Hassler type core holder and injecting air, the measured air permeability (k_{air}) values are corrected with the consideration of the Klinkenberg effect and converted to liquid permeability (k_L) (Klinkenberg, 1941). Results of core analysis conducted at TPAO are shown in Table D.1 (TPAO, 2011).

Table D. 1. Results of Core Analysis conducted at TPAO

Core Sample	Dia. (cm)	Length (cm)	Porosity (frac.)	k_{air} (md)	k_L (md)	Grain Density (g/cc)
E3	3.8	4.96	0.213	286.70	266.70	2.66

Measurements of porosity and permeability on core sample E3 under overburden pressure is also conducted at TPAO with CMS-300 test system by applying 800, 1500 and 3000 psig net overburden pressure (NOP). Change in porosity and permeability in core sample E3 with different net overburden pressures is

obtained, as tabulated in Table D.2 and shown in Figure D.1 and D.2 (TPAO, 2011).

Table D. 2. Change in porosity and permeability in core sample E3 with different net overburden pressures

NO P (psi)	Pore volume, V_p (cc)	Porosity, ϕ (frac.)	k_L (md)	k_{air} (md)	$\Delta\phi$ [$(\phi / \phi_{800psi}) \times 100$] (%)	Δk_L [$(k / k_{800psi}) \times 100$] (%)
800	11.6	0.206	283	296	100	100
1500	11.5	0.204	279	292	99.0	98.6
3000	11.3	0.202	274	287	98.1	96.8

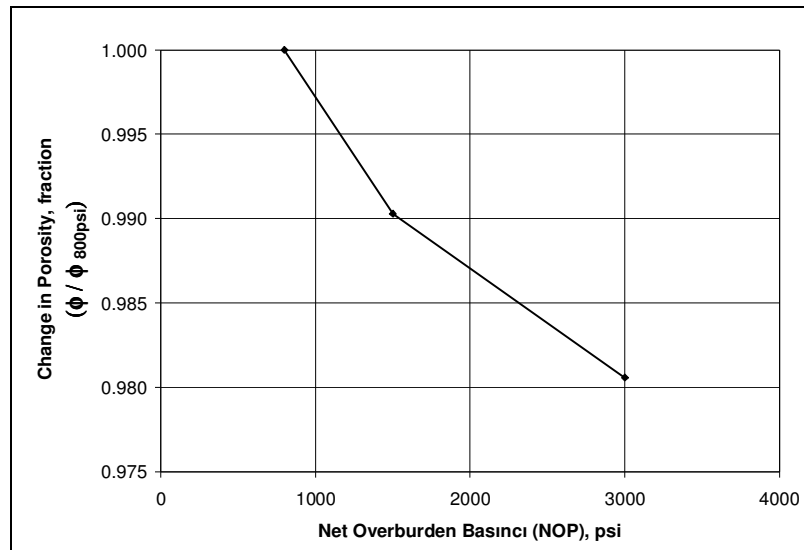


Figure D. 1. Change in porosity with net overburden pressure

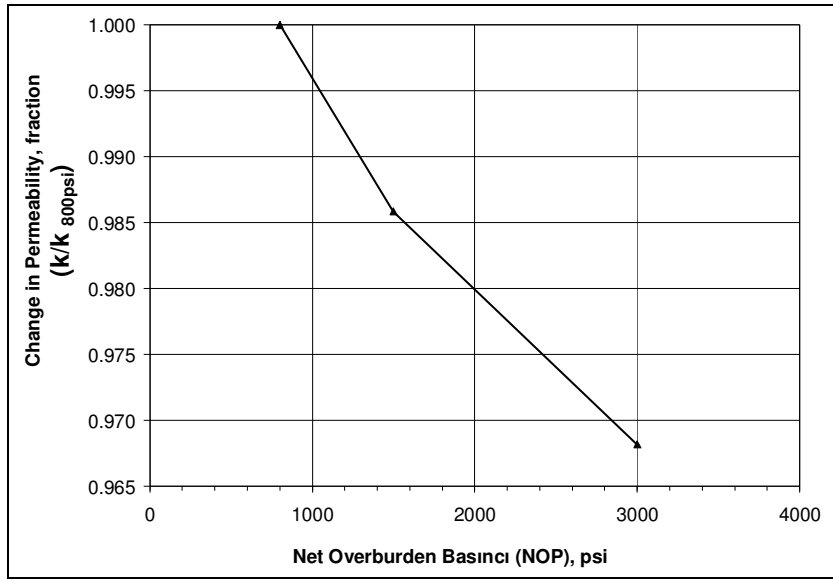


Figure D. 2. Change in permeability with net overburden pressure

Capillary pressure tests are conducted by mercury injection method using Micromeritics' AutoPore IV 9500 Series Equipment at TPAO. By applying various levels of pressures between 0.5-60 000 psia and determining the volumes of mercury (non-wetting phase) that enters the pores of the sample, capillary pressure curve is constructed as shown in Figure D.3. Pore size distribution is also obtained for the sample as shown in Figure D.4 (TPAO, 2011).

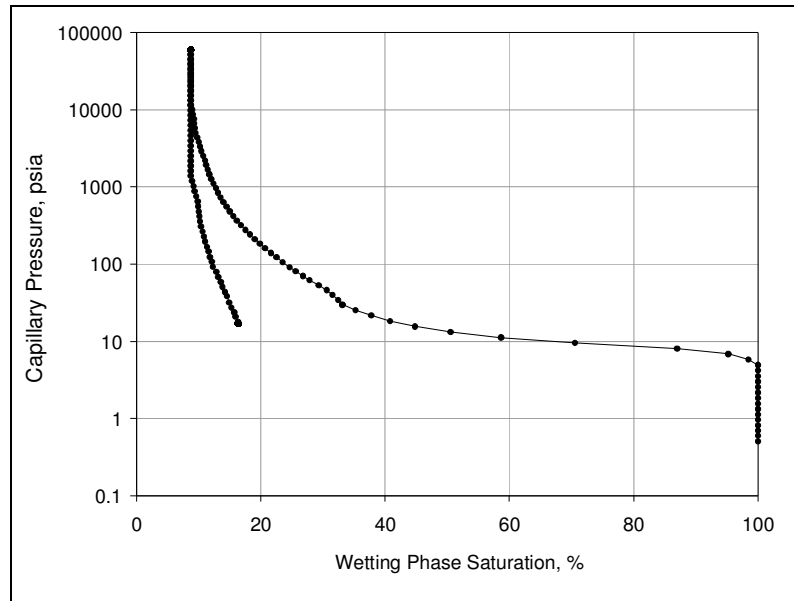


Figure D. 3. Capillary Pressure Curve of the Core E3

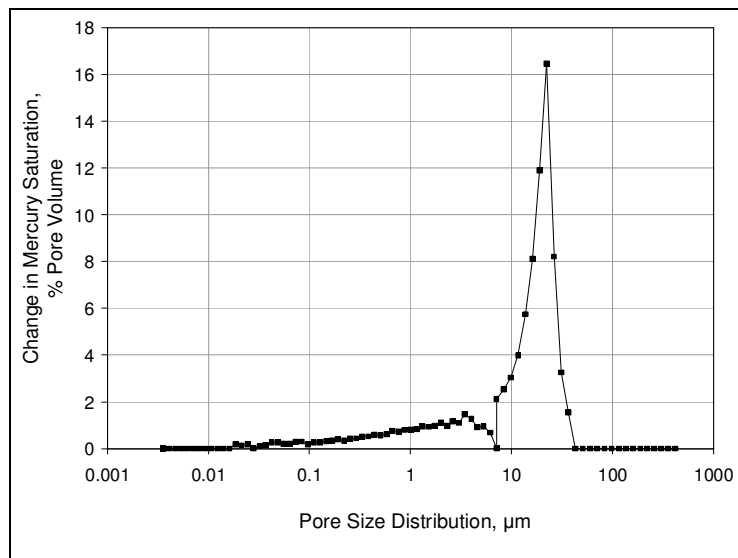


Figure D. 4. Pore Size Distribution of the Core E3

For relative permeability measurements at TPAO, core sample E2 is saturated with 5 wt% KCl aqueous solution. From the bottom, KCl solution is started to be injected at a rate of 0.24 cc/min (1 ft/day) and water permeability values (k_w) are obtained. A back pressure of 250 psi and an overburden pressure of 750 psi are applied. n-decane is injected until no more water production is obtained. By this way, residual water saturation condition is reached and n-decane permeability at residual water saturation ($k_o @ S_{wir}$) is determined. In the next step, at constant flow rate, KCl aqueous solution is injected and necessary time, pressure, brine and n-decane production data is recorded. When n-decane production ceased, brine saturation at residual n-decane saturation ($k_w @ S_{or}$) is determined. Relative permeability calculations are performed with Johnson-Bossler-Naumann (JBN) method (Johnson, Bossler and Naumann, 1959). Permeability, porosity and end point data is tabulated in Table D.3. Relative permeability curve obtained is shown in Figure D.5 and Figure D.6 (TPAO, 2011).

Table D. 3. Permeability, porosity and end point data

Core Sample	ϕ (frac.)	k_L (md)	k_w (md)	S_{wi} (%)	$k_o @ S_{wi}$ (k_{base}) (md)	S_{or} (%)	$k_w @ S_{or}$ (md)
E2	20.5	266.7	80.1	35.4	19.23	27.6	17.17

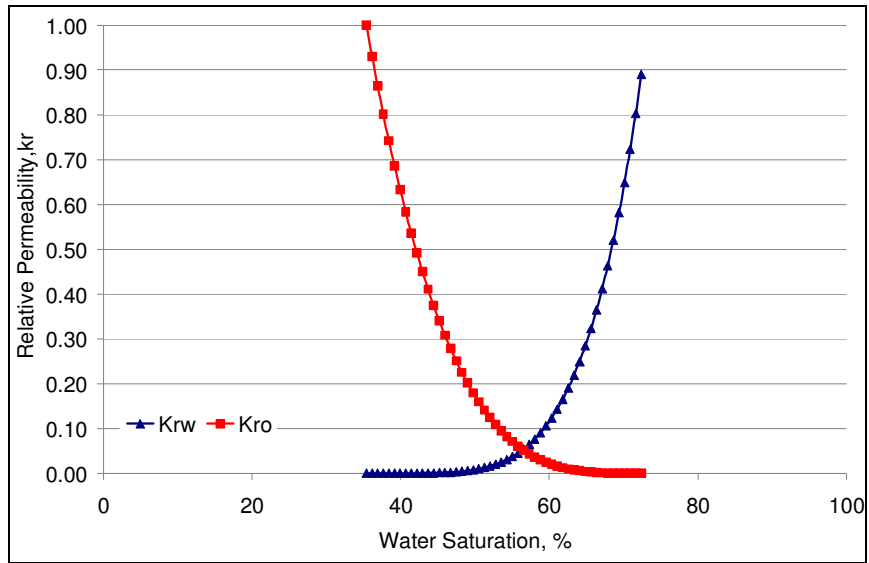


Figure D. 5. Relative permeability curve

APPENDIX E

SOLUBILITY OF CO₂, CH₄ AND N₂ IN N-DECANE AT 70 °C AND 250 PSI

E.1. Solubility of CO₂ in n-decane at 70 °C and 250 psi

In Figure E.1, pressure composition diagram of CO₂ in n-decane is presented (Reamer and Sage, 1963). As shown in the Figure E.1., mole fraction of CO₂ in liquid phase at 70 °C (158 °F) and 250 psi in the CO₂-n-decane system corresponds to a value of 0.14.

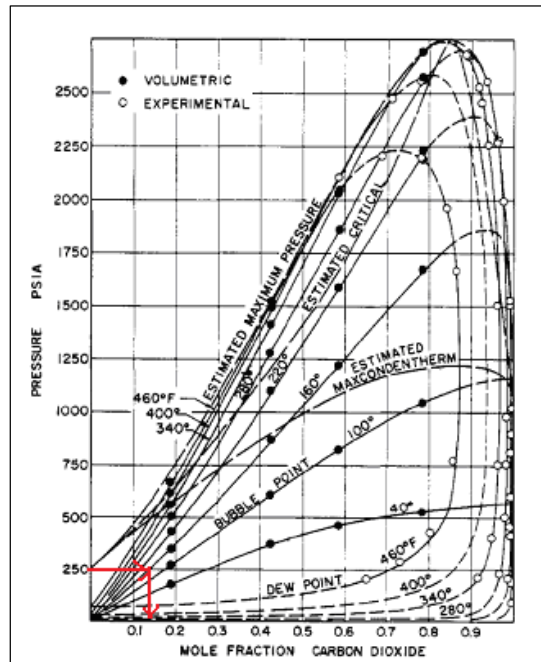


Figure E. 1. Pressure Composition Diagram of CO₂-n-decane System (Reamer and Sage, 1963)

E.2. Solubility of CH₄ in n-decane at 70 °C and 250 psi

In Figure E.2, pressure composition diagram of CH₄ in n-decane is presented (Srivastan, 1992). As shown in the Figure E.2., mole fraction of CH₄ in liquid phase at 70 °C (343.15 °K) and 250 psi (1.72 MPa) in the CH₄-n-decane system corresponds to a value of around 0.07 (Beaudin and Kohn, 1967; Srivastan, 1992).

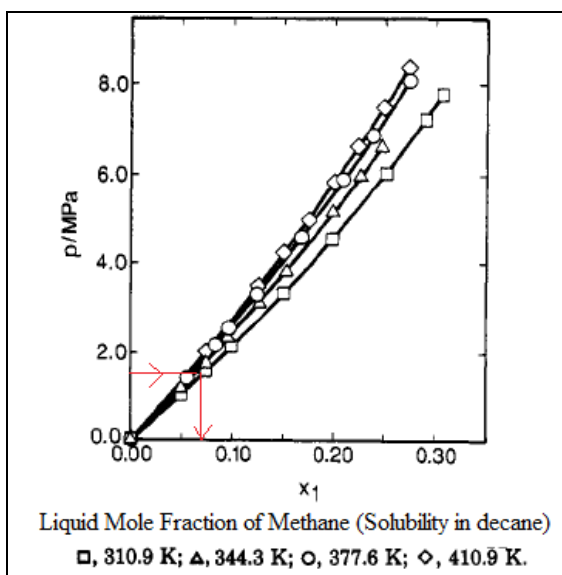


Figure E. 2. Methane Solubility in Decane (Srivastan, 1992)

E.3. Solubility of N₂ in n-decane at 70 °C and 250 psi

In Figure E.3, pressure composition diagram of N₂ in n-decane is presented (Azarnoosh and McKetta, 1963). As shown in the Figure E.3, mole fraction of N₂ in liquid phase at 70 °C (158 °F) and 250 psi in the N₂-n-decane system corresponds to a value of around 0.026.

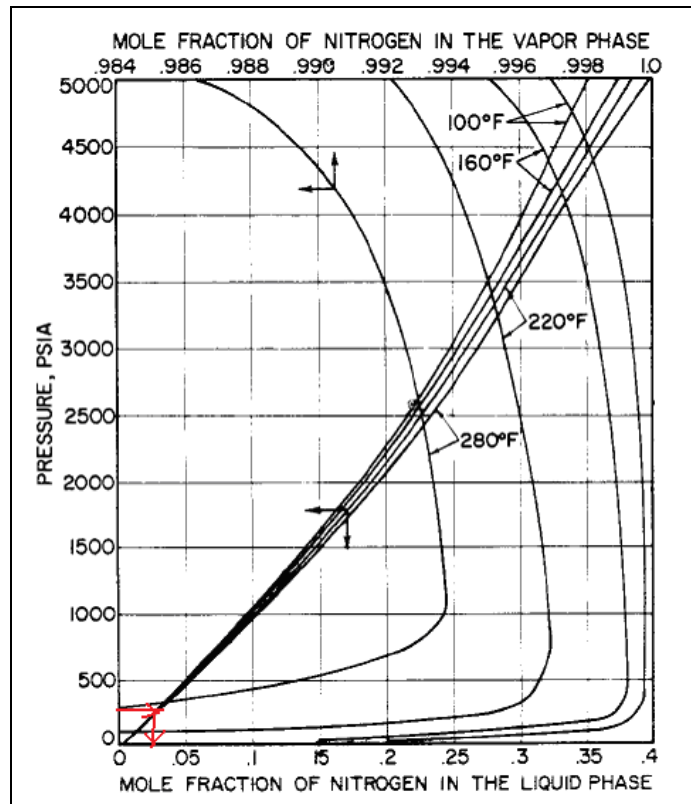


Figure E. 3. Pressure Composition Diagram of N₂-n-decane System (Azarnoosh and McKetta, 1963).

APPENDIX F

MIXTURE DENSITY AND VISCOSITY OF N-DECANE-CO₂, CH₄ & N₂

Table F. 1. Density and Viscosity of n-Decane- CO₂ Mixtures with Different CO₂ Mole Fractions (Culllck And Mathls, 1984)

CO ₂ Mole Frac.	Temp, °K	Pres, MPa	ρ_{mixture} kg/m ³	μ_{mixture} (10 ⁻⁶ Pas)	Temp, °K	Pres, MPa	ρ_{mixture} kg/m ³	μ_{mixture} (10 ⁻⁶ Pas)
0.15	310.93	6.93	728.1	666.6	373.13	7.1	678.3	333.6
	310.93	14.08	734.1	704.5	373.13	13.96	687.4	371.5
	310.93	28.37	745	812.3	373.13	27.75	702.3	432.3
	310.93	34.63	749.3	864.7	373.13	34.68	708.1	464.6
	344.32	6.72	701.5	446.2	403.08	7.19	652.4	269.5
	344.32	14.17	709.5	484.1	403.08	14.48	665.6	292.3
	344.32	27.89	722.1	558.8	403.08	27.96	683.7	342.6
	344.32	34.58	726.9	587.7	403.08	34.06	690.4	363.7
0.301	310.9	7.16	735.1	547.1	374.02	6.76	676.7	288.1
	310.9	14.28	740.9	589.2	374.02	13.72	687.5	309.5
	310.9	27.72	752.9	669.9	374.02	27.75	705.1	366.1
	310.9	34.09	757.8	709.9	374.02	33.96	711.9	390.5
	344.31	7.02	704.4	388.7	403.22	7.1	650.8	225.8
	344.31	14.13	712.7	413.7	403.22	14.24	664.4	246
	344.31	27.83	727.4	476.3	403.22	27.78	685.6	291.4
	344.31	34.51	733.1	506.1	403	33.89	693.3	308.6
0.505	311.21	7.12	750.5	360.1	373.36	10.6	685.4	212.9
	311.21	13.87	758.9	393.5	373.36	13.82	692.7	222.2
	311.21	27.65	774.6	447.7	373.36	27.75	717.2	266.1
	311.21	30.94	778	464	403.3	11.58	652.8	169.2
	343.18	6.93	712.9	289.3	403.3	13.91	659	174.9
	343.18	13.63	724.7	286.6	403.3	21.37	677.9	199
	343.18	20.54	735.4	325.5	403.3	27.99	691.1	215.3
	343.18	27.58	744.6	333.6				

Table F. 2. Density and Viscosity of n-Decane- CH₄ Mixtures with Different CH₄ Mole Fractions (Agilio and Padua, 2004)

CH ₄ Mole Frac.	Temp, °K	Pres, MPa	ρ_{mixture} kg/m ³	μ_{mixture} (10 ⁻⁶ Pas)	CH ₄ Mole Frac.	Temp, °K	Pres, MPa	ρ_{mixture} kg/m ³	μ_{mixture} (10 ⁻⁶ Pas)
0	303.15	0.1	722.5	791	0.41	303.15	20.02	674.3	457
0	303.15	5.07	726.1	837	0.41	303.15	25.09	678.8	480
0	303.15	10.1	729.9	886	0.41	303.15	30.05	683	505
0	303.15	15	732.8	935	0.41	303.15	40.12	689.9	541
0	303.15	20	736.5	982	0.41	303.15	49.91	697.1	588
0	303.15	30	743.1	1085	0.41	303.15	60.07	703.6	648
0	303.15	40.1	749.2	1193	0.41	303.15	75.36	713.1	743
0	303.15	50.1	754.5	1309	0.41	323.15	20.05	656.9	356
0	303.15	60.2	759.9	1441	0.41	323.15	24.92	662.1	374
0	303.15	76.2	767.8	1648	0.41	323.15	29.87	666.7	393
0	323.15	0.38	707.4	612	0.41	323.15	40	675.8	435
0	323.15	5.07	711.5	647	0.41	323.15	50.05	682.2	465
0	323.15	10.1	715.7	682	0.41	323.15	60.29	690.1	506
0	323.15	15.1	719.7	719	0.41	323.15	75.61	700.7	576
0	323.15	20	723.1	759	0.41	353.15	20.09	634.2	279
0	323.15	30	730.1	839	0.41	353.15	25.01	640.2	295
0	323.15	40	736.5	921	0.41	353.15	30.01	645.8	312
0	323.15	49.6	742.4	1002	0.41	353.15	39.94	654.5	336
0	323.15	59.4	748	1088	0.41	353.15	50.06	663.3	371
0	323.15	75.6	756.5	1237	0.41	353.15	60.26	671	408
0	353.15	0.26	684.1	441	0.41	353.15	74.95	683.4	456
0	353.15	5.03	689.3	469	0.41	393.15	20.05	602.3	204
0	353.15	10.1	694.2	499	0.41	393.15	25	610	220
0	353.15	15	699	523	0.41	393.15	30.14	617.2	232
0	353.15	20	703	552	0.41	393.15	40	627.9	255
0	353.15	30.1	711	611	0.41	393.15	50.07	638.3	279
0	353.15	40	718.2	667	0.41	393.15	60.03	647.6	306
0	353.15	50.1	724.8	730	0.41	393.15	75.48	660.6	348
0	353.15	60.1	731	791	0.601	303.15	24.84	615.1	274
0	353.15	75.1	739.6	873	0.601	303.15	30.14	621.2	289

Table F. 3. Density and Viscosity of n-Decane- CH₄ Mixtures with Different CH₄ Mole Fractions (Agilio and Padua, 2004) (continued)

CH ₄ Mole Frac.	Temp, °K	Pres, MPa	ρ_{mixture} kg/m ³	μ_{mixture} (10 ⁻⁶ Pas)	CH ₄ Mole Frac.	Temp, °K	Pres, MPa	ρ_{mixture} kg/m ³	μ_{mixture} (10 ⁻⁶ Pas)
0	393.15	0.52	651.9	306	0.601	303.15	40.06	631.3	320
0	393.15	5.03	658	326	0.601	303.15	49.95	640	352
0	393.15	10	664.3	350	0.601	303.15	60.14	648.3	380
0	393.15	15	670.1	373	0.601	303.15	75.15	659.2	425
0	393.15	20.1	675.9	392	0.601	323.15	24.99	596.9	224
0	393.15	30.1	685.9	430	0.601	323.15	30.06	604	239
0	393.15	40	694.5	470	0.601	323.15	40.04	615.9	264
0	393.15	50.1	702.3	512	0.601	323.15	49.98	625.2	290
0	393.15	60.1	709.5	555	0.601	323.15	59.97	634.4	313
0	393.15	75.6	720	627	0.601	323.15	74.99	646	352
0.227	303.15	10.1	702.2	605	0.601	353.15	24.99	569.2	180
0.227	303.15	15	706.2	633	0.601	353.15	30.07	578	193
0.227	303.15	19.9	709.6	668	0.601	353.15	40.07	592.6	216
0.227	303.15	30.2	717.3	734	0.601	353.15	50	603.7	237
0.227	303.15	40.1	722.8	801	0.601	353.15	60.06	613.7	261
0.227	303.15	49.9	728.5	868	0.601	353.15	74.91	626.5	292
0.227	303.15	60.1	734.3	942	0.601	393.15	25.07	541.6	144
0.227	303.15	75.7	742.4	1065	0.601	393.15	29.99	550.3	152
0.227	323.15	9.83	685.5	460	0.601	393.15	40.16	567.5	176
0.227	323.15	15.1	690.3	487	0.601	393.15	50.08	579.6	192
0.227	323.15	20.1	694.4	512	0.601	393.15	59.95	590.5	212
0.227	323.15	30.3	702.1	567	0.601	393.15	74.93	604.8	239
0.227	323.15	40.1	709	620	0.799	303.15	40.11	527.7	147
0.227	323.15	50.9	715.5	680	0.799	303.15	45.04	535.4	160
0.227	323.15	60.3	721.3	736	0.799	303.15	50.1	542.6	162
0.227	323.15	76.1	730.1	827	0.799	303.15	60	553.4	182
0.227	353.15	10.1	661.1	360	0.799	303.15	74.5	566.7	208
0.227	353.15	15.1	666.5	381	0.799	323.15	40.16	508	129

Table F. 4. Density and Viscosity of n-Decane- CH₄ Mixtures with Different CH₄ Mole Fractions (Agilio and Padua, 2004) (continued)

CH ₄ Mole Frac.	Temp, °K	Pres, MPa	ρ_{mixture} kg/m ³	μ_{mixture} (10 ⁻⁶ Pas)	CH ₄ Mole Frac.	Temp, °K	Pres, MPa	ρ_{mixture} kg/m ³	μ_{mixture} (10 ⁻⁶ Pas)
0.227	353.15	20.2	671.9	399	0.799	323.15	45.02	516.7	137
0.227	353.15	30.1	680.7	430	0.799	323.15	50.02	524.1	145
0.227	353.15	40.1	688.9	475	0.799	323.15	60.05	537.6	157
0.227	353.15	50	696.1	513	0.799	323.15	74.98	554.6	185
0.227	353.15	60.1	702.7	556	0.799	353.15	40.07	480.2	106
0.227	353.15	75.4	711.8	622	0.799	353.15	45.09	490.6	113
0.227	393.15	10.1	630.9	254	0.799	353.15	49.96	499.4	120
0.227	393.15	15.1	637.6	273	0.799	353.15	60.09	515.4	132
0.227	393.15	20.3	644.2	288	0.799	353.15	75.1	533.4	152
0.227	393.15	30	655.1	312	0.799	393.15	40	447.6	86
0.227	393.15	39.9	664.1	349	0.799	393.15	45	460.8	94
0.227	393.15	49.9	672.5	380	0.799	393.15	50.03	470.6	98
0.227	393.15	60	681	407	0.799	393.15	60.02	486.7	111
0.227	393.15	75.5	691.9	451	0.799	393.15	75.25	506.8	131

APPENDIX G

PENG ROBINSON EQUATION OF STATE

n-decane- CO₂, CH₄ and N₂ mixture densities are calculated by using Peng Robinson Equation of State by using the following formulation (Peng and Robinson, 1976):

$$P = \frac{RT}{v-b} - \frac{a(T)}{v(v+b)+b(v-b)} \quad (\text{G.1})$$

which can be also expressed as :

$$Z^3 - (1-B)Z^2 + (A - 3B^2 - 2B)Z - (AB - B^2 - B^3) = 0 \quad (\text{G.2})$$

where

$A = \frac{aP}{R^2T^2}$, $B = \frac{bP}{RT}$, $Z = \frac{Pv}{RT}$, v : molar volume, R: gas constant, T: absolute temperature.

Equation of state constants, a and b (Peng and Robinson, 1976):

At the critical temperature (T_c) and critical pressure (P_c):

$$a(T_c) = 0.45724 \frac{R^2T_c}{P_c} \quad (\text{G.3})$$

$$b(T_c) = 0.07780 \frac{RT_c}{P_c} \quad (\text{G.4})$$

$$Z_c = 0.307 \quad (\text{G.5})$$

At temperatures other than critical temperature:

$$a(T) = a(T_c) \alpha(T_r, \omega) \quad (\text{G.6})$$

$$b(T) = b(T_c) \quad (\text{G.7})$$

where

$$\alpha^{1/2} = 1 + \kappa(1 - T_r^{1/2}) \quad (\text{G.8})$$

$$\kappa = 0.37464 + 1.54226\omega - 0.26992\omega^2 \quad (\text{G.9})$$

ω : acentric factor; T_r : reduced temperature. Critical properties and acentric factors of the components are shown in Table G.1 (McCain, Jr, 1990).

Table G.1. Critical Properties and Acentric Factors of Components (McCain, Jr, 1990)

Component	Pc (psia)	Tc (°F)	ω
n-decane	305	652.00	0.4898
CO ₂	1071	87.91	0.2667
CH ₄	673	-116.14	0.0104
N ₂	492	-232.42	0.0372

In the calculation of mixture properties as in the case of the experiments, following expressions are applied for parameters a and b (Peng and Robinson, 1976):

$$a = \sum_i \sum_j x_i x_j a_{ij} \quad (\text{G.10})$$

$$b = \sum_i x_i b_i \quad (\text{G.11})$$

where

$$a_{ij} = (1 - \delta_{ij}) a_i^{1/2} a_j^{1/2} \quad (\text{G.12})$$

x: mole fraction of the component (i,j), δ : binary interaction coefficient

Binary interaction coefficients for n-decane and CO₂, CH₄ and N₂ are determined by using following correlations (Varotsis et al., 1986):

$$k_{ij} = \delta_2 T_{r_j}^2 + \delta_1 T_{r_j} + \delta_0 \quad (\text{G.13})$$

i: CO₂, CH₄ or N₂ component, j: n-decane component

For CO₂-n-decane mixture, Equation 6.19 and 6.20 are used (Varotsis et al., 1986):

$$\begin{aligned} \delta_0 &= 0.4025635 + 0.1748927 \log \omega_j \\ \delta_1 &= -0.94812 - 0.6009864 \log \omega_j \\ \delta_2 &= 0.741843368 + 0.441775 \log \omega_j \end{aligned} \quad (\text{G.14})$$

and for pressure, P:

$$k_{ij}' = k_{ij}(1.044269 - 0.00004P) \quad (\text{G.15})$$

For CH₄- n-decane mixture, Equation 6.21 is used (Varotsis et al., 1986):

$$\begin{aligned} \delta_0 &= -0.01664 - 0.37283 \log \omega + 1.31757 \log \omega^2 \\ \delta_1 &= 0.48147 + 3.35342 \log \omega - 1.0783(\log \omega)^2 \\ \delta_2 &= -0.4114 - 3.5072 \log \omega - 0.78798(\log \omega)^2 \end{aligned} \quad (\text{G.16})$$

For N₂- n-decane mixture, Equation 6.22 is used (Varotsis et al., 1986):

$$\begin{aligned} \delta_0 &= 0.1751787 - 0.7043 \log \omega - 0.862066 (\log \omega)^2 \\ \delta_1 &= -0.584474 + 1.328 \log \omega + 2.035767 (\log \omega)^2 \\ \delta_2 &= 2.257079 + 7.869765 \log \omega + 13.50466 (\log \omega)^2 + 8.3864 (\log \omega)^3 \end{aligned} \quad (\text{G.17})$$

For pressure, P:

$$k_{ij}' = k_{ij}(1.04 - 0.000042P) \quad (\text{G.18})$$

APPENDIX H

INPUT FILE PREPARED FOR MODELING CO₂ EXPERIMENT

RESULTS SIMULATOR GEM 201110

```
INUNIT SI
WSRF WELL 1
WSRF GRID TIME
OUTSRF GRID SO SG SW PRES
OUTSRF RES NONE
WPRN GRID 0
OUTPRN GRID NONE
OUTPRN RES NONE
**$ Distance units: m
RESULTS XOFFSET      0.0000
RESULTS YOFFSET      0.0000
RESULTS ROTATION      0.0000 **$ (DEGREES)
RESULTS AXES-DIRECTIONS 1.0 -1.0 1.0
**$
*****
*****
**$ Definition of fundamental cylindrical grid
**$
*****
*****
GRID RADIAL 3 1 3 *RW      0.001
KDIR DOWN
DI IVAR      0.009525      0.009525      0.00445
DJ JVAR      360
DK ALL
3*0.019 3*0.1135 3*0.012
DTOP
3*0
DUALPOR
SHAPE GK
**$ Property: NULL Blocks Max: 1 Min: 1
**$ 0 = null block, 1 = active block
NULL MATRIX CON      1
**$ Property: NULL Blocks Max: 1 Min: 1
```

**\$ 0 = null block, 1 = active block
NULL FRACTURE CON 1
**\$ Property: Porosity Max: 0.99 Min: 0.2
POR MATRIX KVAR
0.99 0.2 0.99

*MOD

3:3 1:1 2:2 = 0.99
**\$ Property: Porosity Max: 0.99 Min: 0.2
POR FRACTURE KVAR
0.99 0.2 0.99

*MOD

3:3 1:1 2:2 = 0.99
**\$ Property: Permeability I (md) Max: 1330 Min: 266
PERMI MATRIX KVAR
1330 266 1330

*MOD

3:3 1:1 2:2 = 1330
**\$ Property: Permeability I (md) Max: 1330 Min: 266
PERMI FRACTURE KVAR
1330 266 1330

*MOD

3:3 1:1 2:2 = 1330
**\$ Property: Permeability J (md) Max: 1330 Min: 266
PERMJ MATRIX KVAR
1330 266 1330

*MOD

3:3 1:1 2:2 = 1330
**\$ Property: Permeability J (md) Max: 1330 Min: 266
PERMJ FRACTURE KVAR
1330 266 1330

*MOD

3:3 1:1 2:2 = 1330
**\$ Property: Permeability K (md) Max: 1330 Min: 266

PERMK MATRIX KVAR

1330 266 1330

*MOD

3:3 1:1 2:2 = 1330

**\$ Property: Permeability K (md) Max: 1330 Min: 266

PERMK FRACTURE KVAR

1330 266 1330

*MOD

3:3 1:1 2:2 = 1330

**\$ Property: Fracture Spacing J (m) Max: 1e-005 Min: 1e-005

DJFRAC CON 1E-005

**\$ Property: Fracture Spacing I (m) Max: 1e-005 Min: 1e-005

DIFRAC CON 1E-005

**\$ Property: Fracture Spacing K (m) Max: 1e-005 Min: 1e-005

DKFRAC CON 1E-005

**\$ Property: Pinchout Array Max: 1 Min: 1

**\$ 0 = pinched block, 1 = active block

PINCHOUTARRAY CON 1

CPOR FRACTURE 3e-6

CPOR MATRIX 3e-6

**The following is the fluid component

**property data in GEM format.

**The unit system and fluid compositions should

**be specified in the I/O control section.

**The units and compositions specified in WinProp

**are included here as comments for informational purposes.

** PVT UNITS CONSISTENT WITH *INUNIT *FIELD

**COMPOSITION *PRIMARY

** 1.0000000E-03 9.9900000E-01

**COMPOSITION *SECOND

** 1.0000000E+00 0.0000000E+00

**\$ Model and number of components

**\$ Model and number of components

MODEL PR

NC 2 2

COMPNAME 'CO2' 'NC10'

HCFLAG

0 0

VISCOR HZYT

MIXVC 1

VISCOEFF 1.0230000E-01 2.3364000E-02 5.8533000E-02 -4.0758000E-02
 9.3324000E-03
 MW
 4.4010000E+01 1.4228600E+02
 AC
 0.225 0.49
 PCRIT
 7.2800000E+01 2.0800000E+01
 VCRIT
 9.4000000E-02 6.0300000E-01
 TCRIT
 3.0420000E+02 6.1760000E+02
 PCHOR
 78 433.5
 SG
 0.818 0.734
 TB
 -78.4761 174.15
 OMEGA
 0.457236 0.457236
 OMEGB
 0.0777961 0.0777961
 VSHIFT
 0 0
 HEATING_VALUES
 0 6.82976e+006
 VISVC
 9.4000000E-02 6.0300000E-01
 BIN
 1.1000000E-01

TRES 70
 DIFFUSION 1.500000 0.000001 0.000000
 ROCKFLUID

RPT 1

**\$ Sw krw krow

SWT

0.354	0	1
0.418	0	0.561795
0.482	0	0.274971
0.496875	0.000217285	0.226569
0.51175	0.00173828	0.184209
0.526625	0.0058667	0.147488
0.5415	0.0139063	0.116004
0.556375	0.0271606	0.0893523

0.57125	0.0469336	0.0671317	
0.586125	0.0745288	0.048939	
0.601	0.11125	0.0343714	
0.615875	0.158401	0.0230262	
0.63075	0.217285	0.0145004	
0.645625	0.289207	0.00839146	
0.6605	0.375469	0.00429643	
0.675375	0.477375	0.00181256	
0.69025	0.59623	0.000537054	
0.705125	0.733337	6.71317e-005	
0.72	0.89	0	
**\$	SI	kg	krog
SLT			
0.554	1	0	
0.57875	0.823975	0.000170892	
0.6035	0.669922	0.00136713	
0.62825	0.536377	0.00461408	
0.653	0.421875	0.0109371	
0.67775	0.324951	0.0213615	
0.7025	0.244141	0.0369126	
0.72725	0.177979	0.0586159	
0.752	0.125	0.0874966	
0.77675	0.0837402	0.12458	
0.8015	0.0527344	0.170892	
0.82625	0.0305176	0.227457	
0.851	0.015625	0.295301	
0.87575	0.0065918	0.375449	
0.9005	0.00195313	0.468927	
0.92525	0.000244141	0.57676	
0.95	0	0.699973	
0.975	0	0.841089	
1	0	1	

INITIAL

USER_INPUT

**\$ Property: Pressure (kPa) Max: 1724 Min: 1724

PRES MATRIX CON 1724

**\$ Property: Pressure (kPa) Max: 1724 Min: 1724

PRES FRACTURE CON 1724

**\$ Property: Water Saturation Max: 0.203 Min: 0.203

SW MATRIX CON 0.203

**\$ Property: Water Saturation Max: 0.203 Min: 0.203

SW FRACTURE CON 0.203

**\$ Property: Global Composition(CO2) Max: 0.001 Min: 0.001

ZGLOBALC 'CO2' MATRIX CON 0.001

```

**$ Property: Global Composition(CO2) Max: 1 Min: 1
ZGLOBALC 'CO2' FRACTURE CON      1
**$ Property: Global Composition(NC10) Max: 0.999 Min: 0.999
ZGLOBALC 'NC10' MATRIX CON      0.999
**$ Property: Global Composition(NC10) Max: 0 Min: 0
ZGLOBALC 'NC10' FRACTURE CON      0
**$ Property: Initial Water Saturation Max: 0.203 Min: 0.203
SWINIT MATRIX CON      0.203
**$ Property: Initial Water Saturation Max: 0.203 Min: 0.203
SWINIT FRACTURE CON      0.203
**$ Property: Block Temperature (C) Max: 70 Min: 70
TEMPER MATRIX CON      70
**$ Property: Block Temperature (C) Max: 70 Min: 70
TEMPER FRACTURE CON      70
NUMERICAL
DTMIN 1e-16
RUN
DATE 2011 1 1
DTWELL 1e-006
**$
WELL 'Well-1'                **$ UBA  ff Status      WELL 'Well-2'
INJECTOR 'Well-1'           Connection              PRODUCER 'Well-2'
INCOMP SOLVENT              **$      rad geofac      OPERATE MIN
1. 0.                        wfrac skin              BHP 101. CONT
OPERATE MAX                  GEOMETRY K              OPEN 'Well-2'
BHP 1724. CONT              0.001 0.37 1. 0.      DATE 2011 1
**$      rad geofac          PERF GEOA 'Well-       2.00069
wfrac skin                   2'                       **$
GEOMETRY K                   **$ UBA  ff Status      WELL 'Well-1'
0.001 0.37 1. 0.           Connection              INJECTOR 'Well-1'
PERF GEOA 'Well-            1 1 3 1. OPEN          INCOMP SOLVENT
1'                             FLOW-TO                 1. 0.
**$ UBA  ff Status          'SURFACE'               OPERATE MAX
Connection                    SHUTIN 'Well-2'         BHP 1724. CONT
1 1 1 1. OPEN                DATE 2011 1             OPEN 'Well-1'
FLOW-FROM                     2.00000                 **$
'SURFACE'                     **$                      WELL 'Well-2'
OPEN 'Well-1'                 WELL 'Well-1'           PRODUCER 'Well-2'
**$                             INJECTOR 'Well-1'       OPERATE MIN
**$                             INCOMP SOLVENT          BHP 101. CONT
WELL 'Well-2'                 1. 0.                   SHUTIN 'Well-2'
PRODUCER 'Well-2'            OPERATE MAX              DATE 2011 1
OPERATE MIN                   BHP 1724. CONT          3.00000
BHP 101. CONT                 SHUTIN 'Well-1'        **$
**$                             **$                      WELL 'Well-1'

```

INJECTOR 'Well-1'
INCOMP SOLVENT
1. 0.
OPERATE MAX
BHP 1724. CONT
SHUTIN 'Well-1'
**\$
WELL 'Well-2'
PRODUCER 'Well-2'
OPERATE MIN
BHP 101. CONT
OPEN 'Well-2'
DATE 2011 1
3.00069
**\$
WELL 'Well-1'
INJECTOR 'Well-1'
INCOMP SOLVENT
1. 0.
OPERATE MAX
BHP 1724. CONT
OPEN 'Well-1'
**\$
WELL 'Well-2'
PRODUCER 'Well-2'
OPERATE MIN
BHP 101. CONT
SHUTIN 'Well-2'
DATE 2011 1
4.00000
**\$
WELL 'Well-1'
INJECTOR 'Well-1'
INCOMP SOLVENT
1. 0.
OPERATE MAX
BHP 1724. CONT
SHUTIN 'Well-1'
**\$
WELL 'Well-2'
PRODUCER 'Well-2'
OPERATE MIN
BHP 101. CONT
OPEN 'Well-2'

DATE 2011 1
4.00069
**\$
WELL 'Well-1'
INJECTOR 'Well-1'
INCOMP SOLVENT
1. 0.
OPERATE MAX
BHP 1724. CONT
OPEN 'Well-1'
**\$
WELL 'Well-2'
PRODUCER 'Well-2'
OPERATE MIN
BHP 101. CONT
SHUTIN 'Well-2'
DATE 2011 1
5.00000
**\$
WELL 'Well-1'
INJECTOR 'Well-1'
INCOMP SOLVENT
1. 0.
OPERATE MAX
BHP 1724. CONT
SHUTIN 'Well-1'
**\$
WELL 'Well-2'
PRODUCER 'Well-2'
OPERATE MIN
BHP 101. CONT
OPEN 'Well-2'
DATE 2011 1
5.00069
**\$
WELL 'Well-1'
INJECTOR 'Well-1'
INCOMP SOLVENT
1. 0.
OPERATE MAX
BHP 1724. CONT
OPEN 'Well-1'
**\$
WELL 'Well-2'
PRODUCER 'Well-2'

OPERATE MIN
BHP 101. CONT
SHUTIN 'Well-2'
DATE 2011 1
6.00000
**\$
WELL 'Well-1'
INJECTOR 'Well-1'
INCOMP SOLVENT
1. 0.
OPERATE MAX
BHP 1724. CONT
SHUTIN 'Well-1'
**\$
WELL 'Well-2'
PRODUCER 'Well-2'
OPERATE MIN
BHP 101. CONT
OPEN 'Well-2'
DATE 2011 1
6.00069
**\$
WELL 'Well-1'
INJECTOR 'Well-1'
INCOMP SOLVENT
1. 0.
OPERATE MAX
BHP 1724. CONT
OPEN 'Well-1'
**\$
WELL 'Well-2'
PRODUCER 'Well-2'
OPERATE MIN
BHP 101. CONT
SHUTIN 'Well-2'
DATE 2011 1
7.00000
**\$
WELL 'Well-1'
INJECTOR 'Well-1'
INCOMP SOLVENT
1. 0.
OPERATE MAX
BHP 1724. CONT
SHUTIN 'Well-1'

**\$
WELL 'Well-2'
PRODUCER 'Well-2'
OPERATE MIN
BHP 101. CONT
OPEN 'Well-2'
DATE 2011 1
7.00069
**\$
WELL 'Well-1'
INJECTOR 'Well-1'
INCOMP SOLVENT
1. 0.
OPERATE MAX
BHP 1724. CONT
OPEN 'Well-1'
**\$
WELL 'Well-2'
PRODUCER 'Well-2'
OPERATE MIN
BHP 101. CONT
SHUTIN 'Well-2'
DATE 2011 1
8.00000
**\$
WELL 'Well-1'
INJECTOR 'Well-1'
INCOMP SOLVENT
1. 0.
OPERATE MAX
BHP 1724. CONT
SHUTIN 'Well-1'
**\$
WELL 'Well-2'
PRODUCER 'Well-2'
OPERATE MIN
BHP 101. CONT
OPEN 'Well-2'
DATE 2011 1
8.00069
**\$
WELL 'Well-1'
INJECTOR 'Well-1'
INCOMP SOLVENT
1. 0.

OPERATE MAX
BHP 1724. CONT
OPEN 'Well-1'
**\$
WELL 'Well-2'
PRODUCER 'Well-2'
OPERATE MIN
BHP 101. CONT
SHUTIN 'Well-2'
DATE 2011 1
9.00000
**\$
WELL 'Well-1'
INJECTOR 'Well-1'
INCOMP SOLVENT
1. 0.
OPERATE MAX
BHP 1724. CONT
SHUTIN 'Well-1'
**\$
WELL 'Well-2'
PRODUCER 'Well-2'
OPERATE MIN
BHP 101. CONT
OPEN 'Well-2'
DATE 2011 1
9.00069
**\$
WELL 'Well-1'
INJECTOR 'Well-1'
INCOMP SOLVENT
1. 0.
OPERATE MAX
BHP 1724. CONT
OPEN 'Well-1'
**\$
WELL 'Well-2'
PRODUCER 'Well-2'
OPERATE MIN
BHP 101. CONT
SHUTIN 'Well-2'
DATE 2011 1
10.00000
**\$
WELL 'Well-1'

INJECTOR 'Well-1'
INCOMP SOLVENT
1. 0.
OPERATE MAX
BHP 1724. CONT
SHUTIN 'Well-1'
**\$
WELL 'Well-2'
PRODUCER 'Well-2'
OPERATE MIN
BHP 101. CONT
OPEN 'Well-2'
DATE 2011 1
10.00069
**\$
WELL 'Well-1'
INJECTOR 'Well-1'
INCOMP SOLVENT
1. 0.
OPERATE MAX
BHP 1724. CONT
OPEN 'Well-1'
**\$
WELL 'Well-2'
PRODUCER 'Well-2'
OPERATE MIN
BHP 101. CONT
SHUTIN 'Well-2'
DATE 2011 1
11.00000
**\$
WELL 'Well-1'
INJECTOR 'Well-1'
INCOMP SOLVENT
1. 0.
OPERATE MAX
BHP 1724. CONT
SHUTIN 'Well-1'
**\$
WELL 'Well-2'
PRODUCER 'Well-2'
OPERATE MIN
BHP 101. CONT
OPEN 'Well-2'

DATE 2011 1	OPERATE MIN	**\$
11.00069	BHP 101. CONT	WELL 'Well-2'
**\$	SHUTIN 'Well-2'	PRODUCER 'Well-2'
WELL 'Well-1'	DATE 2011 1	OPERATE MIN
INJECTOR 'Well-1'	13.00000	BHP 101. CONT
INCOMP SOLVENT	**\$	OPEN 'Well-2'
1. 0.	WELL 'Well-1'	DATE 2011 1
OPERATE MAX	INJECTOR 'Well-1'	14.00069
BHP 1724. CONT	INCOMP SOLVENT	**\$
OPEN 'Well-1'	1. 0.	WELL 'Well-1'
**\$	OPERATE MAX	INJECTOR 'Well-1'
WELL 'Well-2'	BHP 1724. CONT	INCOMP SOLVENT
PRODUCER 'Well-2'	SHUTIN 'Well-1'	1. 0.
OPERATE MIN	**\$	OPERATE MAX
BHP 101. CONT	WELL 'Well-2'	BHP 1724. CONT
SHUTIN 'Well-2'	PRODUCER 'Well-2'	OPEN 'Well-1'
DATE 2011 1	OPERATE MIN	**\$
12.00000	BHP 101. CONT	WELL 'Well-2'
**\$	OPEN 'Well-2'	PRODUCER 'Well-2'
WELL 'Well-1'	DATE 2011 1	OPERATE MIN
INJECTOR 'Well-1'	13.00069	BHP 101. CONT
INCOMP SOLVENT	**\$	SHUTIN 'Well-2'
1. 0.	WELL 'Well-1'	DATE 2011 1
OPERATE MAX	INJECTOR 'Well-1'	15.00000
BHP 1724. CONT	INCOMP SOLVENT	**\$
SHUTIN 'Well-1'	1. 0.	WELL 'Well-1'
**\$	OPERATE MAX	INJECTOR 'Well-1'
WELL 'Well-2'	BHP 1724. CONT	INCOMP SOLVENT
PRODUCER 'Well-2'	OPEN 'Well-1'	1. 0.
OPERATE MIN	**\$	OPERATE MAX
BHP 101. CONT	WELL 'Well-2'	BHP 1724. CONT
OPEN 'Well-2'	PRODUCER 'Well-2'	SHUTIN 'Well-1'
DATE 2011 1	OPERATE MIN	**\$
12.00069	BHP 101. CONT	WELL 'Well-2'
**\$	SHUTIN 'Well-2'	PRODUCER 'Well-2'
WELL 'Well-1'	DATE 2011 1	OPERATE MIN
INJECTOR 'Well-1'	14.00000	BHP 101. CONT
INCOMP SOLVENT	**\$	OPEN 'Well-2'
1. 0.	WELL 'Well-1'	DATE 2011 1
OPERATE MAX	INJECTOR 'Well-1'	15.00069
BHP 1724. CONT	INCOMP SOLVENT	**\$
OPEN 'Well-1'	1. 0.	WELL 'Well-1'
**\$	OPERATE MAX	INJECTOR 'Well-1'
WELL 'Well-2'	BHP 1724. CONT	INCOMP SOLVENT
PRODUCER 'Well-2'	SHUTIN 'Well-1'	1. 0.

OPERATE MAX
BHP 1724. CONT
OPEN 'Well-1'
**\$
WELL 'Well-2'
PRODUCER 'Well-2'
OPERATE MIN
BHP 101. CONT
SHUTIN 'Well-2'
DATE 2011 1
16.00000
**\$
WELL 'Well-1'
INJECTOR 'Well-1'
INCOMP SOLVENT
1. 0.
OPERATE MAX
BHP 1724. CONT
SHUTIN 'Well-1'
**\$
WELL 'Well-2'
PRODUCER 'Well-2'
OPERATE MIN
BHP 101. CONT
OPEN 'Well-2'
DATE 2011 1
16.00069
**\$
WELL 'Well-1'
INJECTOR 'Well-1'
INCOMP SOLVENT
1. 0.
OPERATE MAX
BHP 1724. CONT
OPEN 'Well-1'
**\$
WELL 'Well-2'
PRODUCER 'Well-2'
OPERATE MIN
BHP 101. CONT
SHUTIN 'Well-2'
DATE 2011 1
17.00000
**\$
WELL 'Well-1'

INJECTOR 'Well-1'
INCOMP SOLVENT
1. 0.
OPERATE MAX
BHP 1724. CONT
SHUTIN 'Well-1'
**\$
WELL 'Well-2'
PRODUCER 'Well-2'
OPERATE MIN
BHP 101. CONT
OPEN 'Well-2'
DATE 2011 1
17.00069
**\$
WELL 'Well-1'
INJECTOR 'Well-1'
INCOMP SOLVENT
1. 0.
OPERATE MAX
BHP 1724. CONT
OPEN 'Well-1'
**\$
WELL 'Well-2'
PRODUCER 'Well-2'
OPERATE MIN
BHP 101. CONT
SHUTIN 'Well-2'
DATE 2011 1
18.00000
**\$
WELL 'Well-1'
INJECTOR 'Well-1'
INCOMP SOLVENT
1. 0.
OPERATE MAX
BHP 1724. CONT
SHUTIN 'Well-1'
**\$
WELL 'Well-2'
PRODUCER 'Well-2'
OPERATE MIN
BHP 101. CONT
OPEN 'Well-2'

DATE 2011 1
18.00069
**\$
WELL 'Well-1'
INJECTOR 'Well-1'
INCOMP SOLVENT
1. 0.
OPERATE MAX
BHP 1724. CONT
OPEN 'Well-1'
**\$
WELL 'Well-2'
PRODUCER 'Well-2'
OPERATE MIN
BHP 101. CONT
SHUTIN 'Well-2'
DATE 2011 1
19.00000
**\$
WELL 'Well-1'
INJECTOR 'Well-1'
INCOMP SOLVENT
1. 0.
OPERATE MAX
BHP 1724. CONT
SHUTIN 'Well-1'
**\$
WELL 'Well-2'
PRODUCER 'Well-2'
OPERATE MIN
BHP 101. CONT
OPEN 'Well-2'
DATE 2011 1
19.00069
**\$
WELL 'Well-1'
INJECTOR 'Well-1'
INCOMP SOLVENT
1. 0.
OPERATE MAX
BHP 1724. CONT
OPEN 'Well-1'
**\$
WELL 'Well-2'
PRODUCER 'Well-2'

OPERATE MIN
 BHP 101. CONT
 SHUTIN 'Well-2'
 DATE 2011 1
 20.00000
 **\$
 WELL 'Well-1'
 INJECTOR 'Well-1'
 INCOMP SOLVENT
 1. 0.
 OPERATE MAX
 BHP 1724. CONT
 SHUTIN 'Well-1'
 **\$
 WELL 'Well-2'
 PRODUCER 'Well-2'
 OPERATE MIN
 BHP 101. CONT
 OPEN 'Well-2'
 DATE 2011 1
 20.00069
 **\$
 WELL 'Well-1'
 INJECTOR 'Well-1'
 INCOMP SOLVENT
 1. 0.
 OPERATE MAX
 BHP 1724. CONT
 OPEN 'Well-1'
 **\$
 WELL 'Well-2'
 PRODUCER 'Well-2'
 OPERATE MIN
 BHP 101. CONT
 SHUTIN 'Well-2'
 DATE 2011 1
 21.00000
 **\$
 WELL 'Well-1'
 INJECTOR 'Well-1'
 INCOMP SOLVENT
 1. 0.
 OPERATE MAX
 BHP 1724. CONT
 SHUTIN 'Well-1'

**\$
 WELL 'Well-2'
 PRODUCER 'Well-2'
 OPERATE MIN
 BHP 101. CONT
 OPEN 'Well-2'
 DATE 2011 1
 21.00069
 **\$
 WELL 'Well-1'
 INJECTOR 'Well-1'
 INCOMP SOLVENT
 1. 0.
 OPERATE MAX
 BHP 1724. CONT
 OPEN 'Well-1'
 **\$
 WELL 'Well-2'
 PRODUCER 'Well-2'
 OPERATE MIN
 BHP 101. CONT
 SHUTIN 'Well-2'
 DATE 2011 1
 22.00000
 **\$
 WELL 'Well-1'
 INJECTOR 'Well-1'
 INCOMP SOLVENT
 1. 0.
 OPERATE MAX
 BHP 1724. CONT
 SHUTIN 'Well-1'
 **\$
 WELL 'Well-2'
 PRODUCER 'Well-2'
 OPERATE MIN
 BHP 101. CONT
 OPEN 'Well-2'
 DATE 2011 1
 22.00069
 **\$
 WELL 'Well-1'
 INJECTOR 'Well-1'
 INCOMP SOLVENT
 1. 0.

OPERATE MAX
 BHP 1724. CONT
 OPEN 'Well-1'
 **\$
 WELL 'Well-2'
 PRODUCER 'Well-2'
 OPERATE MIN
 BHP 101. CONT
 SHUTIN 'Well-2'
 DATE 2011 1
 23.00000
 **\$
 WELL 'Well-1'
 INJECTOR 'Well-1'
 INCOMP SOLVENT
 1. 0.
 OPERATE MAX
 BHP 1724. CONT
 SHUTIN 'Well-1'
 **\$
 WELL 'Well-2'
 PRODUCER 'Well-2'
 OPERATE MIN
 BHP 101. CONT
 OPEN 'Well-2'
 DATE 2011 1
 23.00069
 **\$
 WELL 'Well-1'
 INJECTOR 'Well-1'
 INCOMP SOLVENT
 1. 0.
 OPERATE MAX
 BHP 1724. CONT
 OPEN 'Well-1'
 **\$
 WELL 'Well-2'
 PRODUCER 'Well-2'
 OPERATE MIN
 BHP 101. CONT
 SHUTIN 'Well-2'
 DATE 2011 1
 24.00000
 **\$
 WELL 'Well-1'

INJECTOR 'Well-1'	OPEN 'Well-2'	**\$
INCOMP SOLVENT	DATE 2011 1	WELL 'Well-2'
1. 0.	25.00069	PRODUCER 'Well-2'
OPERATE MAX	**\$	OPERATE MIN
BHP 1724. CONT	WELL 'Well-1'	BHP 101. CONT
SHUTIN 'Well-1'	INJECTOR 'Well-1'	SHUTIN 'Well-2'
**\$	INCOMP SOLVENT	DATE 2011 1
WELL 'Well-2'	1. 0.	27.00000
PRODUCER 'Well-2'	OPERATE MAX	**\$
OPERATE MIN	BHP 1724. CONT	WELL 'Well-1'
BHP 101. CONT	OPEN 'Well-1'	INJECTOR 'Well-1'
OPEN 'Well-2'	**\$	INCOMP SOLVENT
DATE 2011 1	WELL 'Well-2'	1. 0.
24.00069	PRODUCER 'Well-2'	OPERATE MAX
**\$	OPERATE MIN	BHP 1724. CONT
WELL 'Well-1'	BHP 101. CONT	SHUTIN 'Well-1'
INJECTOR 'Well-1'	SHUTIN 'Well-2'	**\$
INCOMP SOLVENT	DATE 2011 1	WELL 'Well-2'
1. 0.	26.00000	PRODUCER 'Well-2'
OPERATE MAX	**\$	OPERATE MIN
BHP 1724. CONT	WELL 'Well-1'	BHP 101. CONT
OPEN 'Well-1'	INJECTOR 'Well-1'	OPEN 'Well-2'
**\$	INCOMP SOLVENT	DATE 2011 1
WELL 'Well-2'	1. 0.	27.00069
PRODUCER 'Well-2'	OPERATE MAX	**\$
OPERATE MIN	BHP 1724. CONT	WELL 'Well-1'
BHP 101. CONT	SHUTIN 'Well-1'	INJECTOR 'Well-1'
SHUTIN 'Well-2'	**\$	INCOMP SOLVENT
DATE 2011 1	WELL 'Well-2'	1. 0.
25.00000	PRODUCER 'Well-2'	OPERATE MAX
**\$	OPERATE MIN	BHP 1724. CONT
WELL 'Well-1'	BHP 101. CONT	OPEN 'Well-1'
INJECTOR 'Well-1'	OPEN 'Well-2'	**\$
INCOMP SOLVENT	DATE 2011 1	WELL 'Well-2'
1. 0.	26.00069	PRODUCER 'Well-2'
OPERATE MAX	**\$	OPERATE MIN
BHP 1724. CONT	WELL 'Well-1'	BHP 101. CONT
SHUTIN 'Well-1'	INJECTOR 'Well-1'	SHUTIN 'Well-2'
**\$	INCOMP SOLVENT	STOP
WELL 'Well-2'	1. 0.	DATE 2011 3
PRODUCER 'Well-2'	OPERATE MAX	2.00069
OPERATE MIN	BHP 1724. CONT	**\$
BHP 101. CONT	OPEN 'Well-1'	

CURRICULUM VITAE

Name Sevtaç BÜLBÜL

E-mail sevtacbulbul@gmail.com

Date of Birth 5th April 1981

Place of Birth Ankara

Nationality Turkish

Education

B.Sc.

- | | |
|-----------|--|
| 1999-2004 | Middle East Technical University (METU), Ankara
Petroleum and Natural Gas Engineering
Cumulative GPA: 3.04 out of 4.00 (Honour) |
| 2002-2004 | Middle East Technical University (METU), Ankara
Minor Program of Faculty of Engineering-
Geographical Information Systems and Remote Sensing |
| 2003-2007 | Anadolu University, Open Education Faculty
Business Administration |

M.Sc.

September 2004- February 2007

Middle East Technical University (METU), Ankara
Department of Petroleum and Natural Gas Engineering
Cumulative GPA: 4.00 out of 4.00

Ph.D.

February 2007-present

Middle East Technical University (METU), Ankara
Department of Petroleum and Natural Gas Engineering

Languages

English- Good command of written and spoken English
German- Beginner
Turkish- Native language

Computer Skills

Operating System: MS Windows

Language: C Programming Language (elementary),
MATLAB (intermediate)

Software: MS Office Applications (Word, Excel, PowerPoint, Outlook), Aquifer Simulation Model (ASM), Visual Modflow, TNT MIPS, PETREL, CMG Builder, CMG GEM, CMG WinProp

Experience

- 10.06.2002- 30.06.2002 Summer practice at Turkish Petroleum Corporation (TPAO), Adıyaman.
(At the departments of Production & Well Completions)
- 16.06.2003-11.07.2003 Summer practice at Turkish Pipeline Corporation (BOTAŞ), Ankara
(At the department of Natural Gas Sales and Marketing)
04. 10. 2004- 15.09.2011 Research & teaching assistant
(Department of Petroleum & Natural Gas Engineering, Middle East Technical University (METU)).

Short Courses Attended

- 1) Short course presented by Assoc. Prof. Dr. Tayfun BABADAĞLI (University of Alberta) on “Fundamentals of Fluid Flow in Fractured Porous Media”, 20th June, 2005, Ankara, Turkey.
- 2) Short course held by the Chamber of Petroleum Engineers on “Geothermal Energy”, 18-20th April 2007, Ankara, Turkey.
- 3) Short course presented by Salih Saner, V. Prof. Dr. on “X-Ray Computerized Tomography (CT) Principles and Petrophysical Applications”, February 2010.
- 4) LabVIEW and Data Aquisition Hands-On Training, 22nd March, 2010.
- 5) Short course held by the Chamber of Petroleum Engineers on “LPG Filling Plant and Station Managing”, 4-6th March 2011, Ankara, Turkey.

International Congresses Attended

10th International Conference on Greenhouse Gas Control Technologies, Amsterdam, the Netherlands, September 19-23, 2010.

6th CO₂GeoNet Open Forum, Venice, San Servolo Island, Italy, May 9-11, 2011.

Awards

Course Performance Award, Graduate School of Natural and Applied Sciences, METU, May 2006.

Projects Participated

- TUBITAK KAMAG 106G110: “Assessment of CO₂ Storage Potential in Turkey, Modeling and a Prefeasibility Study for Injection into an Oil Field”, October 2009.
- PhD Research Project funded by Shell Global Solutions International entitled as "Matrix-Fracture Interaction in Sandstone Rocks during CO₂, N₂ and CH₄ Injection" (Contract No. 4600004372).
- CO₂ Geological Storage- CGS Europe Project, "Pan-European coordination action on CO₂ Geological Storage", project funded within the 7th Framework Programme of the European Community

Presentations

- 1) S. Bülbül, F. Gümrah, I. Dirik and A. Altıntaş: “Analytical Modeling of CO₂ Sequestration in Saline Aquifers”, presented at IPETGAS 2005 & on CD, 15th International Petroleum and Natural Gas Congress and Exhibition of Turkey, May 11-13, 2005, Ankara, Turkey.

- 2) S. Bülbül, M. Parlaktuna, T. Mehmetoğlu, U. Karabakal: “Hydrate Formation Conditions of Methane Hydrogen Sulfide Mixtures”, presented at IPETGAS 2007 & on CD, 16th International Petroleum and Natural Gas Congress and Exhibition of Turkey, May 29-31, 2007, Ankara, Turkey.

- 3) S. Bülbül, M. Parlaktuna: “Matrix Fracture Interaction in Sandstone Rocks During Carbon Dioxide Injection”, presented at IPETGAS 2011, 18th International Petroleum and Natural Gas Congress and Exhibition of Turkey, May 11-13, 2011, Ankara, Turkey.

Publications

- 1) I. Dirik, S. Bülbul, A. Altıntaş and F. Gümrah, “Analytical Modeling of CO₂ Sequestration in Saline Aquifers”, Proceedings of Canadian International Petroleum Conference, 55th Annual Technical Meeting, June 8-10, 2004, Calgary, Alberta, Canada, on CD & presented.
- 2) S. Bülbul, F. Gümrah, I. Dirik and A. Aslınas, “Tuzlu Su Akiferlerinde CO₂ Depolanmasının Analitik Modellemesi”, Türk Petrol ve Doğal Gaz Dergisi, Cilt: 11, Sayı: 2, June 2005.
- 3) S. Bülbul, M.Sc. Thesis: “Hydrate Formation Conditions of Methane Hydrogen Sulfide Mixtures”, METU Petroleum Engineering Department, February 2007. Supervisor: Prof. Dr. Tanju Mehmetoğlu, Co-Supervisor: Prof. Dr. Mahmut Parlaktuna.
- 4) Ç. Acar, S. Bülbul, F. Gümrah, Ç. Metin, M. Parlaktuna: “Petrol ve Doğal Gaz”, ODTÜ Yayıncılık, November 2007.
- 5) E. Okandan, Y. Karakece, H. Çetin, İ. Topkaya, M. Parlaktuna, S. Akın, S. Bulbul, C. Dalkha, S. Anbar, C. Cetinkaya, İ. Ermis, M. Yılmaz, V. Ustun, K. Yapan, A.T. Erten, Y. Demiralın, E. Akalan: “Assessment of CO₂ Storage Potential in Turkey, Modeling and a Prefeasibility Study for Injection into an Oil Field”, Energy Procedia 4, GHGT-10, 2011.
- 6) S. Bulbul, A. Kadoura, S. Merey, M. Parlaktuna: “Hydrate Inhibition with PEO (Poly 2-ethyl-2-oxazoline)”, Energy Sources, Part A: Recovery, Utilization, and Environmental Effects, accepted on March 2011-not published yet.
- 7) S. Bulbul, M. Parlaktuna, T. Mehmetoglu, U. Karabakal: “Hydrate Formation Condition of Methane Hydrogen Sulfide Mixtures”, Energy Sources, Part A: Recovery, Utilization, and Environmental Effects, accepted on March 2011-not published yet.
- 8) S. Bulbul, M. Parlaktuna, T. Mehmetoglu, U. Karabakal: “Black Sea Hydrate Formation Conditions of Methane Hydrogen Sulfide Mixtures”, Energy Sources, Part A: Recovery, Utilization, and Environmental Effects, accepted on January 2011-not published yet.

Interests

Turkish Classical Music, reading, writing short stories& poems.

Membership

2005- present	Chamber of Petroleum Engineers
2004- present	METU Alumni Association
2002- present	Society of Petroleum Engineers (SPE)
2000- present	METU Clasical Turkish Music Club (member of the METU Clasical Turkish Music Chorus)